RESERVOIR PARAMETERS ESTIMATION USING ROCK PHYSICS MODELLING AND AVO ANALYSIS FOR CHARACTERIZATION OF LOWER GORU FORMATION

By

Muhammad Ehsan Rafique

M.Phil Geophysics

(2018 - 2020)

Department of Earth Sciences

Quaid-i-Azam University Islamabad, Pakistan

*"In The Name of **ALLAH**, the Most Merciful & Mighty"*

"PAY THANKS TO ALLAH EVERY MOMENT AND GO TO EXPLORE THE HIDDEN TREASURES, ITS ALL FOR YOUR BENEFIT" (AL-QURAN).

CERTIFICATE

It is certified that **Muhammad Ehsan Rafique** s/o **Hafiz Muhammad Rafique** carried out the work contained in this dissertation under my supervision and accepted in its present form by Department of Earth Sciences, Quaid-i-Azam University Islamabad, Pakistan as satisfying the requirements for **M.Phil** degree in **Geophysics**.

RECOMMENDED BY:

Dr. Matloob Hussain _____

Supervisor

Department of Earth Sciences

QAU, Islamabad.

Dr. Aamir Ali _____

Chairman

Department of Earth Sciences

QAU, Islamabad.

External Examiner _____

DEDICATION

I would like to dedicate this thesis work to my parents, brothers, teachers and friends whose love, encouragement, guidance and prays build me so high and make me able to achieve such success and honour. Also dedicated to all those who love me and whom I love.

Acknowledgement

First and foremost, all praises to **Allah Almighty**, the most beneficent and the most merciful. Secondly, my humblest gratitude to the **Holy Prophet Muhammad (Peace Be upon Him)** whose way of life has been a continuous guidance and knowledge of humanity for me. This thesis appears in its current form due to the assistance and guidance of several people. It gives me great pleasure to express my gratitude to all those who supported me and have contributed in making this thesis possible. I thank Allah for giving me strength and ability to carry out this study.

I am especially indebted to my honourable supervisor **Dr. Matloob Hussain** for giving me the opportunity to work under his supervision. His continuous support, motivation and untiring guidance have made this thesis possible. Thanks to him for bearing my mistakes and whenever I could not meet the deadlines. I express my gratitude to **Dr. Aamir Ali** for their inspiration for dedication to the profession and guidance in the preparation of this thesis and their assistance in any way that I may have asked. His vast knowledge, calm nature and positive criticism motivated me to starve for pleasant results.

Besides my supervisor, I am thankful to my respectable friends especially to Yawar Amin for his cooperation and guidance during this research work. To me, there is nothing better than having good friends, so great pride is with me while thanking especially Hamza Latif, Bilal Ahmed, Muhammad Mubashir Rana, Hassan Sardar, Muhammad Azam Khan, Muhammad Wajahat khan, Aqeel Nawaz, Sarmad Rameez, Jamal Abdul Nasir, Javed Iqbal, Muhammad Fahad, Daniyal Aziz and Umar Farooq for their moral support during my study. Words are lacking to express my humble obligation for their helping attitude, and Kind Cooperation. The time spent with them will remain unforgettable for me.

Last but not least, I would like to acknowledge my **Parents, Brothers (**Hafiz Muhammad Zeeshan Rafique & Hafiz Muhammad Nouman Rafique)**, Cousins** and my **Family** for their constant support, unceasing prayers and best wishes. They uplifted my morale whenever I needed.

I do thank all those who have helped me directly or indirectly in the Successful completion of my thesis. Anyone missed in this acknowledgement are also Thanked.

Muhammad Ehsan Rafique

M.Phil Geophysics (2018 – 2020)

ABSTRACT

Although Seismic interpretation is important in terms of reservoir detections, the characterization of reservoirs is based upon well analysis. The problem with this analysis is one dimensionality. In order to deal with this problem, use of other methods are essential. Apart from post stack data analysis, pre stacked data analysis is a key tool to study the varying behavior of reservoirs with variation in their characteristics. Models for pre stacked analysis have been generated throughout the years which can be utilized to either distinguish reservoir sands into different classes and can play an essential part for inverting for a particular parameter if the model results for varying of a specific variable is geostatistically correlated with the pre-stack data of the area.

Focus of this study is to quantitatively characterize reservoir within study area and to check for variation within the reservoir using Rock Physics Models and Amplitude Versus Offset (AVO) analysis. The procedure starts with demarcation of horizons on the basis of seismic to well tie. Structural interpretation is important to study any existing petroleum play. The structural interpretation was therefore carried out including horizon marking of Lower Goru formation and C-interval. Fault polygon were demarcated to analyze two dimensional trend of the faults within the area. Petro-physical analysis concluded presence of reservoirs within the shaly sand lithology of Lower Goru formation. Zones were marked within the sand patches which showed favorable results.

In order to study the pre stacking trend for the reservoir marked using the above mentioned techniques, T- matrix and Non Interactive Approximation RPMs were utilized to obtain the dry rock properties. The porosity within the models was varied to check the effect on the elastic parameters. Wood's equation was used for determination of effective properties of fluid which was then inculcated into the dry rock model with the help of Gassmann's equation. The saturation level within the Wood's equation was varied to check the response of the models under differing saturations. Reflectivity series for varying offset (angle) were determined using Rugger's approximation. The trend showed presence of Class I sands in the reservoir. Results from the models under influence of varying input variables were compared and the trends were discussed. AVO synthetics were generated for each scenario using both the RPMs. The results upon comparison showed a comparatively sharper traces in case of elastic parameters obtained from T – matrix compared to NIA.

CONTENTS

LIST OF FIGURES

LIST OF TABLES

CHAPTER 1

INTRODUCTION

Geophysical prospecting comprises the study of the isolated Earth by means of physical dimensions, generally on or above the ground surface. It also embraces analysis of the dimensions in terms of subsurface structures and phenomena. Geophysical studies are quantitative and physical, whereas geological studies are qualitative and evocative.

Hydrocarbon extraction, no doubt, shows an important role to elevate the economy of a country. As the energy demand surges, exploration sector catch their eyes over unexplored areas for new energy resources excavation. Therefore, our aim is to run a two dimensional (2D) or three dimensional (3D) geological model to petroleum engineers for reservoir performance replication and for well planning (Slatt, 2006), Examination of earth through goophysical method involves taking measurements to check the variation both vertically and horizontally by calculating its physical properties (Bust et al., 2011). Different methods are being utilized by the geoscientists for the hydrocarbon exploration like gravity, magnetic, resistivity etc. but the foremost widely used effective tool is seismic reflection method. Seismic reflection method commonly employed in order to attain a target depth of reservoir with improved mapping of subsurface geological geometry (Badley, 1988). Seismic method marks Reflection coefficients velocity amplitude and angle of offset with distance and density information (Yincan et al., 2018). The recorded data at the surface depend on the subsurface varying rock composition like lithology and fluid saturation (Yilmaz, 2001).

The interpretation of a petrophysical log is unique of the most valuable and noteworthy tools accessible to the geologist and geophysicist. Petrophysics is fundamental and no formation assessment seismic interpretation or geo-mechanical investigation can be undertaken deprived of a brief and full petrophysical interpretation. Petro physical parameters must be successfully extracted from the seismic data because they are useful as hydrocarbon pointers. A vital task of petrophysical analysis is to achieve the appropriate physical parameters for determining fluid and lithology from log data. (Yuedong and Hongwei, 2007).

The reservoir characteristics are the quantification of important physical properties of the reservoir. Wireline is one of the methods used to characterize a reservoir to evaluate the physical

and chemical properties of a reservoir (Asquith et al., 2004). To complete the reservoir analysis the following rock properties are required such as Shale-Volume, Total-Porosity, Effective Porosity and water-saturation (Fischetti et al., 2002; Wilcox, 2016; Vilmaz, 200l; Bacon et al. 2007; Badely, 1985; Stewan, 2012). After you have successfully labeled the reservoir, the next step is to define the reservoir fluid and its lithology. Assessment of the physical properties of rocks based on well log data and cross plot analysis are useful for assessing reservoirs. (Omudu et al., 2007). Attribute cross plot based on rock physics distinguish between fluid type and lithology. LMR (λ, μ, ρ) technique is extensively used for this purpose. The rock physics modeling integrated with petrophysical analysis is used to classify the different lithologies and reservoir properties (Dworkin et al., 2015).

1.1 Introduction to Sawan area

Early-late cretaceous Lower Goru sands have become evident as main producer in Lower Indus basin of Pakistan during last two decades. Great discoveries have been made in fields such as Miano, Kadanwari, Sawan and Badin. Sawan area is located in Khairpur District, Sindh Province, Pakistan, near the proximity of lower Indus basin.

The Sawan region is well known for its gas production which is why it is also called Sawan Gas Field which is located in the Thar Desert about 300 km northeast of Karachi and has been discovered in 1998. It is a joint venture between OMV Pakistan (19.74%), PPL (26.18%), ENI Pakistan (23.68%), Government Holdings Private Limited (22.50%) and Moravske Naftove Doly (7.90%).

The operator of the Sawan gas field is OMV Pakistan. It was and still is considered to be one of the largest gas discoveries in Pakistan. A total of 15 wells were drilled in the Sawan gas field 14 of which supply 270 x 10^6 cubic feet of gas to Sui northern gas pipelines and 40 x 10^6 cubic feet to Sui Southern Gas Company. Total gas sold from the Sawan field in 2009-10 was 104,754 x 10^6 cubic feet compared to 123,485 x 10^6 cubic feet in 2008-09. It is one of the key gas producing fields with the early-late Cretaceous lower Goru formation serving as a potential reservoir. Over the past two decades, these sands have become an important source of hydrocarbons in the middle and lower Indus basin of southern Pakistan. (Munir et al., 2011).

1.2 Location of study area

According to petroleum concession of Pakistan, the coordinates of the area are latitude 26°59' N to 26° 98' N and Longitude 68° 32' E to 68° 58' E (Figure 1.1, Figure 1.2). This area has thick strata of Mesozoic Tertiary deposits covered with Quaternary deposits. The zone was tectonically steady until the Jurassic and perhaps the Early Cretaceous but the rift began to emerge in the Late Cretaceous and Early Paleocene among which effects can be observed in seismic sections where post Eocene strata remain unchanged or very less deformed. Cretaceous rocks are widespread in different parts of the lower Indus basin. These rocks exhibit a wide range of lithological heterogeneity mainly due to changes in sediment availability and environmental conditions (Kadri, 1995).

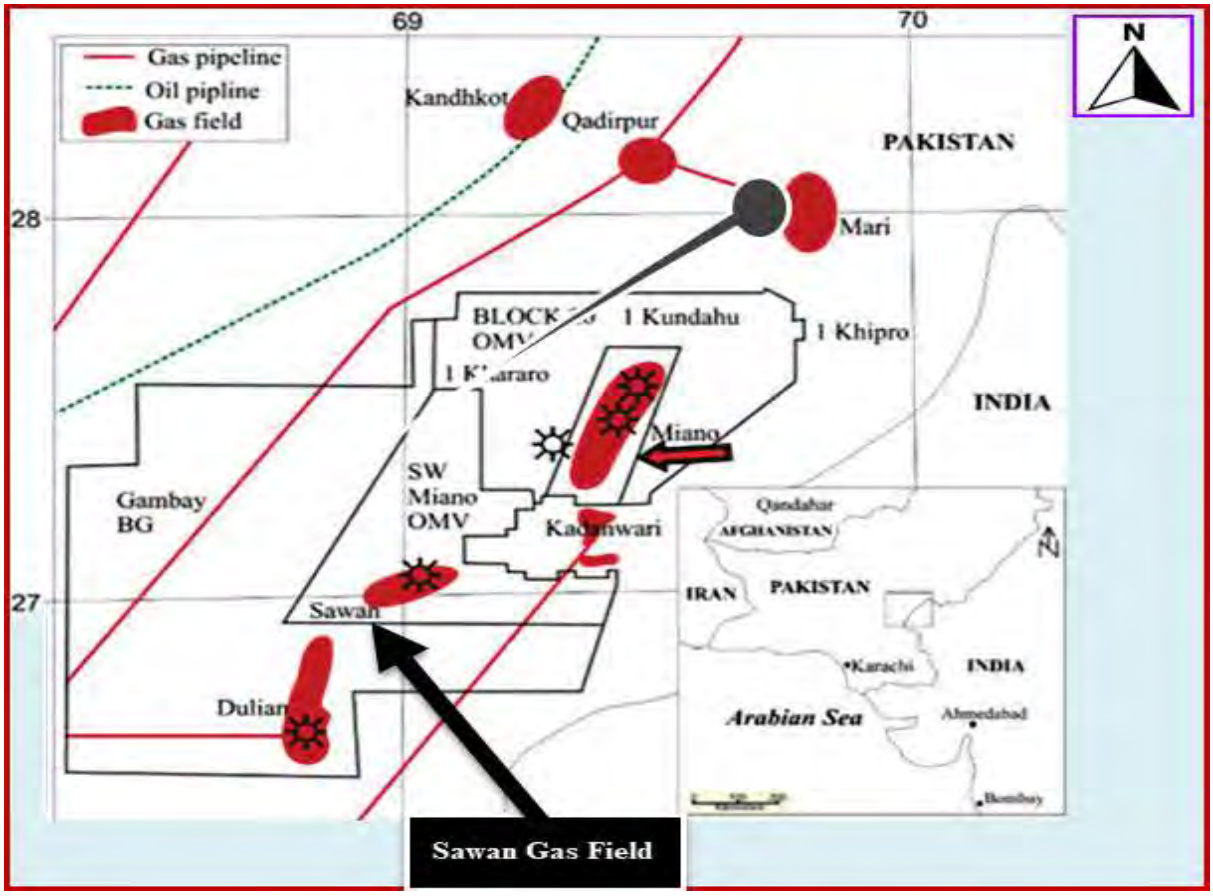

Figure 1.1: Site Map of the area (Kadri, 1995).

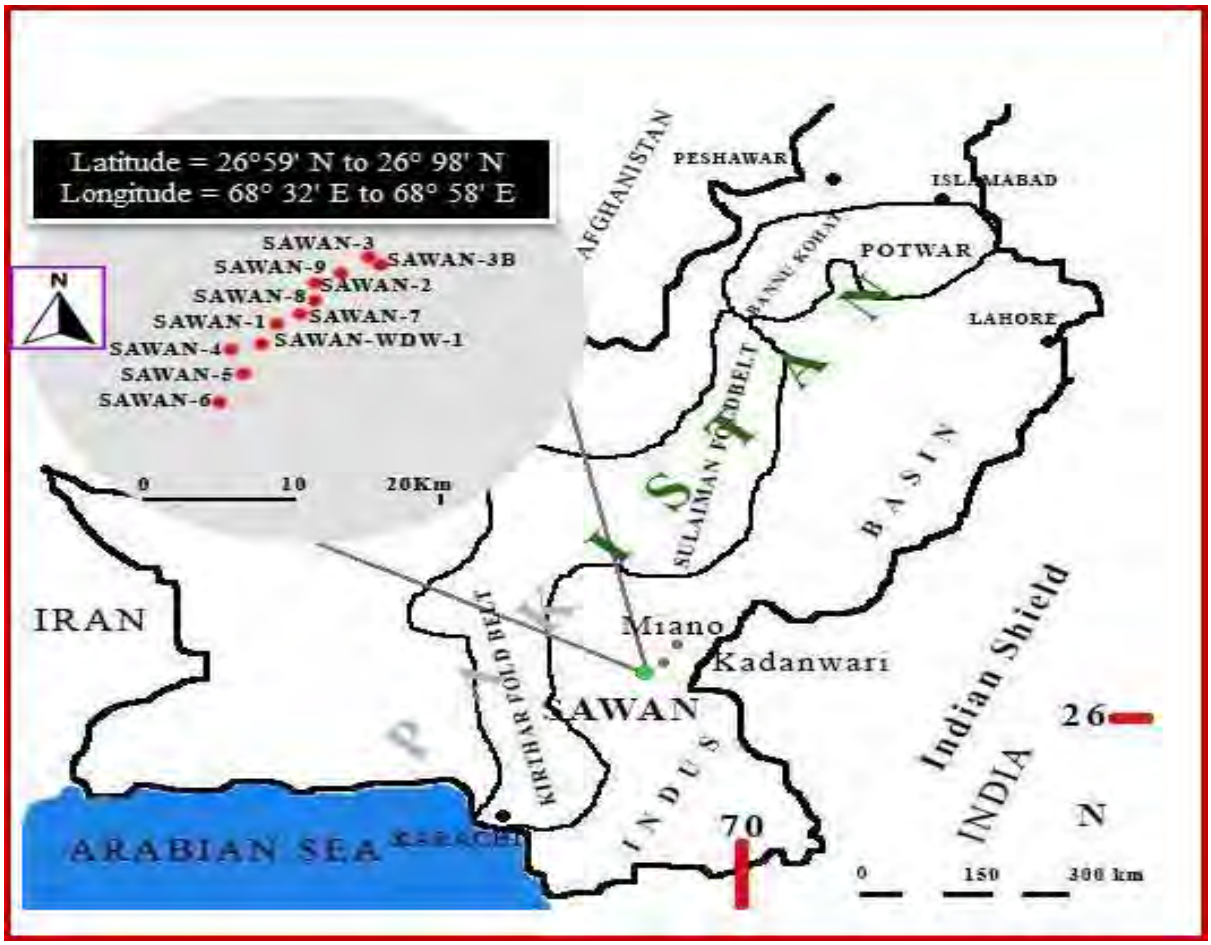

Figure 1.2: Location map of Sawan Field, highlighted with geographical co-ordinates and all wells (Anwer et al., 2017).

1.3 Base Map

Base map Figure 1.3 provides information about in-lines as well as cross-lines and well location of study area. The 3D cube is represented with respected to its geographical references i.e. latitude and longitude. The preparation of base map is carried out by importing SEG-Y and navigation files of seismic lines in Kingdom Suit (software used for interpretation). The well data is loaded in LAS format.

Basically three wells Sawan-01, Sawan-02 and Sawan-07 are loaded and all In-lines ranged 520-910 and Cross-lines 870-1020 are posted on map.

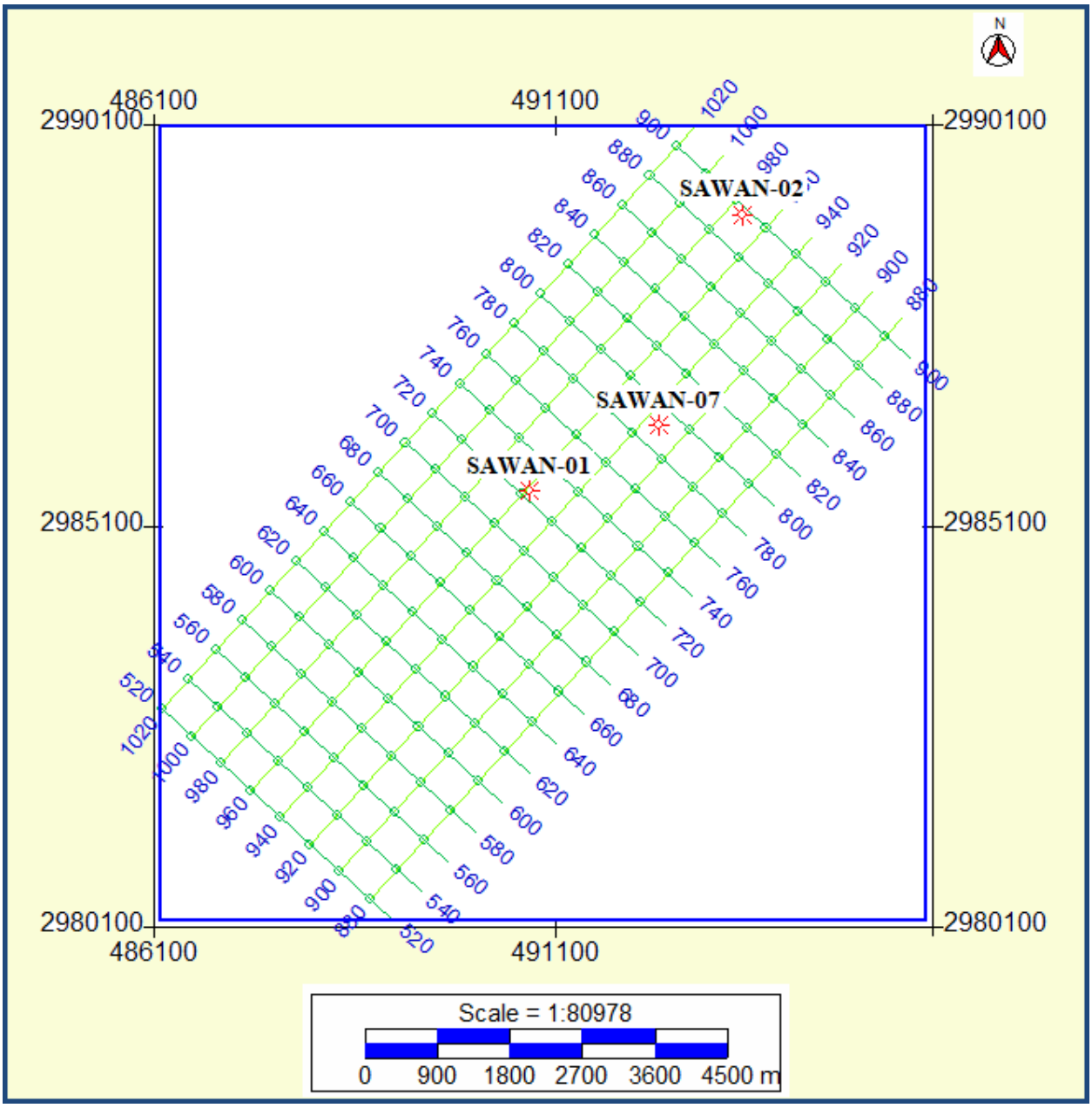

Figure 1.3 Base Map

1.4 Data Sets

Table 1.1: Description of Wells.

Well Name	Latitude	Longitude	Status	Class	TD (m)
SAWAN-01	26.991828	68.906992	GAS	Exploratory	3587
SAWAN-02	27.022972	68.933806	GAS	Appraisal	3500
SAWAN-05	26.954733	68.884303	GAS	Development	3370

SAWAN-06	26.933886	68.867250	GAS	Development	3340
SAWAN-07	26.999283	68.923317	GAS	Development	3400
SAWAN-08	27.009156	68.933394	GAS	Development	3430
SAWAN-09	27.028303	68.951461	GAS	Development	3445

Table 1.2: Well Tops Information at different wells location.

Formation	Sawan-01	Sawan-02	Sawan-05	Sawan-06	Sawan-07	Sawan-08	Sawan-09
Habib Rahi	274	273	269	253	285	284	299
Ghazij	301.5	301	291.5	275	304	305	320
SML*	1117	1109	1103	1084	1116	1121	1121
Ranikot	1259	1251.3	1246	1232	1261	1260	1266
Upper Goru	2448	2412	2463.5	2445	2444	2434	2415
Lower Goru	2696	2683	2715	2670	2691	2716	2704
D Interval	3182	3171	3204	-	-	3196	-
C Interval	3246	3259	3260	3167	3243	3240	-
B Interval	3460	3450		3214	-	-	-

*SML= Sui Main Limestone

1.5 Objectives

Following are the main objectives of this research; achieved by using seismic and well log data.

1. Detailed interpretation of 3D seismic data for subsurface mapping and determination of the boundaries of a new prospective zone.
2. Wireline petro physical analysis for estimation of important reservoir characteristics.
3. To investigate sensitivity of elastic properties with varying porosity and fluid substitution within different Rock Physics Models.
4. AVO modeling using Rugger approximation at varying saturation and porosity to evaluate reservoir performance.

1.6 Methodology

The methodology adopted for research work is as following:

1. Develop a base map with the help of navigation file and coordinates of the study area.
2. Add wells to the base map and load las files.
3. Generate a synthetic seismogram using sonic and density logs of Sawan-07 well.
4. Correlate the seismic section to the well with the help of synthetic seismogram for demarcation of horizons.
5. Mark the Lower Goru and C Interval horizons on seismic data with the help of synthetic seismogram.
6. Fault identification and demarcation of fault polygons.
7. Generation of time and depth grid and contour maps.
8. Petrophysical analysis of Sawan_01, Sawan_02 and Sawan_07 well for reservoir characterization.
9. Modify Non Interactive Approximation (NIA), T-Matrix and Gassmann Rock Physics Models (RPMs) to check sensitivity of elastic parameters with porosity and saturation variation within the modeled reservoir.
10. Plot the elastic parameters with porosity variation and fluid substitution to compare the results from the above listed RPMs.
11. Plot the Reflection coefficients obtained from the Rugger approximation with angle to quantitatively and qualitatively examine the intercept and gradient values.
12. AVA analysis using Rugger approximation to check the response of Amplitude with angle variation for different porosities and saturation levels.

The General Sequence of Research work is illustrated below in Figure 1.4.

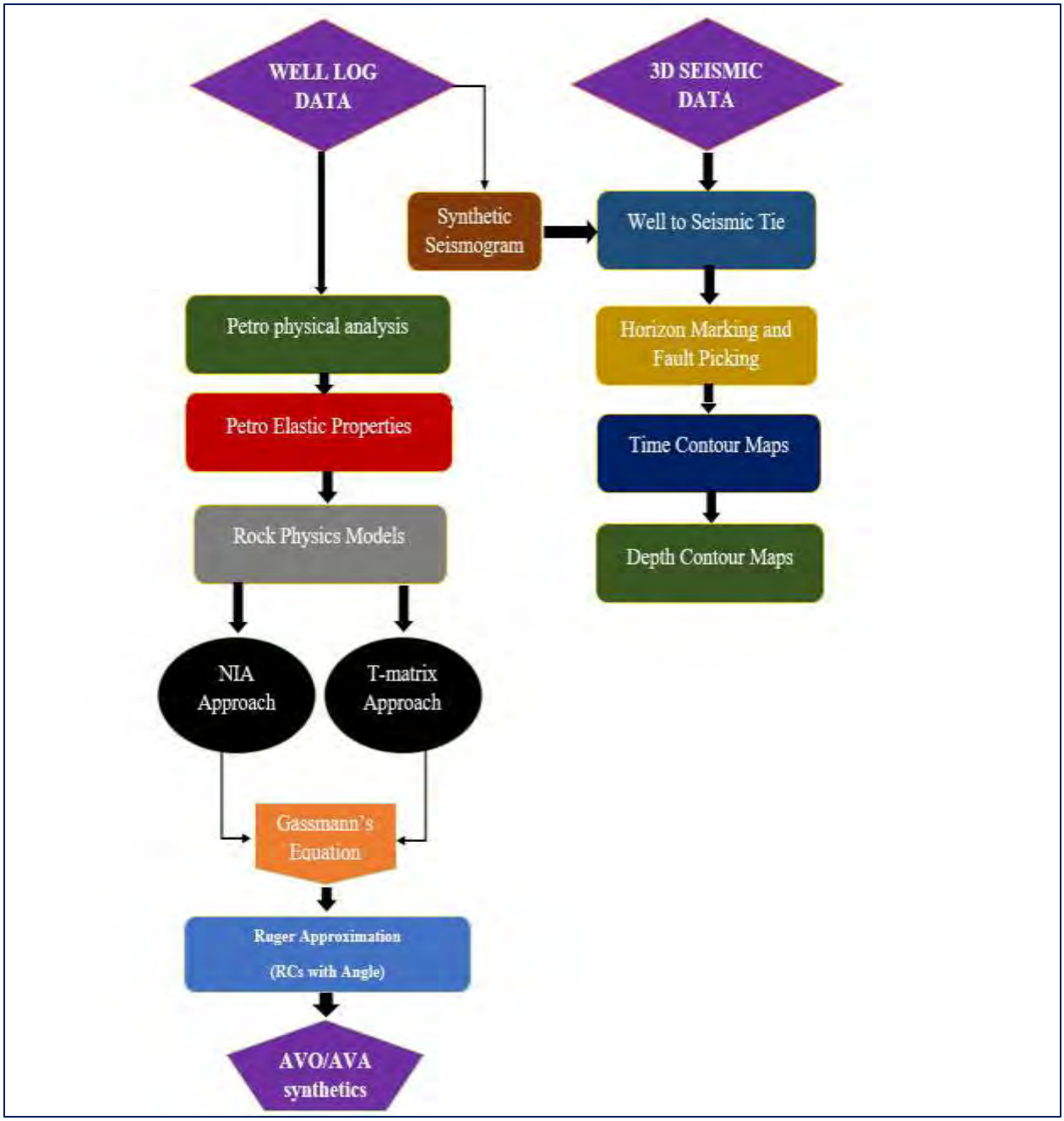

Figure 1.4: Block Plan of Sequential illustration of Thesis Work

CHAPTER 2

GEOLOGY AND TECTONICS OF THE STUDY AREA

For the interpretation of the seismic data geology has a salient role. Geology describes the origin, structural style, mode of deformation and environment of deposits. To understand the full geology of the study area three parameters need to be investigated such as basin tectonics, sedimentary sequences, and basin modifying tectonics. (Kingston et al., 1983). Structural geology reduces the risk of exploration. The interpreter must have geological knowledge of the terrain its stratification unconformities and underlying structures to overcome complexities as the same effects on velocity can be caused by different formations. (Kazmi and Jan, 1997).

This chapter delivers a brief description of the geology tectonic structure and stratigraphy of the study area.

2.1 General Geology and Tectonic Setting

Sawan field is positioned on the south eastern verge from North to South, which tends up to Jacobabad Haripur as Shown in Figure 2.1. The structural and stratigraphic style of the Sawan region is controlled by three main tectonic events uplift and erosion of the Upper Cretaceous layer, the Paleocene luteum fault, and the rise of the Jacobabad Khairpur level in the Upper Tertiary (Ahmad et al., 2004). As a result of these events, the stratigraphic sequence of the study area has evolved and distorted. The first event occurred as a late Cretaceous stratum uplift near the k-T boundary, as evidenced by the thinning of the Ranikot fragment at the paleo high and its thickening away from there.

In the second step, the counterclockwise rotation of the Indian plate and their impact with the Eurasian plate caused to induce wrench faulting (Zaigham and Mallick, 2000; Ahmed et al., 2004). Basement commenced from NNW to SE, the main fractures crossed the entire Cretaceous section. These faults have taken root in single faults and change character as echelon faults near the Upper Goru Formation and dismiss against the backdrop of Tertiary unconformity, developing a negative floristic structure. These effects are more prominent in the eastern part. Finally, the uplifting of Jacobabad Haripur disordered the structure of the Sawan field in the late

Tertiary. As a result of the uplift, the sands of the Lower Goru Formation changed from a shallow marine environment to a structurally deep marine environment, where shales of the Goru formation were dumped over there by cyclic rise of sea level which provide a seal to sands.

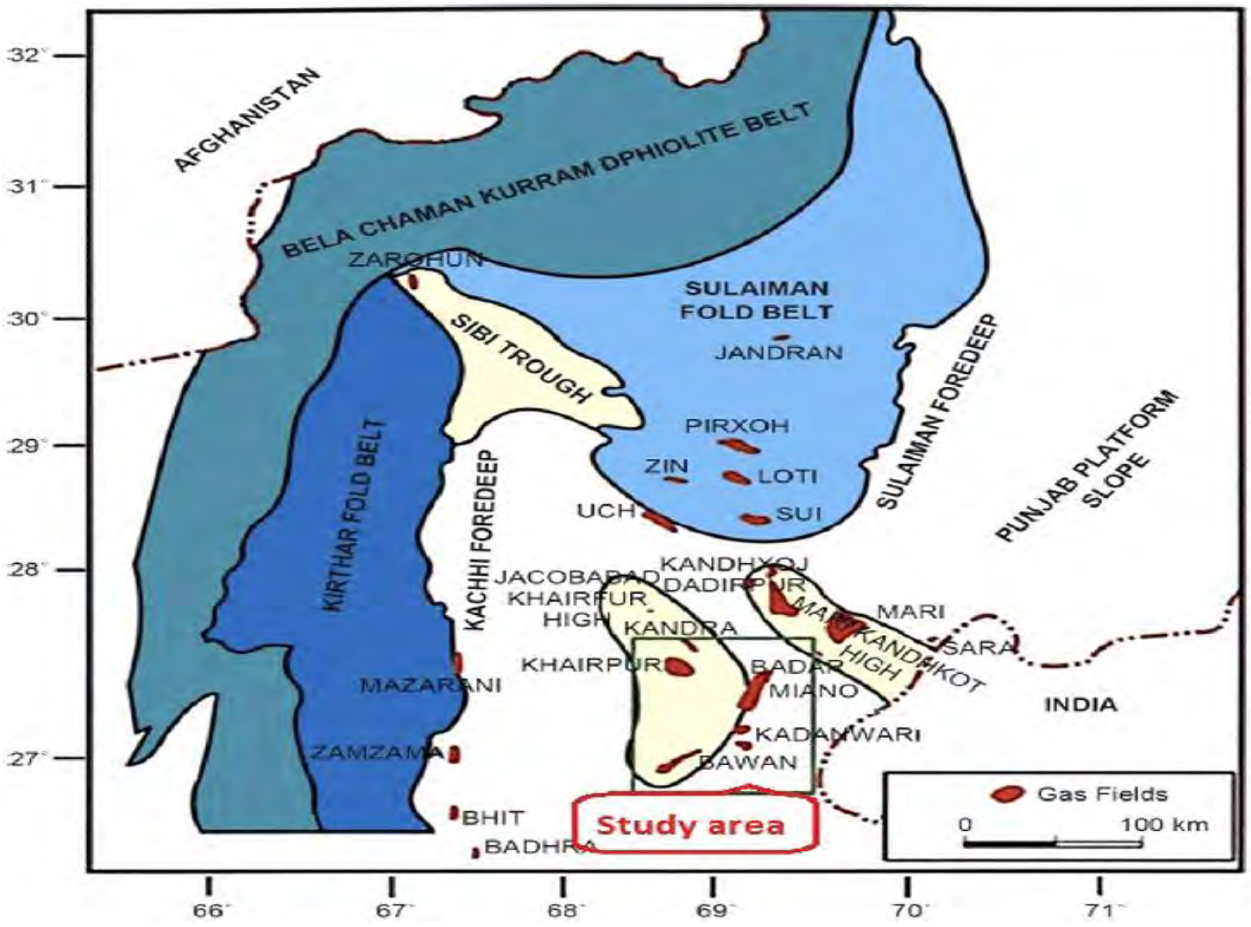

Figure 2.1: Regional-tectonic-map-showing-the-location-of-Sawan-Gas-Field (Krois et al., 1998)

Lower Goru breakthrough mainly occurred at structural high features such as Jacobabad Khairpur High, Mari high etc. in the central and lower Indus Basin in Pakistan as shown in Figure 2.2. These structures as well as the stratigraphic characteristics are very favorable for migratory pathways, the reservoir charge timing and the accumulation of hydrocarbons (Kazmi and Jan, 1997). The first episode of uplift occurs near the Tertiary Cretaceous K-T boundary and is established as a basic tertiary unconformity. Most of the powerful and subtle faults associated with tectonics end up in this unconformity.

NW-SE faults are intersected by most of the entire cretaceous strata which have changed from a single fault in Chiltan to numerous faults at the lower and upper Goru level. This character is due to the trans-tensional tectonics associated with the first section of the Indian Eurasian plates and therefore to the counter clockwise component of the Indian plate. The second up thrust time of in the lower and central Indus basin is Late Eocene -Oligocene. Structural highs may have experienced frequent periods of disturbance in response to successive west and North West thrust phases. This is probably the time when the shape of the traps has finally improved and there may have been secondary migrations and reservoir charge took place (Ahmad et al., 2004).

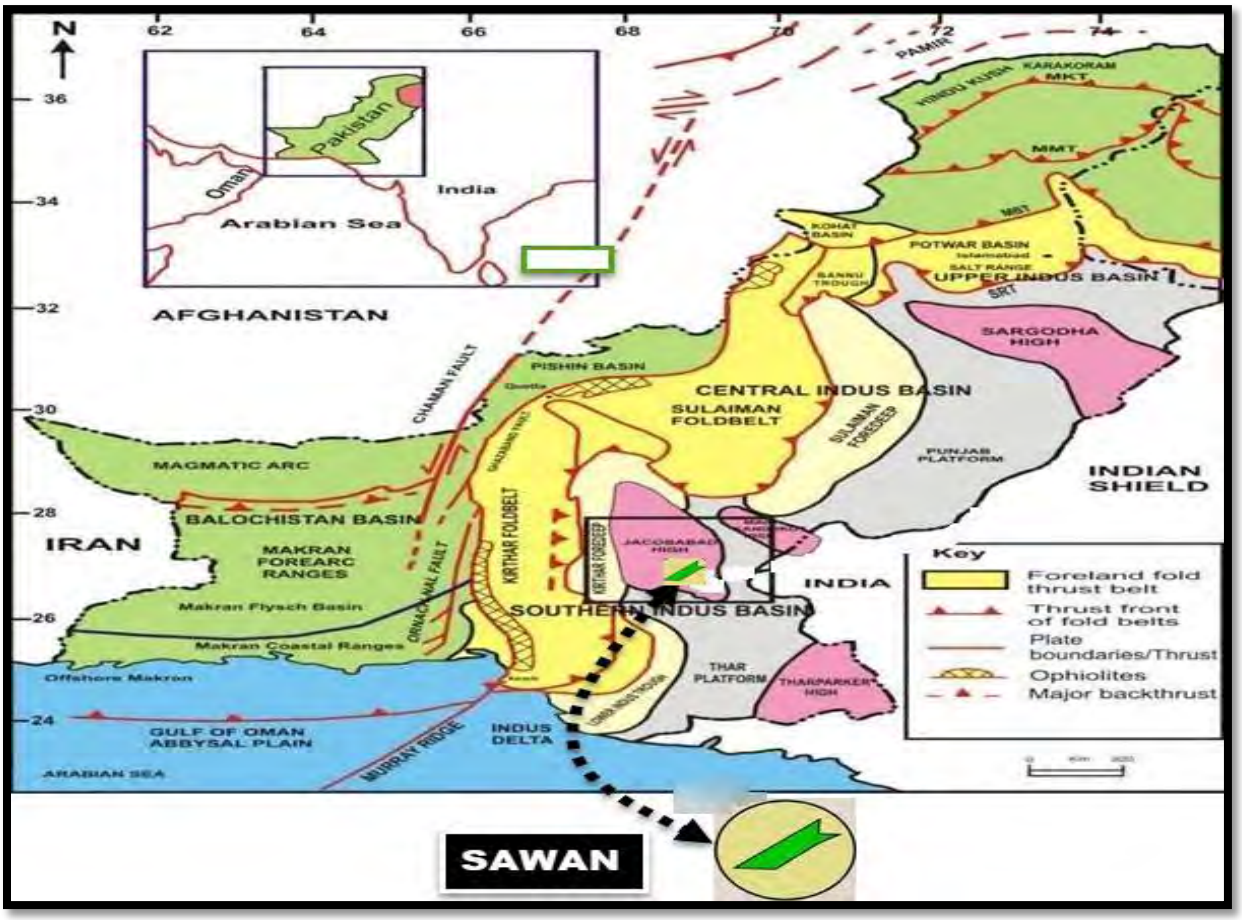

Figure 2.2: Tectonic Map with Sedimentary basins (Anwer et al., 2017).

2.2 Petroleum Play

A system in which the source reservoir and overburden seal rock are considered necessary constituents with the migration of hydrocarbons to setup a petroleum play. The drilling and logging results indicate that the entire Cretaceous age petroleum system was deposited in the Sawan region.

2.2.1 Source Rock

The Early Cretaceous Sember Formation is a potentially rich and proven source rock with TOC values ranging from 1 to 4 in the Middle Indus basin (Aziz et al., 2018). At the beginning of the Cretaceous, the Sember Formation was deposited in a shallow sea. It includes black shale, sandstone, siltstone and nodular sandstone. The main organic material of the Sember formation is type-III kerogen so it indicates promising for gas production (Wandrey et al., 2004). TOC content is estimated by pyrolysis to be 0.5 to 1.7 percent.

2.2.2 Reservoir Rock

The formation of the lower Goru comprises of intermittent layers of sand shales. The lower region of Cretaceous Goru Formation comprises good reservoir quality sandstones further classified as A, B, C and D sand. Sand with the C- interval is the most fertile reservoir of the Sawan field. Seismic stratigraphy and central sedimentological surveys indicate that it is sand of the low stand shelf edge delta system. (Ahmed et al., 2004; Afzal et al., 2009; Munir et al., 2011). The porosity of the C interval sand reservoir varies from 6 to 25 percent and the permeability from 1 to 2000 mD.

2.2.3 Trap and Seal

Structural - stratigraphic traps have been identified in the Sawan region which have been formed during the third phase of a tectonic event called the inversion phase (Ahmad et al., 2004; Berger et al., 2009). During the transgression the shale layer pinchout against prograding C sand wedges in westward providing stratigraphic traps. From Northwest to Southeast trending wrench faults also helps to create a combined trap in the study area. The lower Goru Formation was covered

with a thick layer of transgressive shale. The intraformational lower Goru shale also ensures the cap to reservoir. The Sawan stratigraphic column is shown in Figure 2.3.

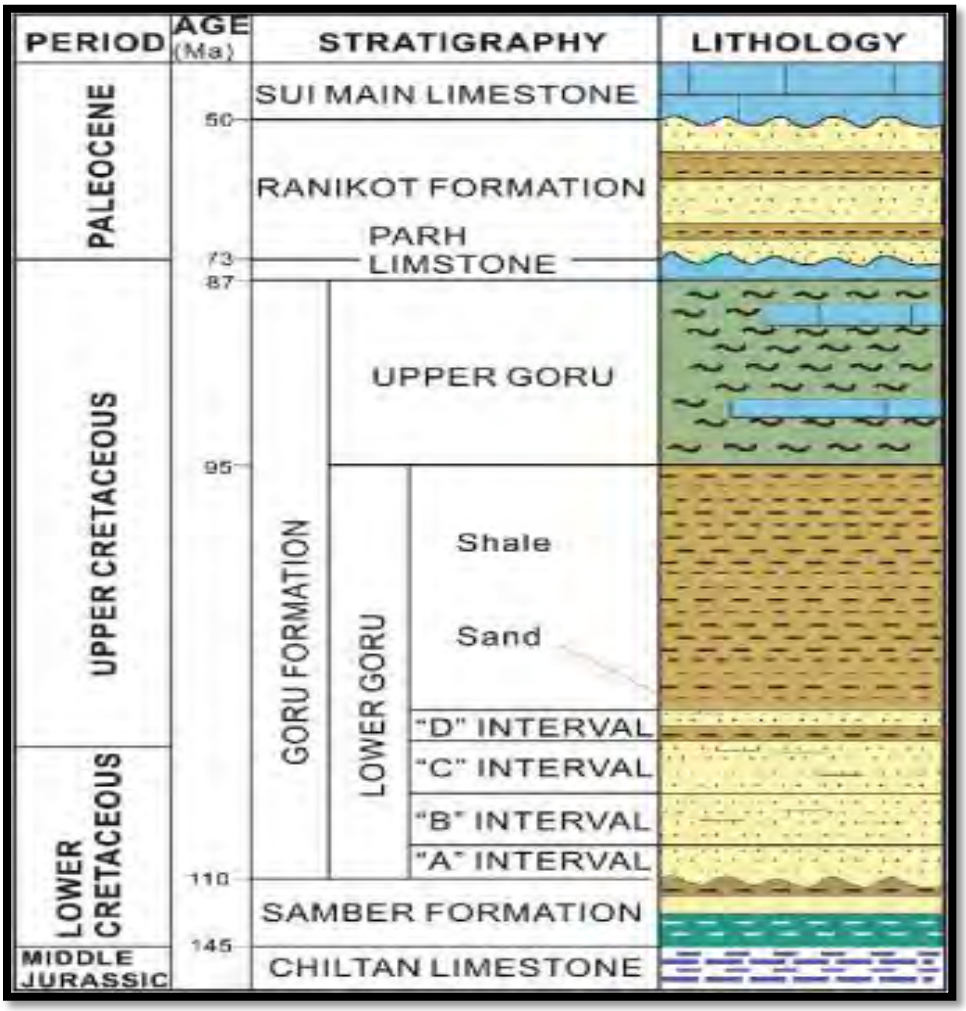

Figure 2.3: Stratigraphic column of Study Area (Krois et al., 1998)

2.3 Sedimentation Environment

The lower Goru C- interval in the research area is formed by LST dominated by waves. The dominant facies are the coastal barrier sands with secondary structural elements such as channel filling sediments. The high seismic amplitude which can be easily read from the 3D seismic data at low acoustic impedance shows a good quality reservoir sand. Stratigraphically, up dip low level wedge LST shows reservoir grade sands that can be found in the Miano, Kadanwari and Sawan fields. (Afzal et al., 2009).

CHAPTER 3

SEISMIC INTERPRETATION

3.1 Introduction

Seismic Interpretation is a sequence to transform a seismic information into subsurface geological picture to find a structural or stratigraphic traps for hydrocarbon accretion (Hubbard, 2008). Mapping of such promising structures helps to drill a new location (Barclay et al., 2007). Three dimensional (3D) seismic interpretation act as a key tool and offer many benefits to seismic exploration regarding interpreting subsurface features. In seismic exploration subsurface horizons were picked and then transferred to other lines for investigation (Bacon et al., 2007). 3D seismic is a very commanding tool in seismic delineating hydrocarbon over whole 3D cube bearing zones (Tonnies, 2006; Admasu, 2006). Stratigraphic and structural interpretations provide very useful information about presence of hydrocarbons (Coffeen, 1978).

By interpreting seismic data we will capable to infer the sub-surface geological structural analysis like faults, folds, horizons and stratigraphic analysis (seismic stratigraphy). All these struggles are prepared to examine the subsurface for some definite motives like for fresh-ground water deposits, minerals and hydrocarbons examination. On the basis of seismic data interpretation structural analysis and stratigraphic analysis can be made.

3.2 Data Utilized

The 3D seismic cube of Sawan area ranges from in-lines (520-910) and cross-lines (870-1020). The well Sawan-07 lies on the in-line number 792. The seismic data is given in SEG-Y layout while well data is given in LAS layout.

3.3 Methodology

Generalized methodology that has been followed to frame out the structural and stratigraphic style of study area shown in Figure 3.1. Base map is prepared with the help of primary information include navigation data, SEGY and well data. Horizons and faults were marked manually on software. The grids are generated after picking faults and horizons. Time and depth

contour maps of marked horizons are generated to show the geometry of chosen reflection events.

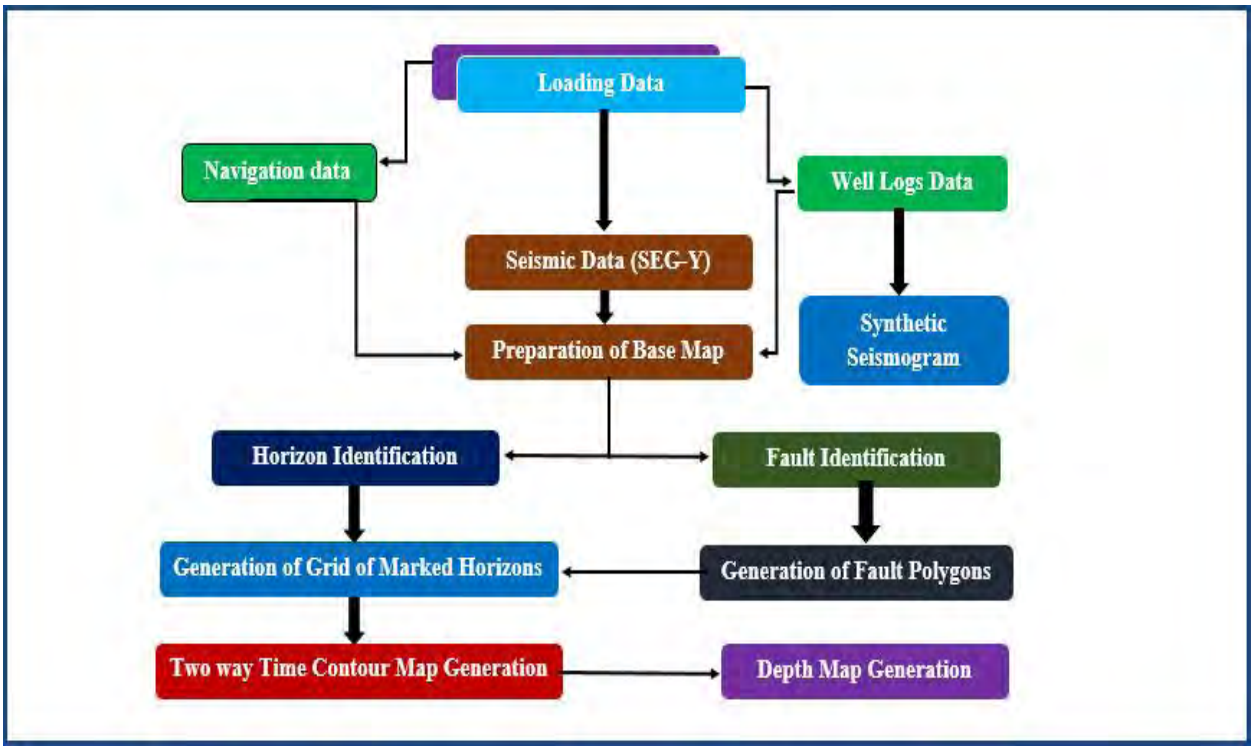

Figure: 3.1 Generalized workflow adopted for interpretation of Study area.

3.4 Synthetic Seismogram

Synthetic seismogram is the correlation of lithological variation within the subsurface and reflectors on seismic profiles. It forms a link between seismic data and subsurface geology by altering a rock properties in terms of impedance into synthetic traces. It is one of the imperative tool for seismic interpretation. In fact, to get more exact result, the seismic data is tied with synthetic seismogram and correlated with well tops (Bacon et al. 2007). Synthetic seismogram plays a fundamental role in forward modeling generated with the help of DT and density log. The velocity is obtained from sonic log and density is obtained from density logs there product results in acoustic impedance. The impedance is convolved with wavelet (extracted) to get synthetic trace. This trace is matched with original trace. Seismic events are tied with formation

tops with the help of synthetic seismogram. Synthetic seismogram is constructed at Sawan-07 well location as shown in Figure 3.2.

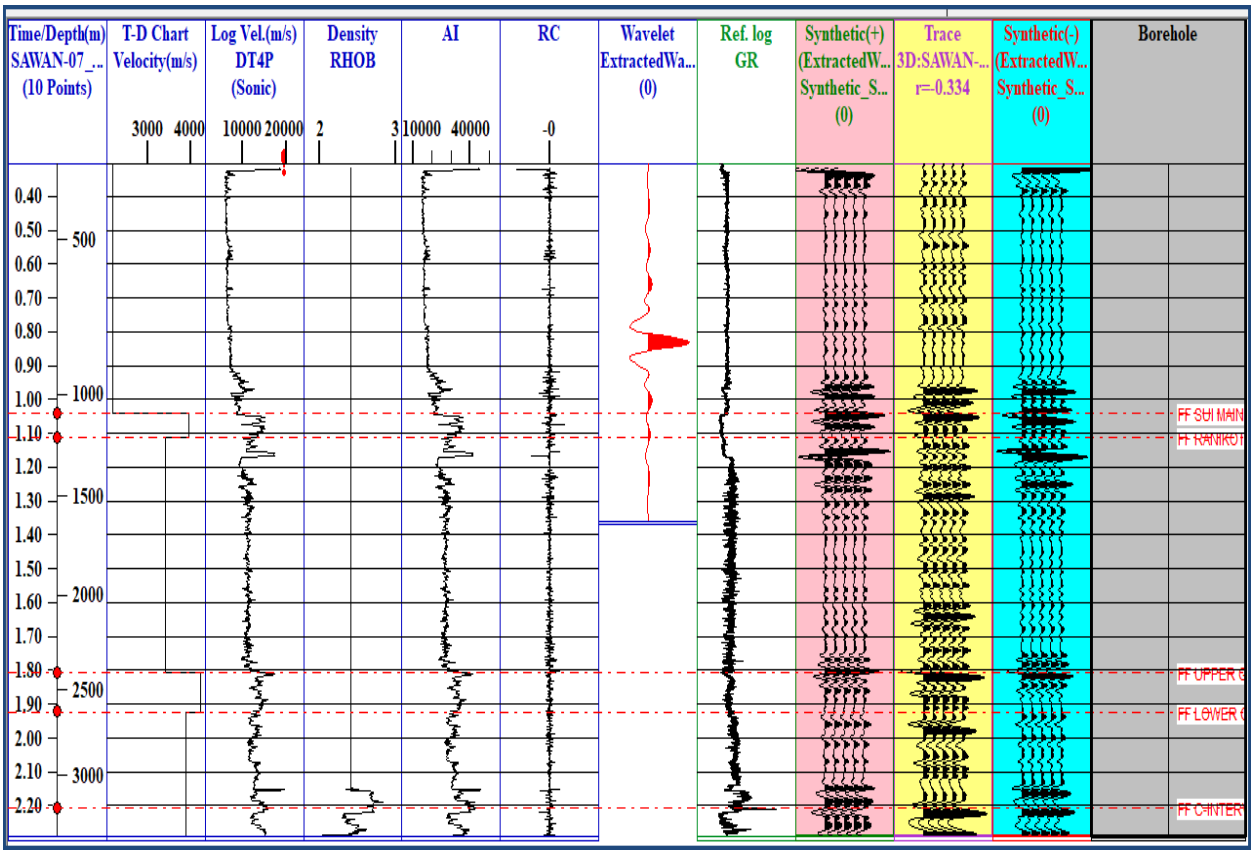

Figure 3.2: Synthetic Seismogram of well Sawan-07

3.5 Horizon and Fault Marking

Seismic horizons are distinct as vertical discontinuities of subsurface formations (Badley, 1987). Horizons are important to mark as we are required to grid and contour our structure, so we can mark different horizons based on synthetic seismogram which we earlier generated. Synthetic wiggle has been created and shown at Sawan-07 well location. On the basis of synthetic seismogram and prominent reflection amplitude of each horizon, two horizons were marked namely Lower Goru and C-Interval (main reservoir) shown in Figure 3.3.

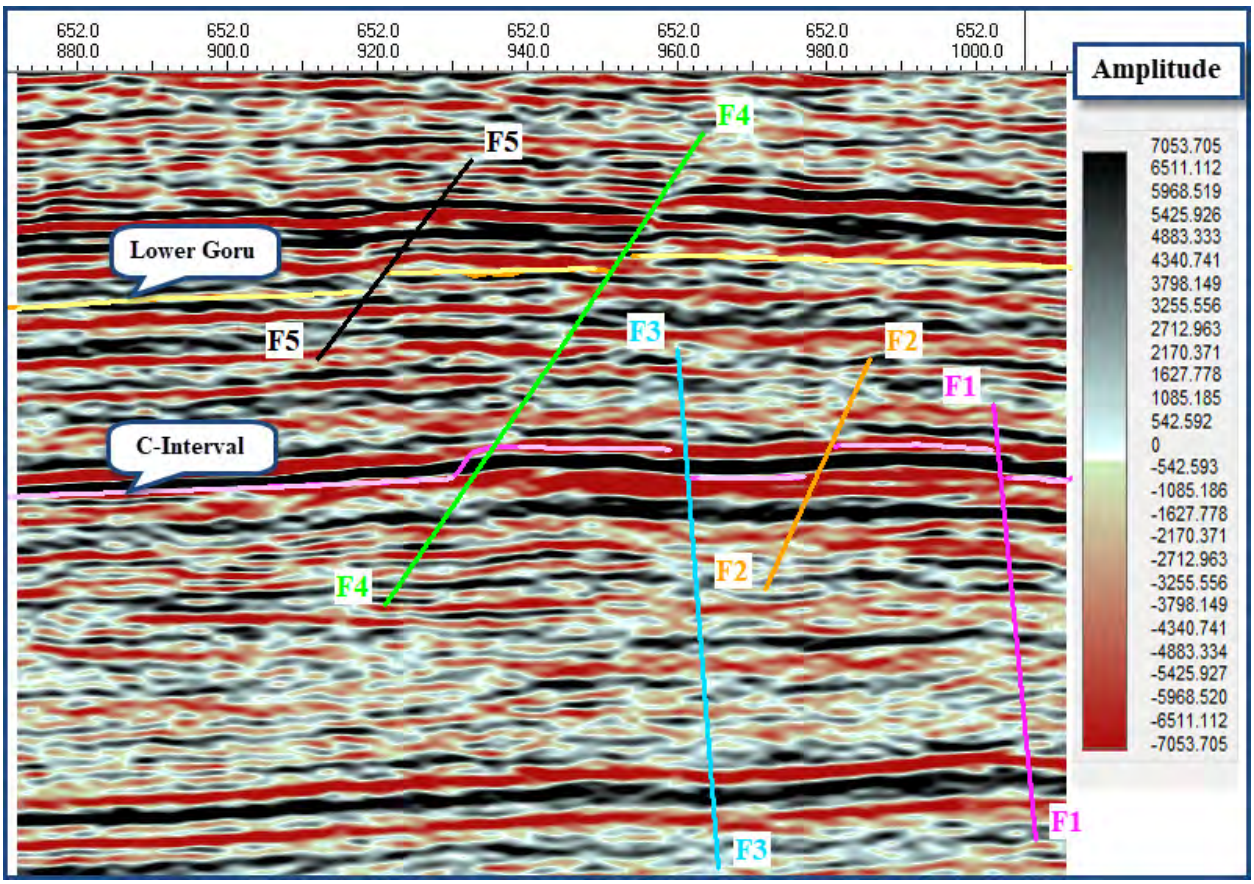

Figure 3.3: Horizon and fault marking of Inline-652

Faults are marked where there is amplitude decay, change in the position of the reflectors, distortion or vanishing of the reflection. Faults were acknowledged and marked at inline location on the base of low amplitude and discontinuities of seismic reflections.

3.6 Contour Maps

The final outputs of all the seismic exploration are the contour maps, time or depth. The mapping is one of the most vital part of the data interpretation on which whole operations depends upon. Contours are lines which join the point of the same values (Coffeen, 1986). Contours represent the three-dimensional earth surface into the two-dimensional earth surface. These contour maps signify the structural relief of the formation, any faulting and folding including dip of the strata.

3.6.1 Time Contour Maps

Two way time maps are made at different levels which depicts the formation subsurface trend on the basis of time variations ranges from 1.871-2.264 sec. In this study, time map is constructed forC-Interval and Lower Goru.

Time structure map of Lower Goru is shown in Figure 3.4 and Time contour map of C-Interval sand is shown in Figure 3.5. In a western side, formation become shallow because formation shale out and forms a up dip stratigraphic traps in a westward direction. Due to outward bulging phenomenon at Sawan central part, formation become deep in NE direction as a result of formation of depocentre. Value of time increases means graben structures and horst structures form where time is decreases.

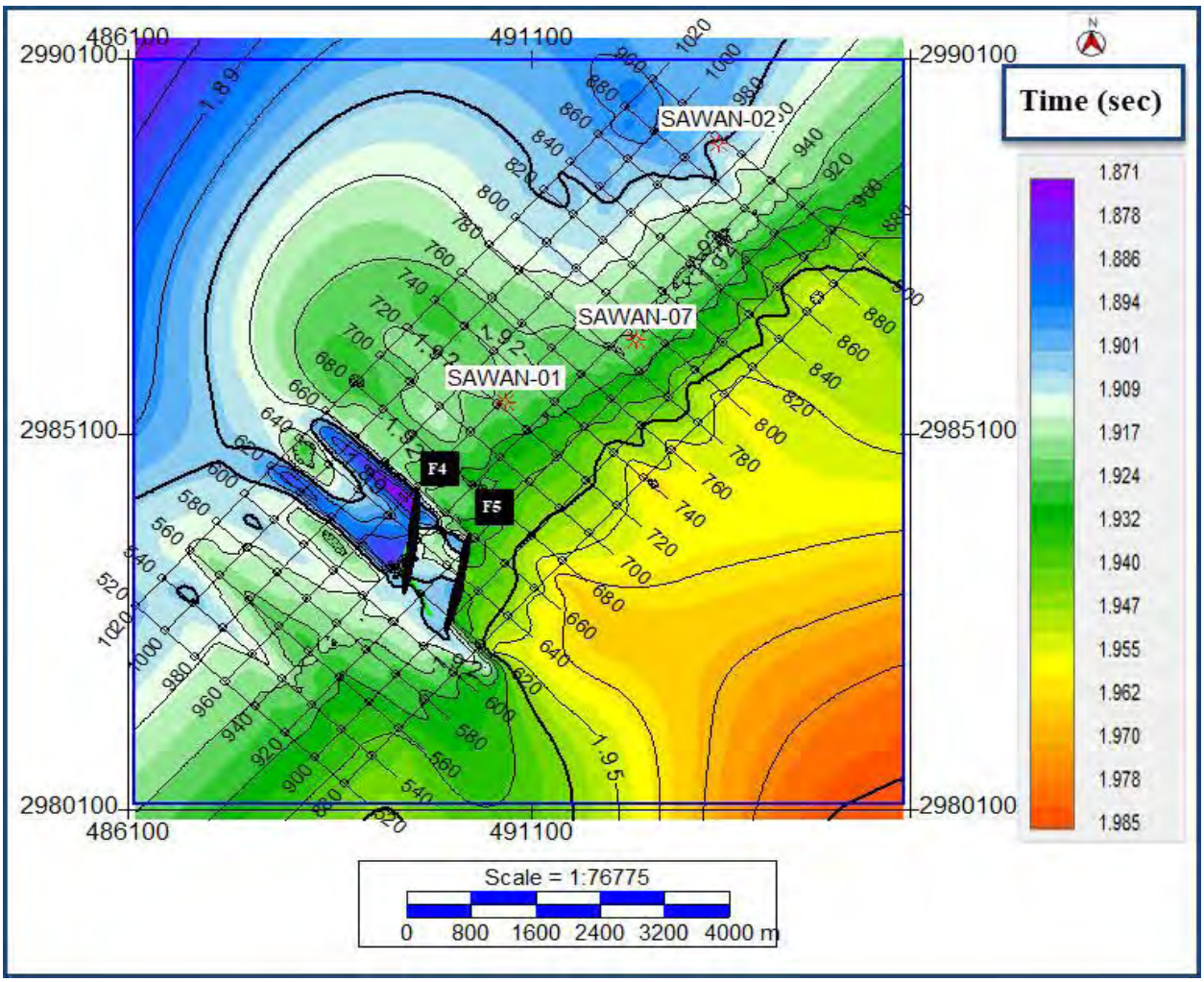

Figure 3.4: Time Contour Map of Lower-Goru

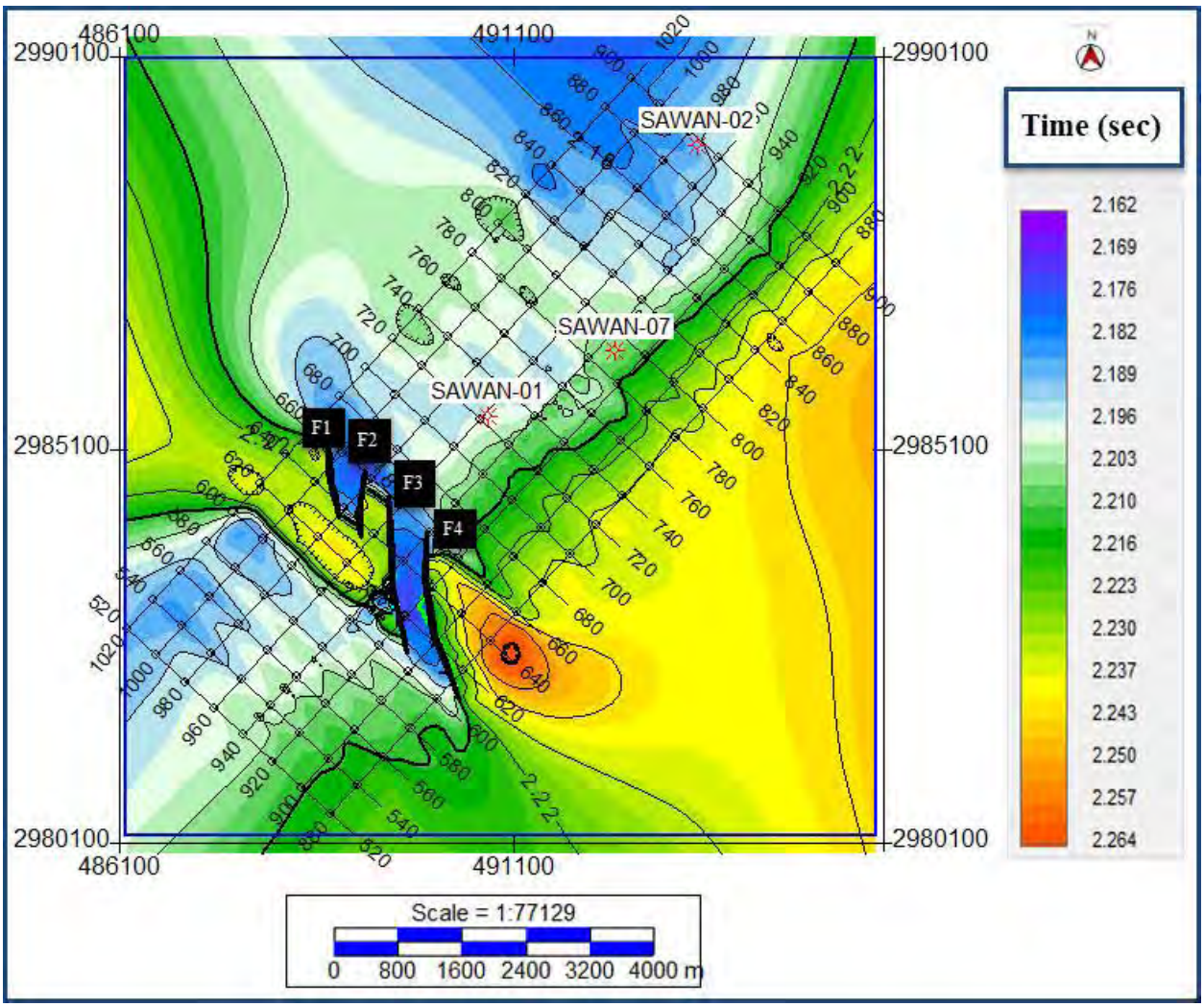

Figure 3.5: Time Contour Map of C-Interval

3.6.2 Depth Contour Maps

Two way depth maps are made at different levels which shows the position of that formation in depth. In this study, depth maps are constructed for Lower Goru and C-Inteval. Depth contour maps shows the different colors on which low values of depth are associated with shallow levels which represents horst blocks. High values of depth are associated with deeper level which represents graben. Depth contour maps of Lower Goru is shown in Figure 3.6 and of C-Interval is shown in Figure 3.7.

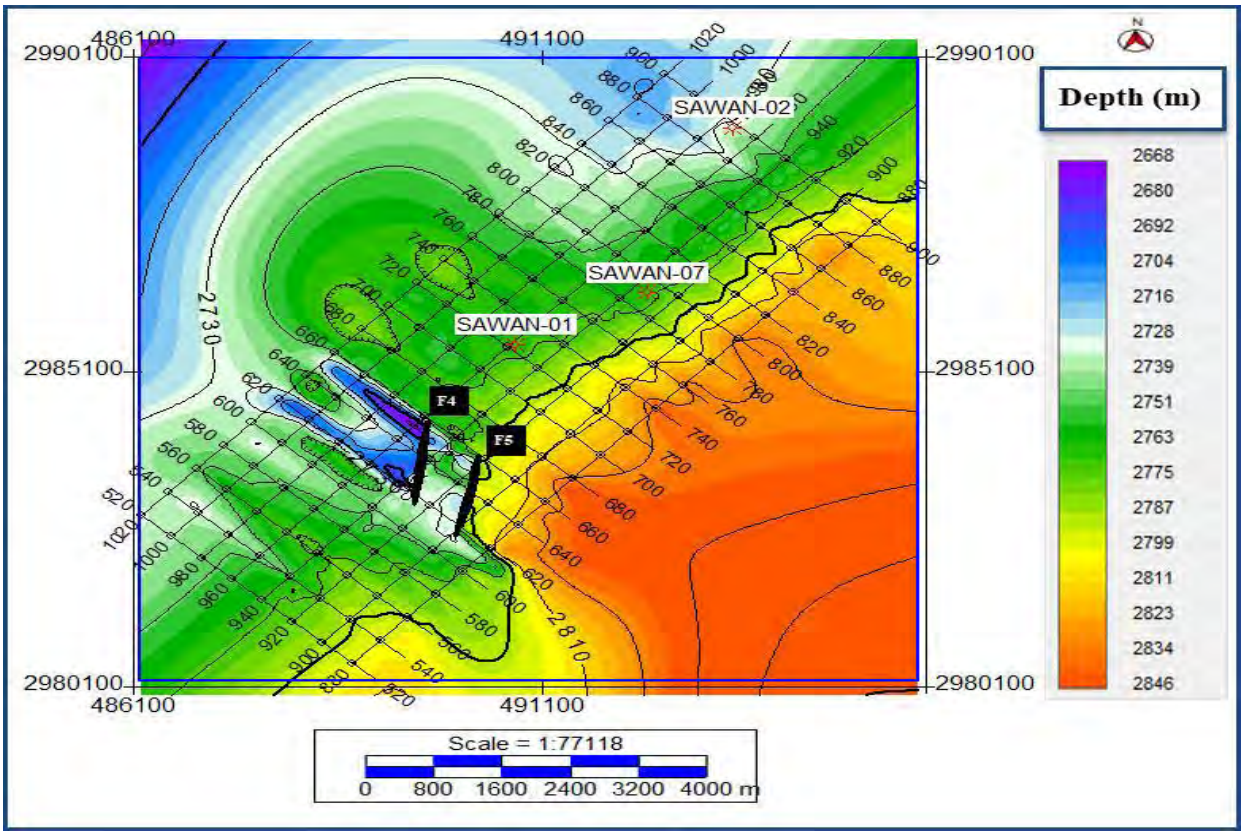

Figure 3.6: Depth Contour Map of Lower Goru

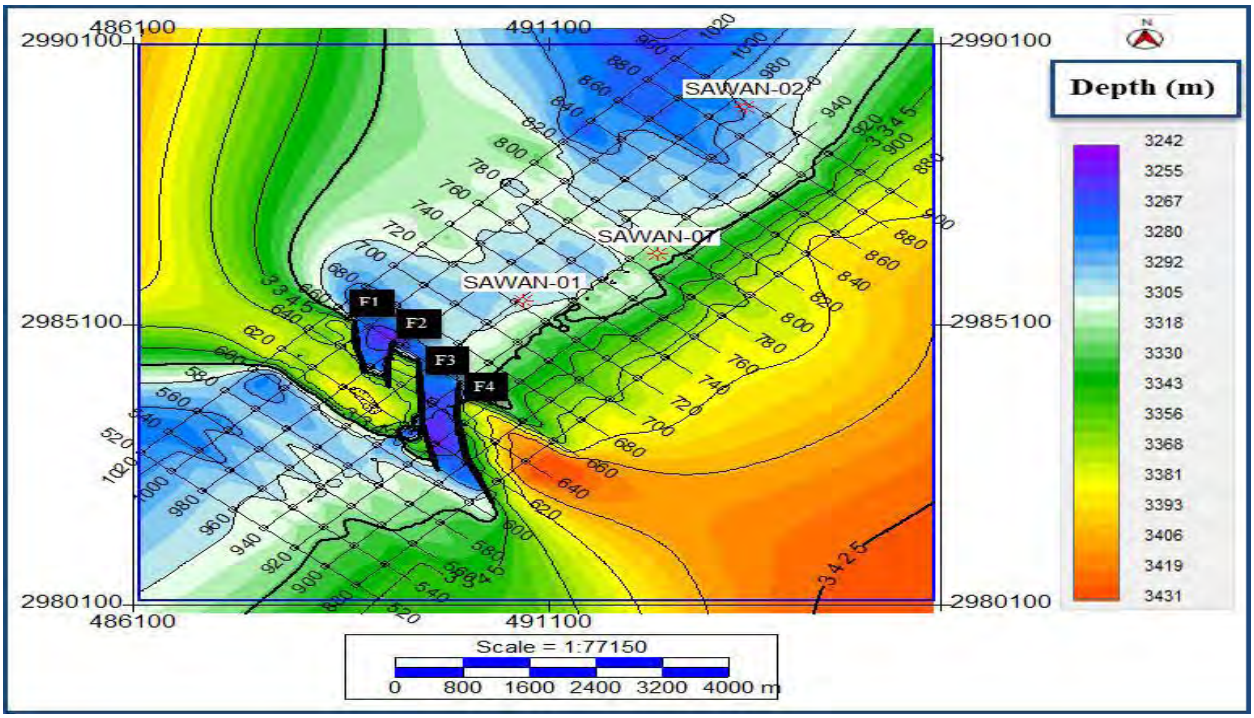

Figure 3.7: Depth Contour Map of C-Interval

Both time and depth contour maps shows variation on both sides of fault polygon and tells the changes in time and depth across faults. In graben structures, value of time and depth is increases but on horst, both time and depth decreases relative to the graben structures.

CHAPTER 4

PETROPHYSICAL ANALYSIS

4.1 Introduction

Petrophysical analysis gives a deep insight of fluid, its identification and quantification in reservoir rocks (Ali et al., 2013). Petrophysical analysis centered on the well log which is continuous record of any geophysical parameter against the depth in the well bore (Rider, 1996). Basically well logs are used to confirm the lithologies and fluid presence in rock. The purpose of Petrophysical analysis is to measure the different rock properties and also their connections to the fluids (Donaldson and Taib, 2004). The potential prospect and non-prospect zones are identified by integrating Petrophysical results with rock physics which authorizes geoscientists to extract essential results. The description of reservoir is done on the basis of Petrophysical results (Daniel, 2003).

There are lot of newly established geophysical well logs be present. Geophysical logs made up of highly focused tools are most well-known among others because of their structure. These logs can be run before casing of well without delay after drilling which is called as Measurement While Drilling (MWD) and also at the time of formation drilling called as Logging While Drilling (LWD). Usually, the deviation of directional well are determined by MWD logs and log type measurements such as resistivity, density and others are done by LWD (Rider, 1996).

4.2 Methodology

Treasured extracted information through log data help to identification of reservoir, separation of payable reservoir zone by applying a constraint on rock properties and volumetric reserve estimation. Petrophysical studies has been accomplished for the classification of reservoir properties of Sawan area. Well logs data of Sawan-07 has been utilized to assess the different formations. Parameters are projected using logs data are shale-volume, density-porosity, effective-porosity, total-porosity, water saturation and hydrocarbon saturation. Wireline log data comprises Gamma ray log (GR), Calliper log, Spontaneous log (SP), Laterolog deep (LLD), Laterolog Shallow (LLS), Micro spherically focused log (MFSL). Neutron-Log (NPHI), Density Log (RHOB) and Sonic Log (DT), Wireline logs placed into three different tracks on the basis of

reservoir properties approximation and working principle shown in Figure 4.1. First track is known as lithology track, second track is known as resistivity track and third track is known as porosity track.

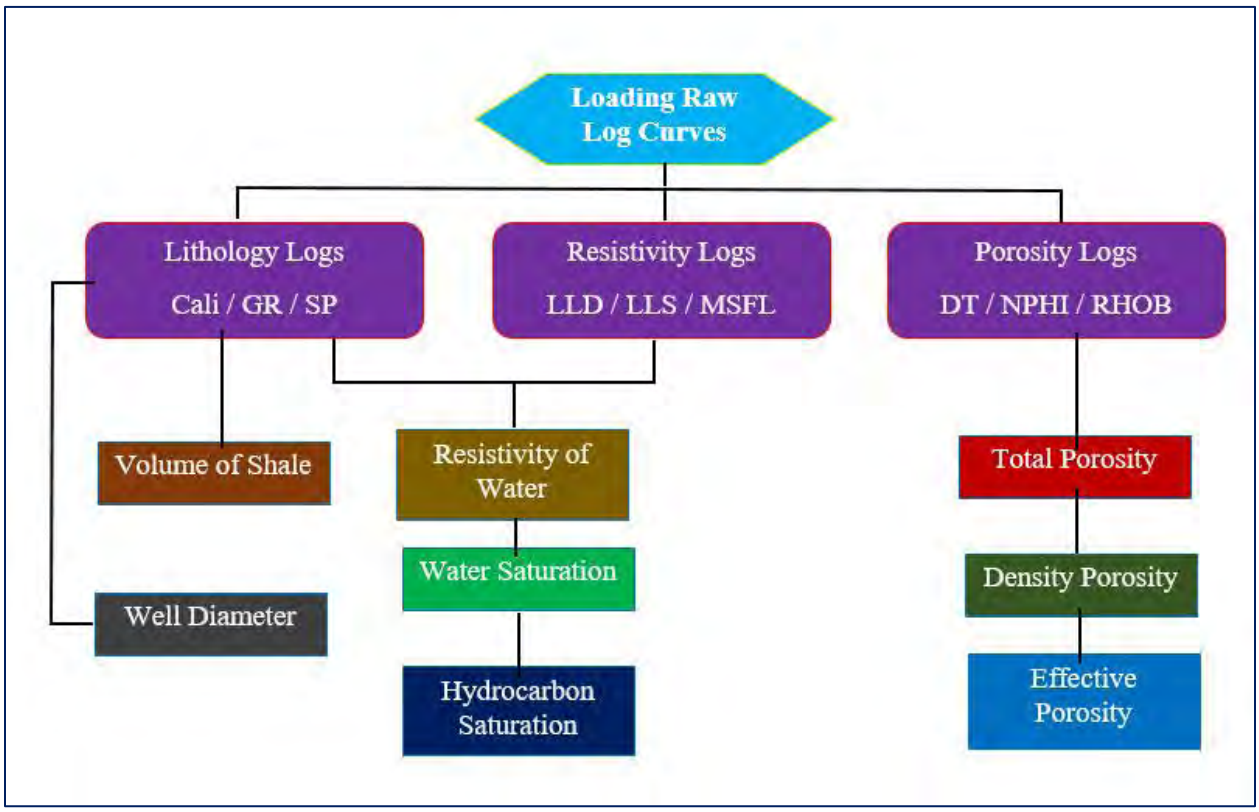

Figure 4.1: Generalized methodology workflow for Petrophysical analysis.

4.3 Objective

The Petrophysical analysis has been carried out in order to measure the reservoir description of the Sawan area using the borehole data of Sawan-07 well. The logs defined above will be used in order to calculate the reservoir parameter such as:

- Volume of shale (Vsh)
- Porosities (PHID, PHIT, PHIE)
- Water Saturation (Sw)
- Hydrocarbon Saturation (H.C)
- Net Pay or Net Reservoir

4.4 Volume of Shale

We have two methods:

- **Linear method**

  In linear method we compute Index Gamma Ray by following formula:

$$IGR = \frac{\text{GR log} - GR\ min}{\text{GR max} - GR\ min}, \tag{4.1}$$

Where, IGR is Index Gamma Ray. GR log is the recorded values of GR, GR min is minimum value of GR log, GR max is maximum value of GR.

IGR can give us maximum volume of shale and we must find minimum volume shale by non-linear method.

- **Non Linear Method**

In non-linear method we have various formulas like Stabier, Larinov and Clavier to compute minimum volume of shale. We apply the one which give us minimum volume of shale. And mostly Stabier give us minimum volume of shale.

- **Stabier:** (Most preferable)

$$Vsh = \frac{\text{IGR}}{3 - 2\ \text{IGR}}, \tag{4.2}$$

Where, IGR=Index Gamma Ray, Vsh is Volume of Shale

- **Larinov:** (Used for older age rocks)

$$\text{Vshale.} = 0.330 \times (2^{2 * \text{IGR}} - 1.0). \tag{4.3}$$

- **Clavier:**

$$\text{Vsh..} = 1.70 - (3.380 - (\text{IGR} + 0.70)^2)^{1/2}. \tag{4.4}$$

4.5 Porosity

In the next step, we have to calculate porosity parameters, like

- Density Porosity
- Sonic Porosity

- Total Porosity
- Effective Porosity
- Neutron Porosity (Given)

4.5.1 Density Porosity

Density-Log is the porosity-log that measure electron-density of the formation (Asquith et al., 2004). Formation electron density is related to bulks density of formation. It is the sum of fluid density multiplies its relative volume plus matrix density time relative volume.
Density-log can be applied to find out the accurate porosity of the formation, if we can identify matrix densities in formation or type of rock (Asquith et al., 2004).

$$\boldsymbol{RHOB}\ \phi = \frac{\textbf{RHOB mat} - \textbf{RHOB log}}{\textbf{RHOB mat} - \textbf{RHOB fluid}}, \tag{4.5}$$

Where $RHOB\ \phi$ is the density porosity, $RHOB\ log$ is density log, *RHOB mat* is value of matrix density, *RHOB fluid* is density of fluid. The value of *RHOB mat* given in the literature is 2.65 g/cm^3, which is for sandstone and *RHOB fluid* is 1 g/cm^3.

4.5.2 Sonic Porosity

Sonic-Logs measure the intermission transit time (Δt) of the compressional sound-wave through the formation. The interval transit time is linked to the formation Porosity. The unit of measure is the microseconds per foot or microseconds per meter (Asquith et al., 2004). Porosity of the formation can be calculated by using the following formula:

$$\boldsymbol{\phi s} = \frac{\textbf{ΔTlog} - \textbf{ΔTmatrix}}{\textbf{ΔTfluid} - \textbf{ΔTmatrix}}, \tag{4.6}$$

Where ϕs represents the sonic porosity, ΔTmatrix is the interval transient time of the matrix, ΔTlog interval transient time of formation, represents the transient time of the fluid (salt mud=185 and fresh mud=189).the interval transient time of the formation depends upon the matrix material, its shape and cementation (Wyllie et al , 1956).If fluid (hydrocarbon or water) is present in the formation, transient interval time is increases and this behavior shows increase in porosity which can be calculated by using sonic log (Asquith et al , 2004).

4.5.3 Total Porosity

Sum of the porosities that are attained from the unalike logs divided by porosity calculated number of logs. Here C-Interval is reservoir for which the average porosity is premeditated, to zone of interest reservoir, all the logs are deduced. The relation is given below through which average porosity is calculated:

$$\phi avg = \frac{\phi n + \phi d + \phi s}{3}, \quad (4.7)$$

Where, ϕavg is the average porosity calculated from the available porosities, ϕn is the neutron porosity, ϕd is the density porosity and ϕs is the sonic porosity.

4.5.4 Effective Porosity

This will define as "the ratio of the volume of interconnected pore spaces in a rock unit to the total volume of the rock by removing shale effect that rock unit". The zone rich in the shale, effective porosity will be zero there. Effective porosity is used to mark the saturated zone. The effective porosity can be calculated by the following formula (Asquith et al, 2004).

$$\phi e = \phi avg \times (1 - Vsh) \quad (4.8)$$

Where ϕe is effective porosity which is to be calculated, ϕavg represent the average porosity and Vsh represent volume of the shale.

4.5.5 Neutron Porosity

Neutron-Log is sensitive to the Hydrogen-atoms present in a formation and determination of the porosity of a formation. Count-rate will be small in high porosity rocks and vice-versa. Neutron porosity is given in the data and calculated by well log with respect to depth.

4.6 Water Saturation (Sw)

Water-saturation in the formation can be described as "The percentage of the pore volume filled by water in the formation". Different models are used for water saturation such as Archie's equation, Indonesian and Dual water based on the lithology. For a clean sand Archie's equation (4.12) gives an accurate result. Indonesian equation is used for dirty formation. Thin interbedded shale sequences degrade the quality of C-Interval sand. So, water saturation is estimated through Indonesian equation (4.9).

$$SW_{\text{Indonesia}} = \left\{ \frac{\sqrt{\frac{1}{Rt}}}{\left(\frac{Vsh^{(1-0.5Vsh)}}{\sqrt{Rsh}}\right) + \sqrt{\frac{\phi_e^m}{a.Rw}}} \right\}^{(2/n)} \quad (4.9)$$

Where, *SW* is a water-saturation. *Rt* is a formation true resistivity, *Vsh* is shale-volume, *Rsh* is a resistivity of shale, ϕe is Effective-porosity, *Rw* is water resistivity value, *m* is a cementation factor and '*a*' is tortuosity factor.

4.7 Resistivity of Water (Rw)

Calculation of resistivity of water (Rw) is key for water saturation. Numerous factors like bottom hole temperature (BHT), surface-temperature, salinity of water in ppm and SP (Static) are important for valuation of water resistivity (Rw) (Amigun et al., 2012).

Two methods has been applied for resistivity of water:

- SP Method
- Pickett cross plot Method

4.7.1 SP Method

In this method, we must have borehole temperature and resistivity of mud filtrate.

$$\mathbf{Ssp} = -\mathbf{K} * \mathbf{log}\left(\frac{\mathbf{Rmf}}{\mathbf{Rw}}\right), \quad (4.10)$$

For K:

$$K=65+0.24*T°C \quad (4.11)$$

We can find value of SSP from *Sp log* curve as SSP is the maximum deflection towards negative side, and *Rmf* is given resistivity of mud filtrate.

So then saturation of water in the formation can be calculated by the following Archie equation:

$$\mathbf{S_w} = \sqrt[\mathbf{n}]{\frac{\mathbf{F \times R_w}}{\mathbf{R_t}}}, \quad (4.12)$$

Where, F is formation factor which is

$$\mathbf{F} = \frac{\mathbf{a}}{\mathbf{\emptyset^m}}, \quad (4.13)$$

Here, Rw is the resistivity of water calculated from above equation (4.10), Rt is the true formation resistivity, n is the saturation exponent, a is the constant, in case of sand represents effective porosity, m is the cementation factor and it value is taken 2.15 for the sandstone.

4.7.2 Pickett Cross Plot Method

The Pickett-Crossplot (pickett, 1972) is unique, easiest and most operative technique. This procedure not only provides evaluations of saturation of water but can also aid to conclude water formation Resistivity (Rw), cementation factor (m) and matrix constraints for porosity logs. The Pickett methods is founded on the observation that true resistivity Rt is a function of three considerations porosity, water saturation (Sw), and Cementation Factor (m). A Pickett Cross Plot is established by plotting logarithmic porosity (PHIA) values with logarithmic deep resistivity (ResD) values on two-by-three cycle log-log paper. Pickett Cross Plot comprises of number of water saturation lines in which lowest or left-most line shows water bearing line with 100% saturation. Data point's lies above this straight line (Ro) represent water saturation less than 100%. Slope of straight line represent cementation factor (m) water bearing line. We have plotted it as shown in Figure 4.2. Water bearing lines represents the Archie relationship as an under:

$$\textbf{Resistivity of Water } (R_o) = \frac{\textbf{Resistivity of Water}}{\textbf{Porosity}} \qquad (4.14)$$

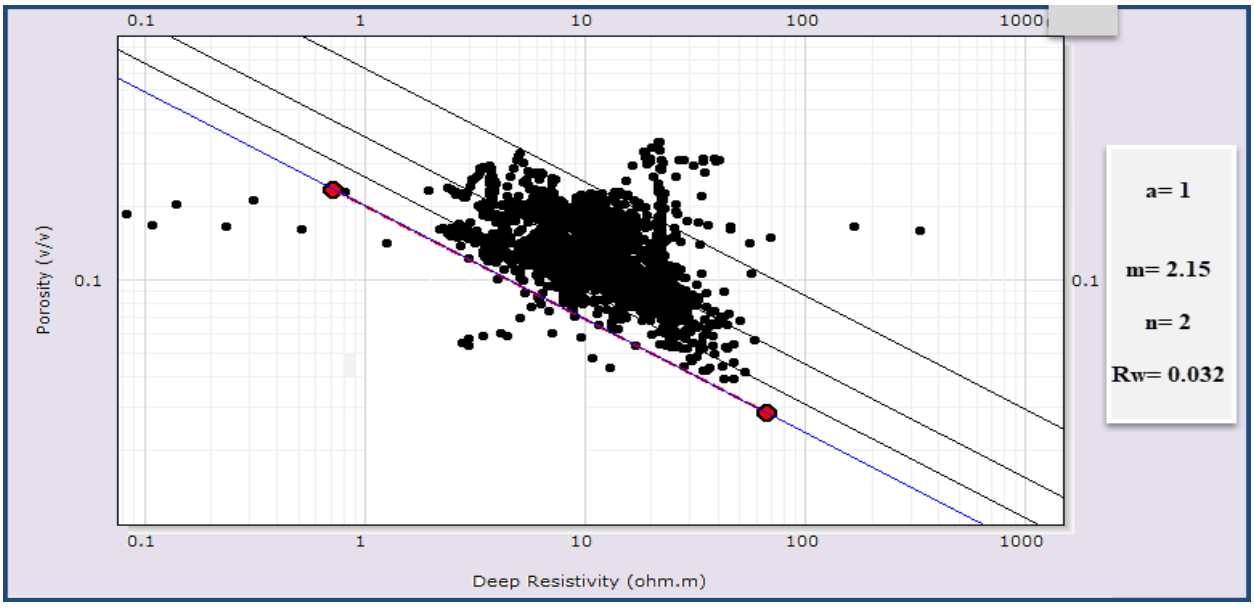

Figure 4.2: Pickett Cross Plot for Rw of Sawan-07

4.8 Hydrocarbon Saturation

Hydrocarbon saturation can be defined as “the pore in formation is filled with hydrocarbon”. It can be designed by using the following mathematical relation:

$$S_{Hydrocarbon} = 1 - S_{Water} \quad (4.15)$$

Where $S_{Hydrocarbon}$ represent hydrocarbon saturation and S_{Water} represent Water-saturation.

4.9 Well Log Interpretation of Sawan-01

Lower Goru formation encountered in sawan-01 well assessed as most prolific sands for hydrocarbon exploration. Two zones of interest, A and B has been marked on the basis of separation between LLD and LLS, large cross over between neutron porosity and density and low volume of shale as shown in Figure 4.3. The calculated Petrophysical results of zone-A listed in Tables 4.1 suggested that Lower Goru formation dominated by clean sand with high effective porosity.The depth of zone-A ranges from 3252-3318 m.

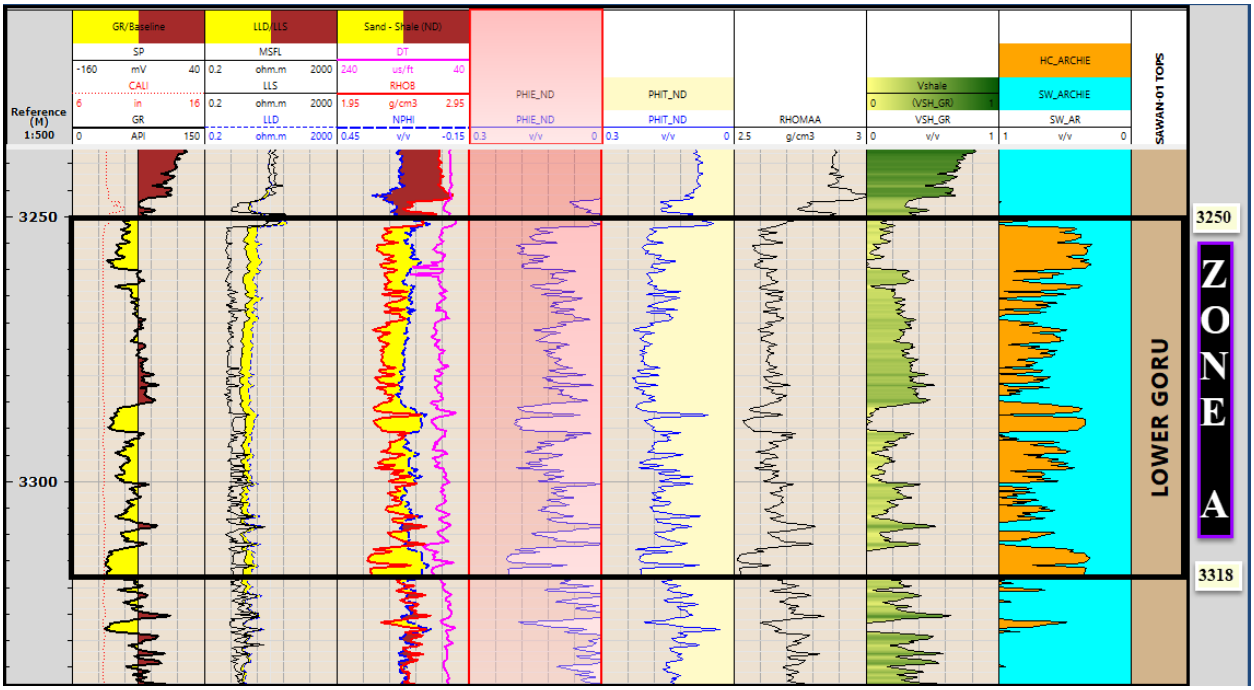

Figure 4.3: Well log plot of Sawan-01

Table 4.1 Petro physical analysis results of zone-A Sawan-01

Serial Number	Calculation Parameter	Percentage
1	Average Volume of Shale = **Vsh**	20 %
2	Average Porosity in (PHIT) Percentage = ϕ_{avg}	17.3 %
3	Average Effective Porosity in Percentage = ϕ_{eavg}	11.4 %
4	Average water Saturation in Percentage = S_{Wavg}	66 %
5	Average Hydrocarbon in Percentage = S_{Havg}	34 %

4.10 Well Log Interpretation of Sawan-02

Lower Goru formation faced in sawan-02 well evaluated as most productive sands for hydrocarbon exploration. On the basis of Petro-physical logs there are two zones in well Sawan-02 (Figure 4.4) having thickness range from 3279-3307 m for zone-A and 3355-3369 m for zone-B. Clean sandy patches in both zones having calculated results in below table 4.2 and table 4.3.

Table 4.2 Petro physical analysis results of zone-A Sawan-02

Serial Number	Calculation Parameter	Percentage
1	Average Volume of Shale = **Vsh**	19.3 %
2	Average Porosity in (PHIT) Percentage = ϕ_{avg}	16.4 %
3	Average Effective Porosity in Percentage = ϕ_{eavg}	12 %
4	Average water Saturation in Percentage = S_{Wavg}	67.6 %
5	Average Hydrocarbon in Percentage = S_{Havg}	32.4 %

Table 4.3 Petro physical analysis results of zone-B Sawan-02

Serial Number	Calculation Parameter	Percentage
1	Average Volume of Shale = **Vsh**	21.7 %
2	Average Porosity in (PHIT) Percentage = ϕ_{avg}	10.7 %
3	Average Effective Porosity in Percentage = ϕ_{eavg}	6.1 %
4	Average water Saturation in Percentage = S_{Wavg}	76 %
5	Average Hydrocarbon in Percentage = S_{Havg}	24 %

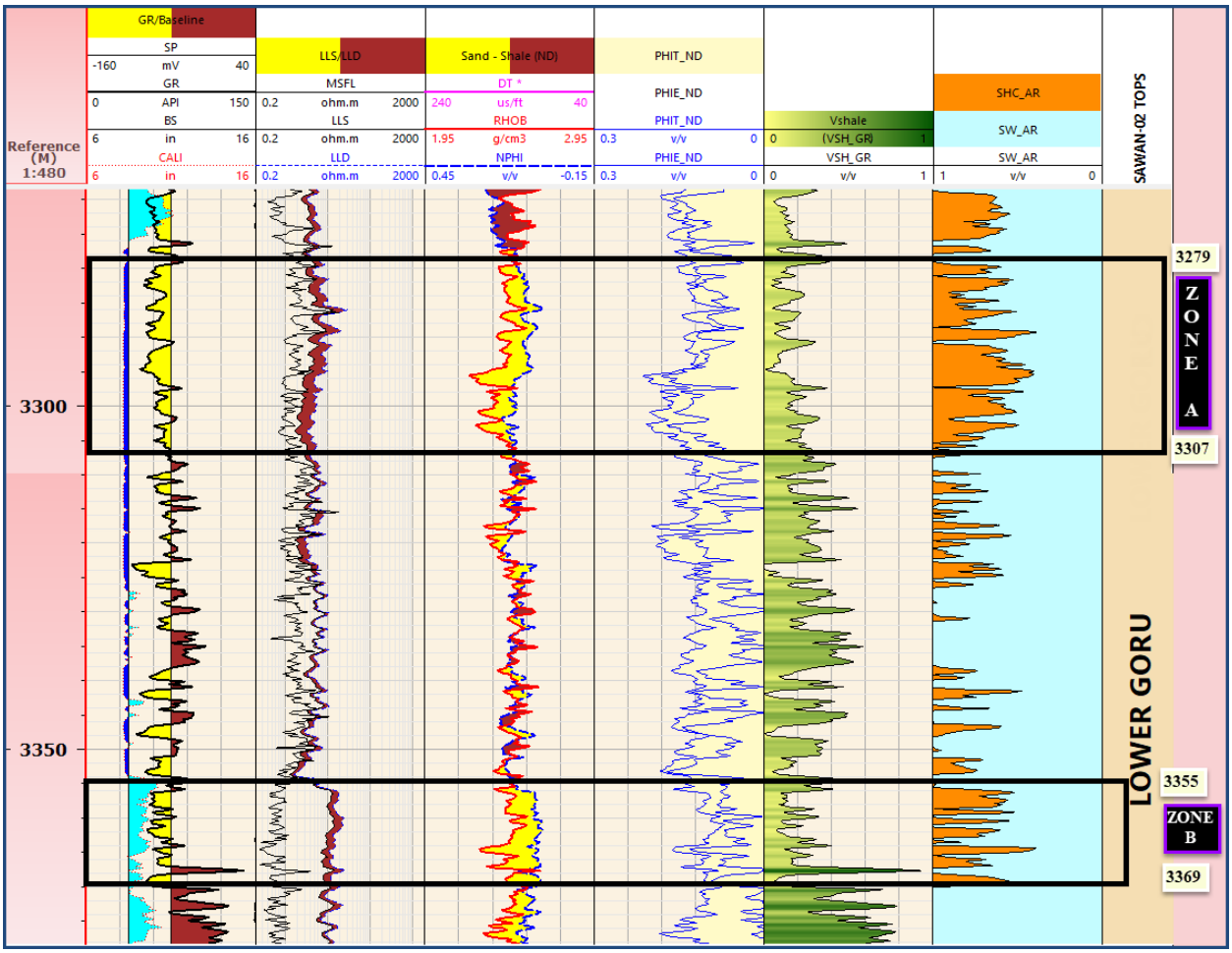

Figure 4.4: Well log plot of Sawan-02

4.11 Well Log Interpretation of Sawan-07

On the basis of log response thickest zone in Lower Goru formation of Sawan-07 marked from depth 3269 to 3335, thickness of 66 meter. As clearly shown in Figure 4.5, there is GR log response is low caliper log is quite stable that there is no wash-outs, separation between LLS and LLD and cross over between NPHI and RHOB which indicates the presence of hydrocarbon in greater amount. Total and effective porosities are good enough and water saturation is decreases in marked zone of Lower Goru. Zone of interest Petro physically analyzed which is shown in Figure 4.6 and results are tabulated in 4.4.

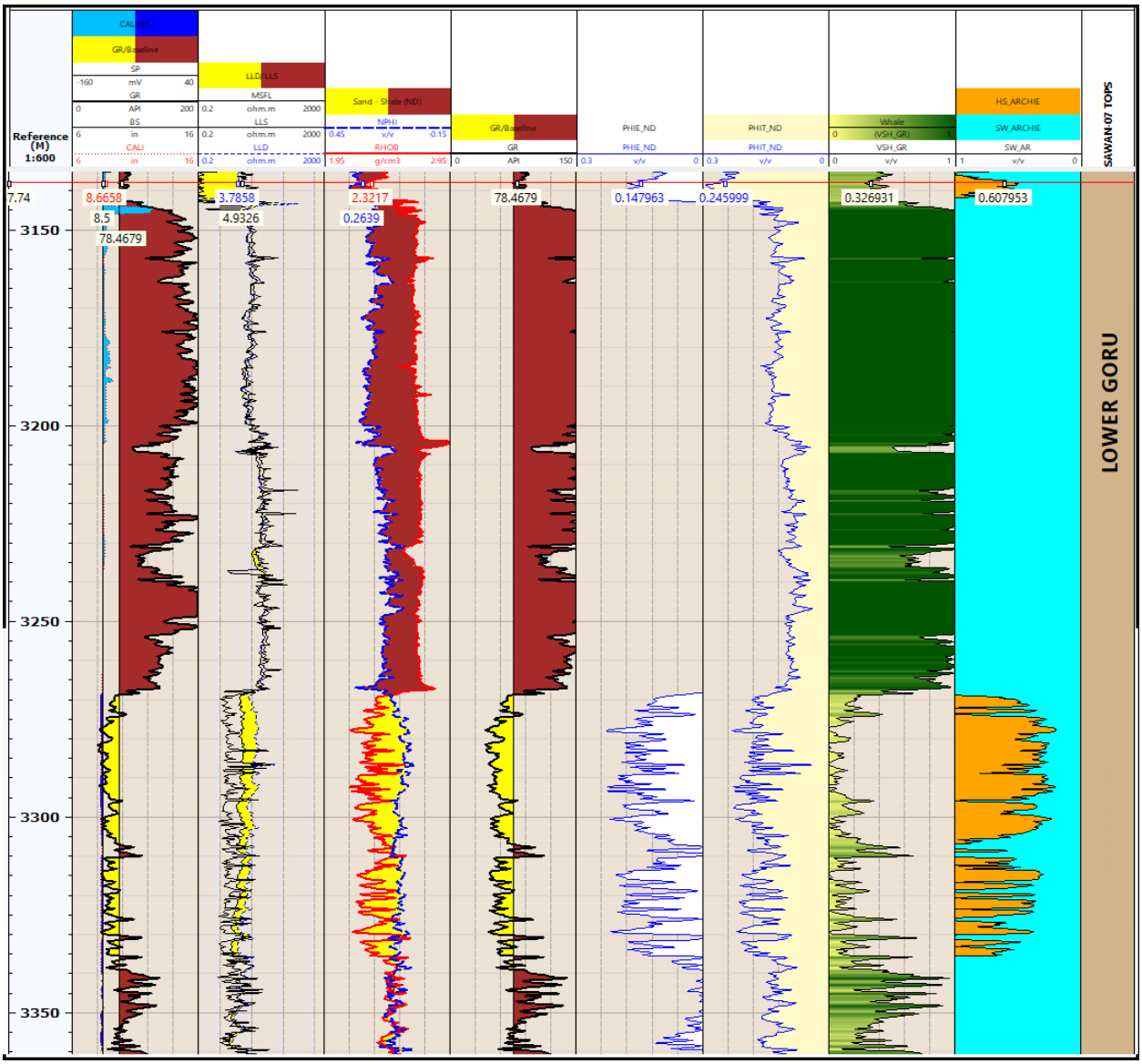

Figure 4.5: Well logs Interpretation of well Sawan-07

Reservoir zone using Well Log Interpretation of Sawan-07

Reservoir zone is marked which is about 66 m thick having clean sand. Water saturation is 52% and rock physics and AVO is interpreted using Sawan-07. Reservoir zone is shown in Figure 4.6 below.

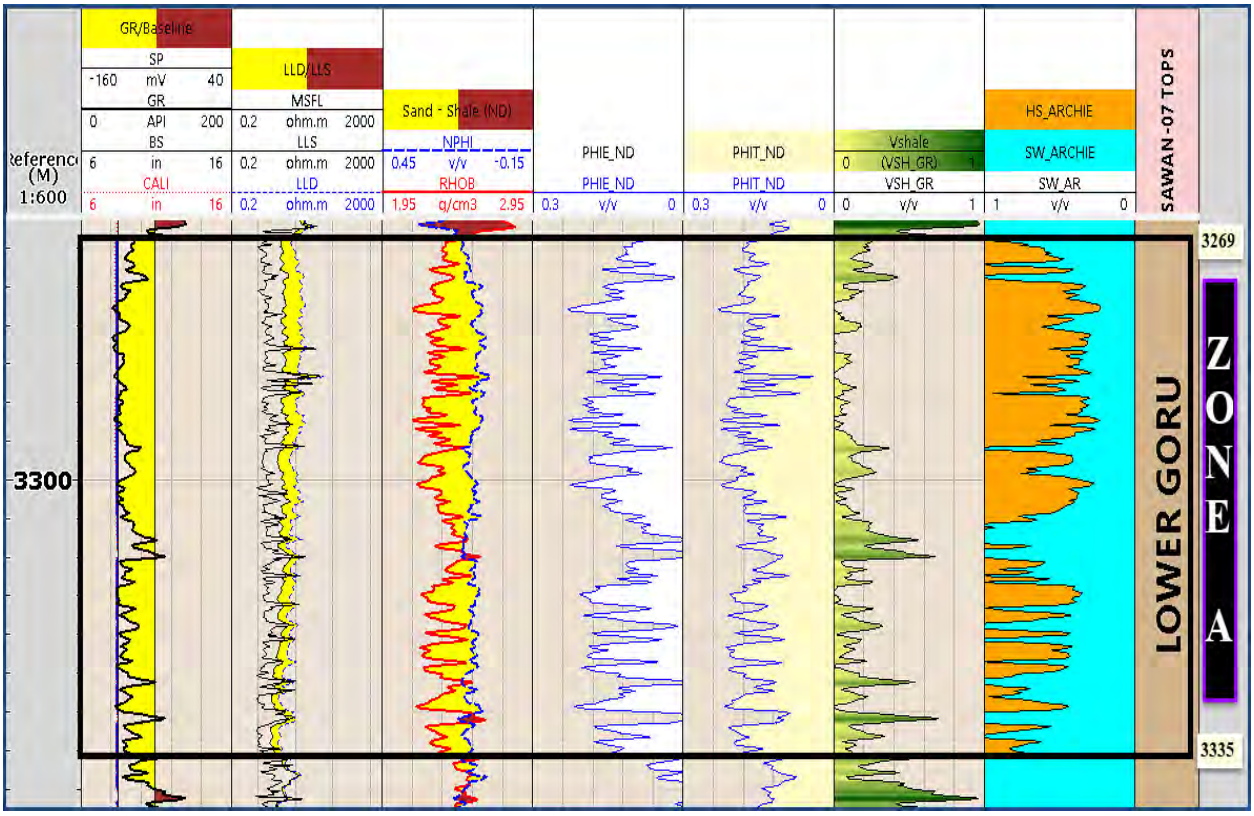

Figure 4.6: Reservoir zone using well logs Interpretation of well Sawan-07

Table 4.4 Petro physical analysis results of zone-A Sawan-07

Serial Number	Calculation Parameter	Percentage
1	Average Volume of Shale = **Vsh**	14.5 %
2	Average Porosity in (PHIT) Percentage = ϕ_{avg}	16.6 %
3	Average Effective Porosity in Percentage = ϕ_{eavg}	12.5 %

4	Average water Saturation in Percentage = $\mathbf{S_{Wavg}}$	52 %
5	Average Hydrocarbon in Percentage = $\mathbf{S_{Havg}}$	48 %

CHAPTER 5

ROCK PHYSICS MODELLING

5.1 Introduction

The purpose of Rock physics is to connect the physical rock properties with the elastic properties of that rock and is the foundation of quantitative seismic interpretation. It has possibly given exploration geophysicists a solid quantifiable basis to their interpretation of seismic data. It plays an essential role as an effective interpretational tool since it connects the fluid with lithology and geological setting of the subsurface zone of interest. RPM is primarily defined in terms of template which provides effective characteristic determination of any reservoir (Andersen and Wijngaarden, 2007; Avseth et al., 2007)

RPM may be developed by taking a single input variable like porosity, or could be functioned to entertain multiple parameters such as content of clay, porosity, saturation of water, saturation of hydrocarbon. The RMPs for fractured lithologies may involve fracture aperture, fracture density and other such parameters as input variable. Although labs and well data are relatively high resolution and therefore have a less chance of being erroneous, the results still depends largely upon the complexity and accuracy with which rock heterogeneity has been incorporated into the model. Rock physical templates involve use of mathematical operations as building blocks. These operations include the physical characteristics of the earth layer in terms of porosity, content of clay and saturation of water being mathematically utilized in terms of logs e.g. GR, NPHI and LLD.

Rocks can be clarified completely by volume fraction, geometric shapes and of components, spatial distributions of constitutes and the properties of distinct component of composite at micro scale. Rocks are heterogeneous at microscopic scale but deliberated as homogenous at macroscopic scales because physical parameters are controlled by average of microscopic parameters. In rock physics, rocks are considered as statistically homogenous i.e. heterogeneous at micro-scale and homogenous at macro-scale. Postulation of statistically homogeneity of rock lets to define the physical properties of medium in term of effective properties (Mavko et al., 2009).

Rock Physics is essentially the connection between reservoir properties and seismic, because it labels the reservoir rock by porosity, rigidity and compressibility etc. When wave travels through medium it will affected by these properties directly. Rock physics is the up-scalar for seismic because it permits interpreter to consider the rock properties with seismic horizon, so that to compute the reservoir properties at seismic horizons.

5.2 Workflow for Rock Physics Modelling

The theme of rock physics is to establish an analytical theory for the detection of properties on seismic. For developing rock physics theory, knowledge about elastic properties of dry rock and pore fluid is required to develop the rock fluid interaction model. A generalized flow chart for Rock physics modeling is shown below in Figure 4.1. Petro physical properties are input for the rock physics modeling.

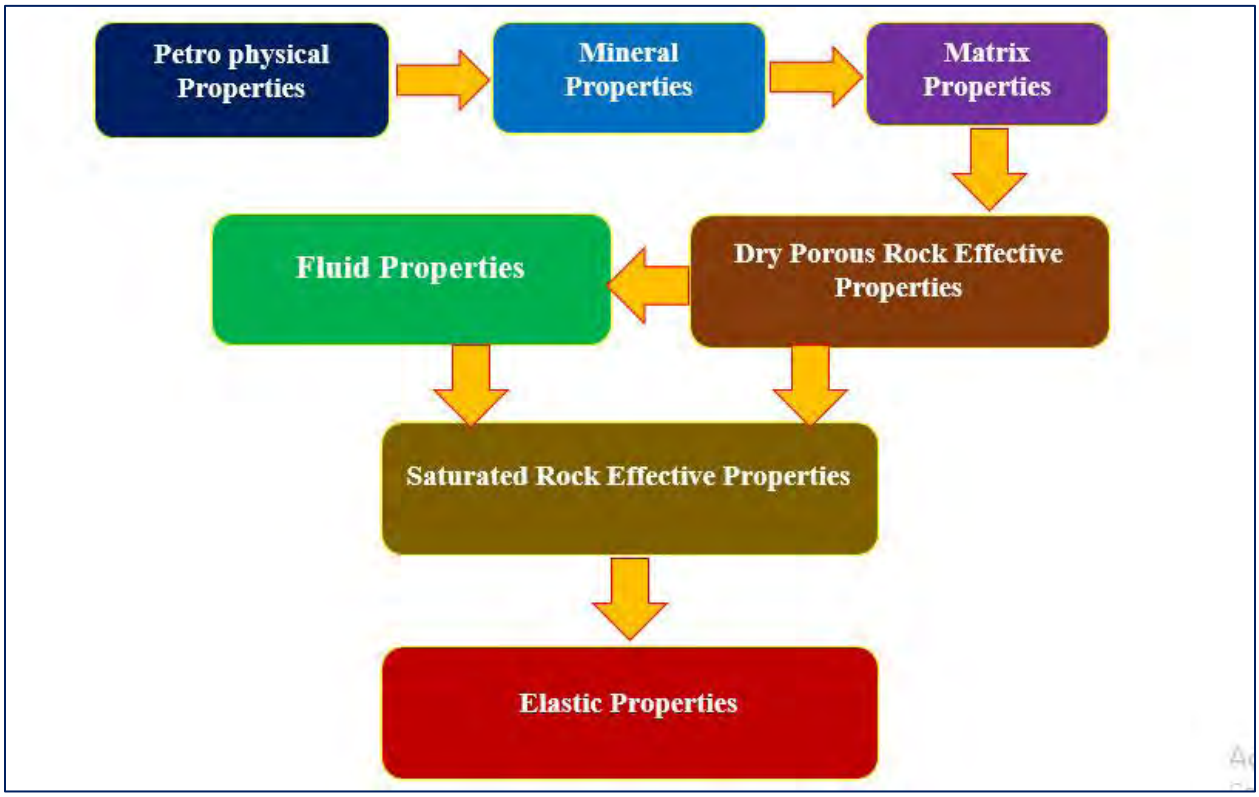

Figure 5.1: Generalized workflow of Rock Physics Modelling for elastic Properties.

5.3 Petrophysical Properties

Petrophysical properties includes porosities, water saturation, hydrocarbon saturation, Volume of shale and densities, calculated already in last chapter.

5.4 Mineral Properties

Density, bulk and shear modulus of mineral are obtained from literature. In our zone of interest, clean layer of sand (quartz) is present and its values from literature are blow.

Table 5.1: Matrix Mineral Properties

Mineral Properties	Value
Bulk Modulus	37 GPa
Shear Modulus	44 Gpa
Density	2.65 g/cm^3

5.5 Matrix Properties

Matrix Properties incorporated rock without pores. If single lithology is dominated in reservoir than mineral properties are identical to matrix properties. If two or more lithologies are present in reservoir than Voigt Reuss Hill mixing technique can be used to calculate the matrix properties.

5.6 Dry Porous Rock Effective Properties

Most important step is of manipulating dry porous rock properties which should be consistent with the real reservoir scenario i.e. sandstone contain spherical pores and micro-cracks and limestone having fractures, these parameters incorporate in dry porous rock properties. There are several approaches which are used to calculate dry porous properties like Inverse Gassmann, NIA approach, T-matrix, Hudson, Backus Averaging etc. In this study we used Inverse Gassmann, NIA and T-matrix.

The statistically homogeneity of rock permits to label the physical properties of medium in term of effective properties. Effective properties are introduced by replacing real discontinuous medium by effective continuous medium. There are numerous approaches available such as T-matrix approach (Jakobsen et al, 2003), Differential Effective Medium theory (Hornby et al.,

1994; Bruggeman, 1935) and Self Consistent approach (Berryman, 1980; Homby et al., 1996) that can be used according to suitable assumptions.

Hook's law improved for the effective clastic medium by leading effective stiffness tensor C or reciprocal of it effective compliance tensor S* (Hornby et al., 1994). Thus, Hooke's law can be written as:

$$\bar{\boldsymbol{\sigma}} = \mathbf{C}^* \bar{\boldsymbol{\varepsilon}} \,, \tag{5.1}$$

$$\bar{\boldsymbol{\varepsilon}} = \mathbf{S}^* \bar{\boldsymbol{\sigma}} \,, \tag{5.2}$$

5.6.1 T-matrix Inclusion Model

T-matrix approach is the most general, modern and suitable for the rock physics applications. T-matrix inclusion model is one approach of estimating effective elastic properties based on quantum scattering theory. T-matrix approach accounts interaction of different cavities on the basis of multiple point correlation function. (Jakobsen et al., 2009) using T-matrix to renew most of existing effective medium approximations.

In T-matrix approach, a statistical homogeneous medium of background stiffness tensor $\mathbf{C_o}$ of having different types of cavities. These inclusions are fragmented into families' r= 1, 2, 3...N, of having shape $a^{(r)}$ and volume fraction $v^{(r)}$. Inclusion of any shape from spherical pores to ellipsoidal shape cavity or even fracture can be modeled through aspect ratio $a^{(r)}$. The general theory of T-matrix not restricted to ellipsoidal shape cavities. (Jakobsen et al. 2009) gives effective elastic stiffness is:

$$\boldsymbol{C^* = C_O + C_1 : (I_4 + C_1^{-1} : C_2)^{-1}} \,, \tag{5.3}$$

Where:

$$\boldsymbol{C_1 = \sum_{r=1}^{N} V^{(r)} t^{(r)}} \,, \tag{5.4}$$

$$\boldsymbol{C_2 = \sum_{r=1}^{N} \sum_{s=1}^{N} V^{(r)} t^{(r)} : G_d^{(rs)} : v^{(s)} t^{(s)}} \,, \tag{5.5}$$

I_4 = Fourth rank identify tensor.

$G_d^{(rs)}$ = Green's tensor.

v = Volume fraction of cavities.

5.6.2 Non-Interacting Approach (NIA)

Non Interactive Approximation has been proposed and described in pronounced detail by (Kachanov et al., 1994, Kachanov 1992 and Shafiro and Kachanov, 1996). NIA was developed to extract the elastic parameters from a rock with incorporated porosity (cavities of varying length) in case of isotropic as well as anisotropic subsurface setting. The effective elastic properties of the non-interacting compliance approach (NIA) (Hornby et al., 1996) is based upon averaging process and continuum hypothesis. Macroscopic description of heterogeneous material volume that is small as compared to interest scale and large as compare to microstructure elaborated by continuum hypothesis. Physical parameters within the volume can be considered as being continuously disturbed over entire volume V.

The simplest solution of converting micro heterogeneous medium into homogencous is Non-interacting approach (NIA). NIA does not incorporate the intersection of cracks, and also neglects the interactions. NIA applied with the assumption of all pores and cracks are isolated i.e. not interacting with each other (Grechka and kachanov, 2006). NIA worked in compliance tensor domain and its equation is:

$$S^* = S_O + \sum_r v^{(r)} (S_O : C^{(r)} - I_4) : K^{(r)} , \quad (5.6)$$

Where S* is effective compliance tensor So is background compliance tensor, and r = 1,2,3...N

(Number of cavities). I_4 is the fourth rank identity tensor, $C^{(r)}$ is related with the pores and cracks and $K^{(r)}$ is known as K-Tensor of Eshelby (1957) which is mentioned by (Jakobsen and Johansen, 2005):

$$K^{(r)} = A^{(r)} : S_O , \quad (5.7)$$

Where

$$A^{(r)} = [I_4 - G^{(r)} : (C^{(r)} - C_O)]^{-1} , \quad (5.8)$$

For dry rock, NIA equation will become by taken out the stiffness parameter.

$$S^* = S_O + \sum_{r=1}^{N} V^{(r)} : K^{(r)} , \quad (5.9)$$

5.7 Fluid Properties

Fluid properties can be assessed by using Voigt, Wood's or Brie equations depending upon the saturation type i.e. for patchy saturation Brie equation can be used for obtaining better results and in case of homogeneous saturation of fluids, the pore fluid properties are locally signified by those of an effective fluid and then Wood's equation can be used to calculate the effective fluid (Unigeo, 2013). We used Wood's equation of homogeneous material to compute Bulk modulus of Pore fluid.

5.7.1 Wood's Equation

Bulk modulus of the mixed pore fluid phase is estimated by utilizing Wood's Equation (kumar, 2006; Mavko et al., 2009). It requires fluid properties.

$$\frac{1}{k_f} = \frac{S_W}{K_w} + \frac{S_O}{K_O} + \frac{S_g}{K_g} \ , \tag{5.10}$$

Table 5.2: Fluid Properties

Materials	*K (GPa)*	*μ (GPa)*	*ρ (g/cm³)*
Water	2.2	0	1.035
Gas	0.0359	0	0.065

Here S_W is saturation of water calculated in last chapter and $(S_o = 1 - S_W)$. We are not incorporating oil in this area. Hydrocarbon is just oil that's why $\{\frac{S_O}{K_O} = 0\}$.

5.8 Saturated Rock Effective Properties

Gassmann, Krief, Wyllie and Duffy-Mindlin models are available for saturating the porous rock with previous calculated fluid properties. Parameter of **pore aspect ratio is 1** in case of sandstone. In this research, Gassmann equation has been used to calculate saturated effective properties.

5.8.1 Gassmann's Equation

The Biot-Gassmann theory (Biot, 1956; Gassmann, 1951) is frequently used to elaborate the saturated rock properties from dry rock properties at low frequencies. Because of low frequency

model, it is preferred over other models because seismic reflection method is low frequency method (Ali and Toqeer, 2017).

Assumptions

It assumes that medium is porous and isotropic and matrix and fluid are homogenous i.e. pores are connected and fully saturated. There is also assumption that fluid-rock system must be closed and fluid does not react chemically with rock (wang and Batzle, 2004, Ali and Toqeer, 2017), Gassmann's equation for the calculation of saturated rock properties is:

$$K_{sat} = K^* + \frac{\left(1 - \frac{K^*}{K_o}\right)^2}{\frac{\phi}{K_{fl}} + \frac{(1-\phi)}{K_o} - \frac{K^*}{K_o^2}}, \quad (5.11)$$

Where, ϕ for porosity, K_o defines bulk modulus of matrix, K^* is known as modulus of dry rock and K_{fl} is fluid bulk modulus.

Effective fluid density valued from equation given as:

$$\boldsymbol{\rho_{sat} = (1-\varphi)\rho_m + \varphi\rho_f} \quad (5.12)$$

Where

$$\boldsymbol{\rho_f = S_w\rho_w + S_g\ \rho_g + S_0\rho_o} \quad (5.13)$$

5.9 Elastic Properties

As we have all information needed to calculate elastic Properties (Vp and Vs). So these are calculated from the equations.

$$\boldsymbol{V_{P\_sat} = \sqrt{\frac{K_{sat} + \frac{4}{3}\mu_{sat}}{\rho_{sat}}}} \quad (5.14)$$

$$\boldsymbol{V_{S\_sat} = \sqrt{\frac{\mu_{sat}}{\rho_{sat}}}} \quad (5.15)$$

5.10 Results of Rock Physics Model

Rock physics model was constructed by considering the matrix material (sandstone), the pore shape (spherical pores) and pore fluid (water and gas). Parameter of aspect ratio is 1 in case of sandstone. Pure quartz considered as the mineral of sandstone and mineral properties are listed in table 5.1.

5.10.1 Sensitivity of Rock Physics Model with Porosity and Elastic Properties

To check the sensitivity of already build rock physics model, knowledge of parameters listed in table 5.1 and 5.2 are utilized to construct the template of porosity versus elastic properties, porosity taken on x-axis and elastic properties on y-axis. These plots are just to investigate the dependence of effective elastic properties (velocities) on porosities.

5.10.1.1 Plots of T-matrix

From figure 5.2, it is clear that P-wave velocities and S-wave velocities are sensitive to porosity and decreases with increase in porosity.

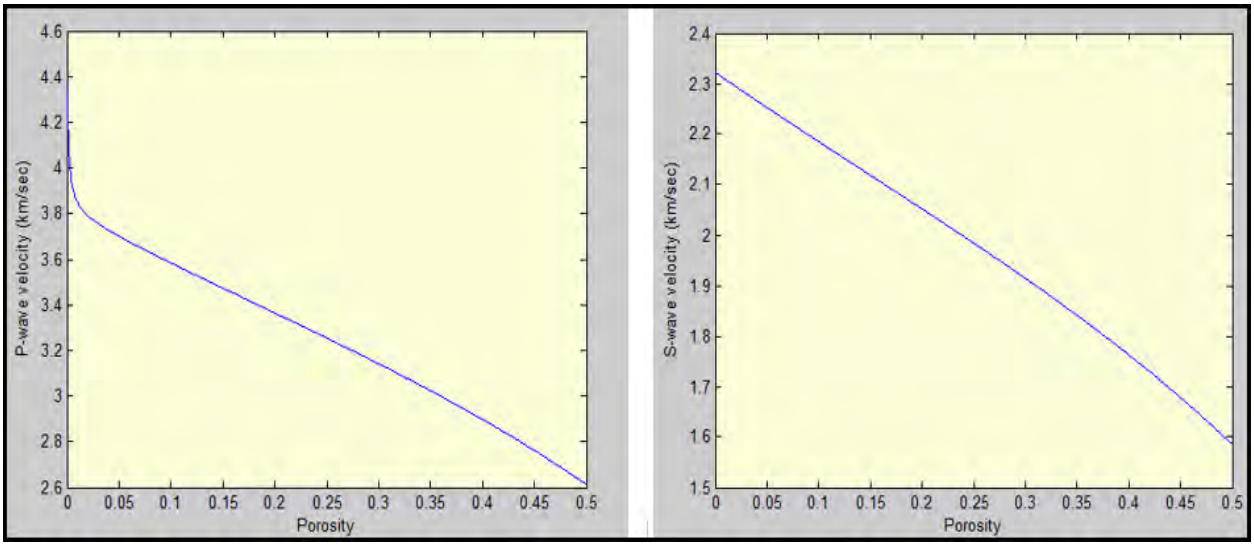

Figure 5.2: Plot of porosity against Vp and Vs for T-matrix

5.10.1.2 Plots of Non-Interacting Approach (NIA)

Figure 5.3 shows that velocities (Vp, Vs) are sensitive to porosity and porosity increases results decrease in P-wave and S-wave velocities.

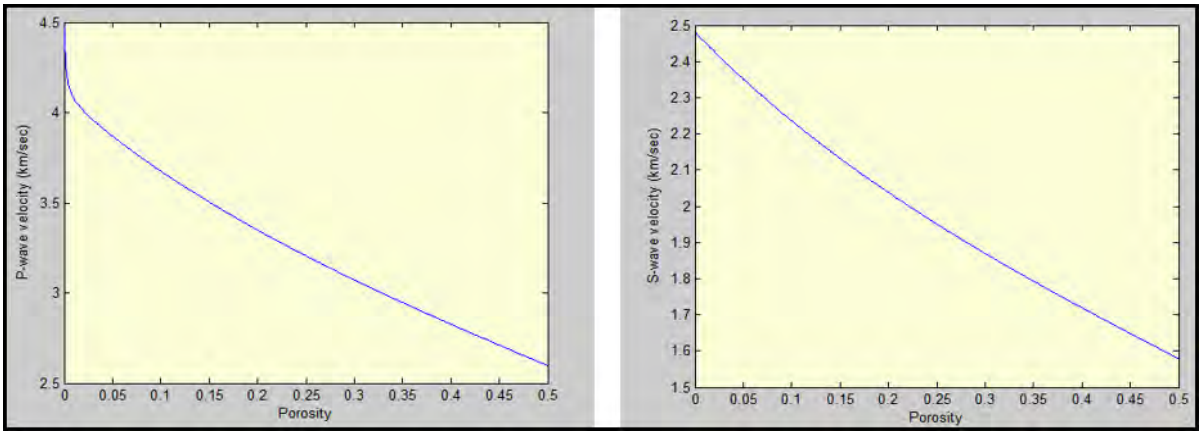

Figure 5.3: Plot of porosity against Vp and Vs for NIA

5.10.2 Sensitivity of Rock Physics Model with Saturation and Elastic Properties

To check the sensitivity of rock physics model with saturation and Velocities (Vp, Vs), template is constructed of saturation versus elastic properties, saturation taken on x-axis ranged from 0 to 1 and elastic properties on y-axis. These plots are to explore the reliance of effective elastic properties (velocities) on saturation.

5.10.2.1 Plots of T-matrix

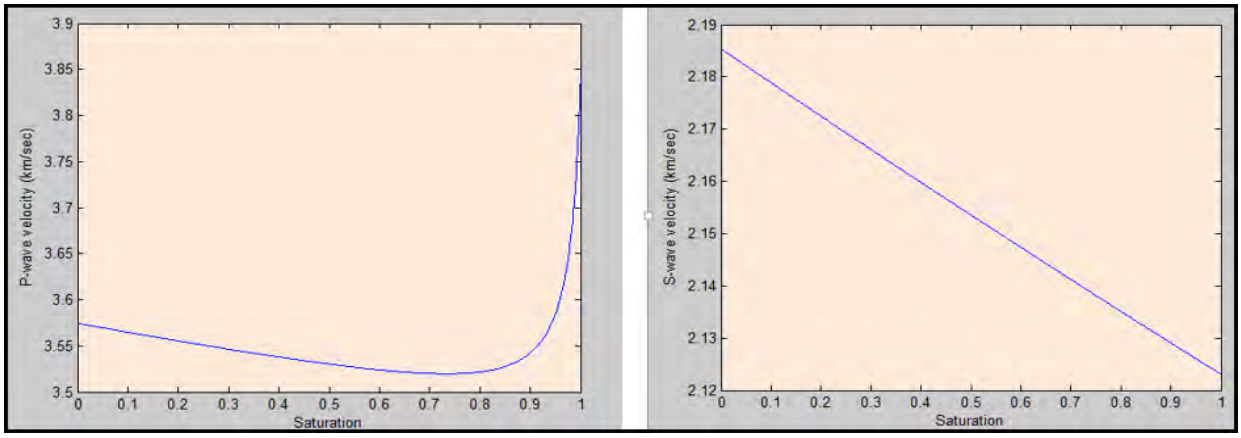

Figure 5.4: Plot of saturation against Vp and Vs for T-matrix

5.10.2.2 Plots of NIA

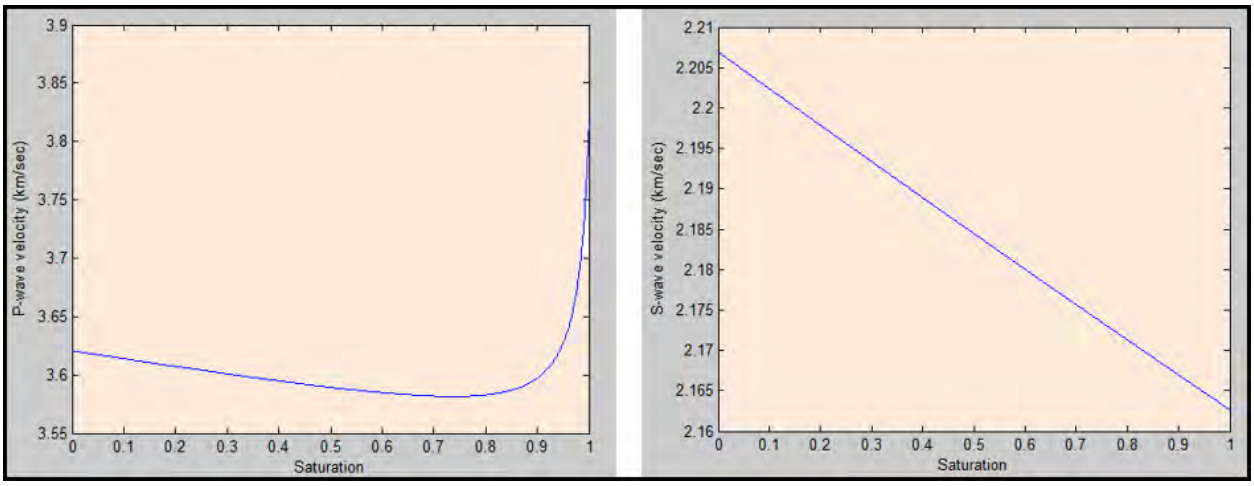

Figure 5.5: Plot of saturation against Vp and Vs for NIA

5.10.2.3 Results of Saturation Plots of T-matrix and NIA

Figure 5.4 and Figure 5.5 are displaying the behavior of Vp and Vs against saturation that velocities are sensitive to saturation. In both models Vp is decreasing with increase in saturation and at last behave as lithology that's why curve is suddenly moved upward.

5.10.3 Sensitivity of Elastic Properties with Porosity and Water Saturation

Sensitivity of P-wave using T-matrix

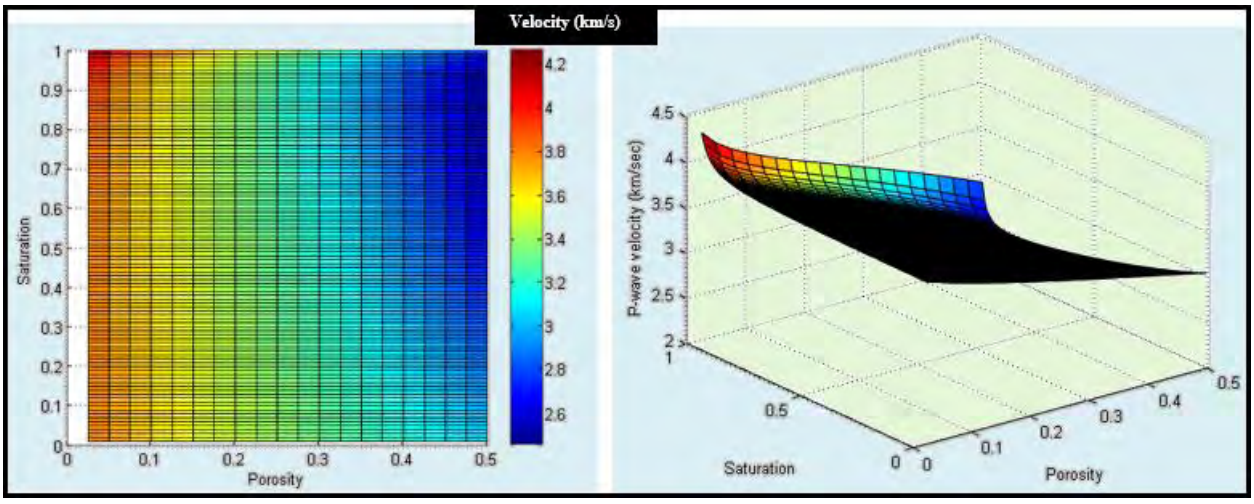

Figure 5.6: Plot of Vp against Porosity and Water Saturation using T-matrix

Sensitivity of S-wave using T-matrix

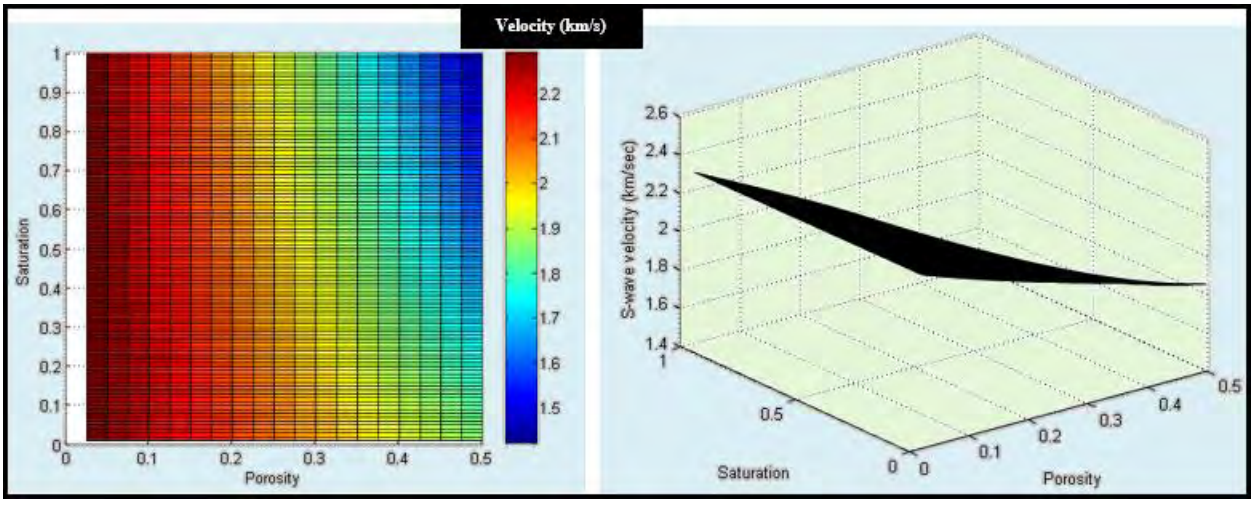

Figure 5.7: Plot of Vs against Porosity and Water Saturation using T-matrix

Sensitivity of P-wave using NIA

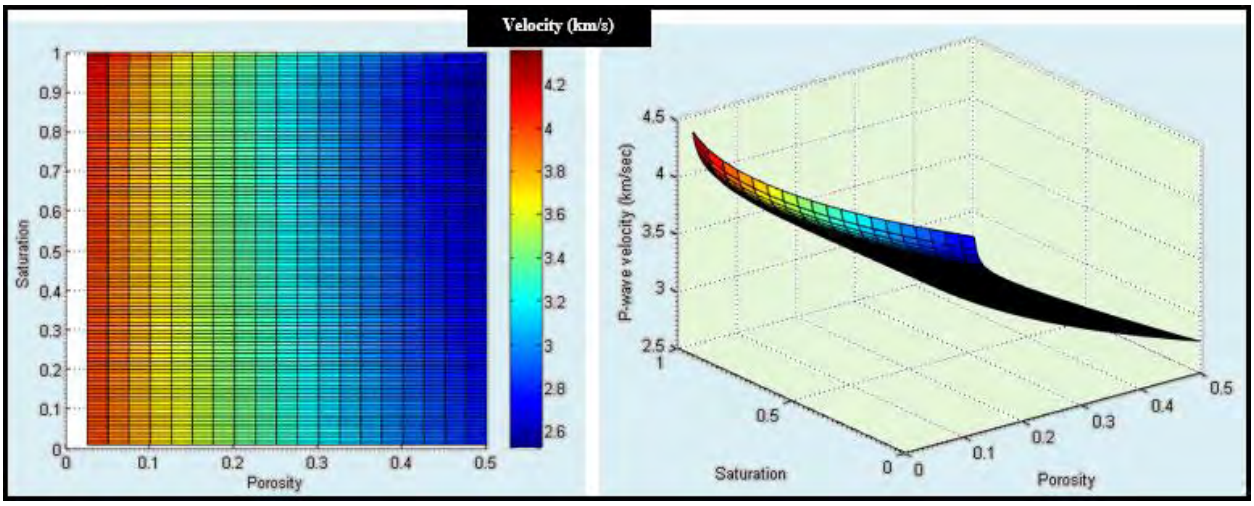

Figure 5.8: Plot of Vp against Porosity and Water Saturation using NIA

Sensitivity of S-wave using NIA

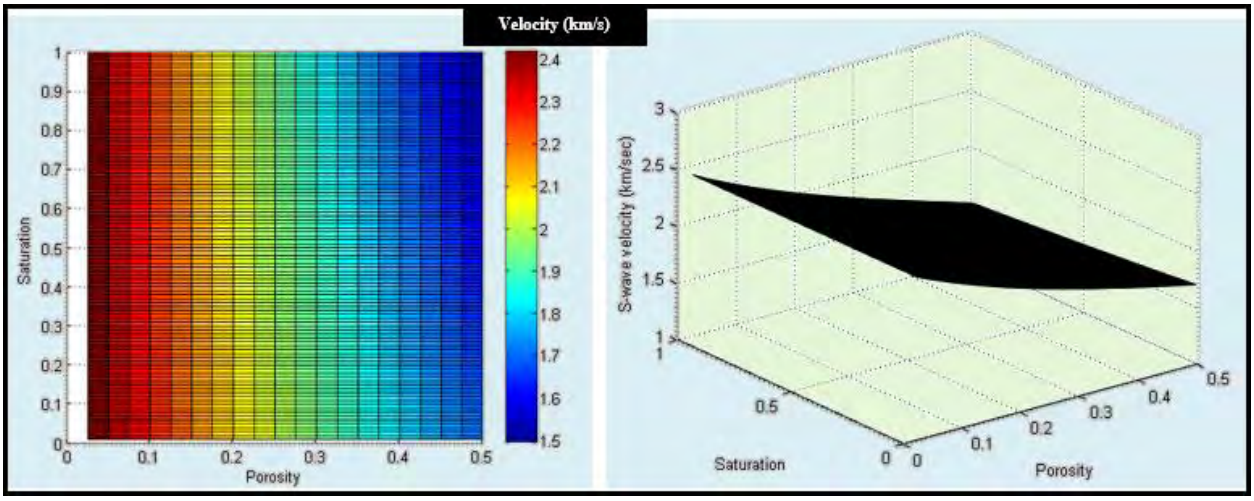

Figure 5.9: Plot of Vs against Porosity and Water Saturation using NIA

To check the sensitivity of already build rock physics model, we build the template of porosity versus water saturation versus Velocities (P-wave, S-wave), porosity taken on x-axis ranges from 0 to 50%, water saturation on y-axis ranges from 0-100% and velocities (P-wave, S-wave) on z-axis (Figure 5.5, 5.6, 5.7, 5.8). It is investigated that effective properties are becoming more sensitive as the porosities are increasing. P-wave velocity is sensitive to the water saturation but S-wave velocity shows insensitivity to water saturation because there is no dependence of shear modulus on saturations. Therefore, saturated shear modulus is equal to dry shear modulus.

CHAPTER 6

AMPLITUDE VERSUS OFFSET/ANGLE (AVO/AVA)

6.1 Introduction

AVO is a lithological and fluid fingerprint. The offset is a geometry-based parameter of surface data acquisition. As a feature of offset, we monitor seismic data, while the angle determines the orientation of the subsurface at which the seismic ray, relative to its normal, hits the horizon of concern. In fact, the angle increases as the offset increases. Zoeppritz-Equations and all their estimates rely on the position, so the surface offset (AVO) must be converted into an incident angle (AVA). The correlation amongst AVO and AVA is ray tracing in abundance and there is a non-linear connection among offset and angle.

The amplitude variation of seismic wave with angle of incidence, or offset (distance between source and receiver), plays a key role in the hydrocarbon exploration, lithology identification (Chao et al., 2013; Anwar et al., 2017). Amplitude versus Offset modeling carried out by considering reservoir as an isotropic medium. However, anisotropy exists in sedimentary rock at different scales (Xu et al., 2005). As AVO analysis has a vital role in seismic monitoring and exploration in last decade's full solution of AVO mathematical equation is Zoeppritz equation (Zeoppritz, 1919). There are lots of approximations to the full Zoeppritz equation are drawn such as Bortfeld approximation, Aki and Richards approximation, Smith and Gidlow approximation, Fatti approximation, Ruger approximation and Novel PP-reflection approximation (Bortfeld, 1961; Yin et al 2018; Aki and Richards, 1980; Fatti et al., 1994, Ruger, 2002: Smith and Gidlow, 1987). This has been also extended in terms of anisotropic AVAZ (Mahmoudian, 2013) and anelastic media (Innanen, 2011a).

In this chapter Ruger assumption is discussed and applied on both models (T-matrix, NIA) and compared their results of reflections and synthetics.

6.2 Workflow for AVO/AVA

Generalized methodology adopted for AVO/AVA is described below in the form of workflow in Figure 6.1.

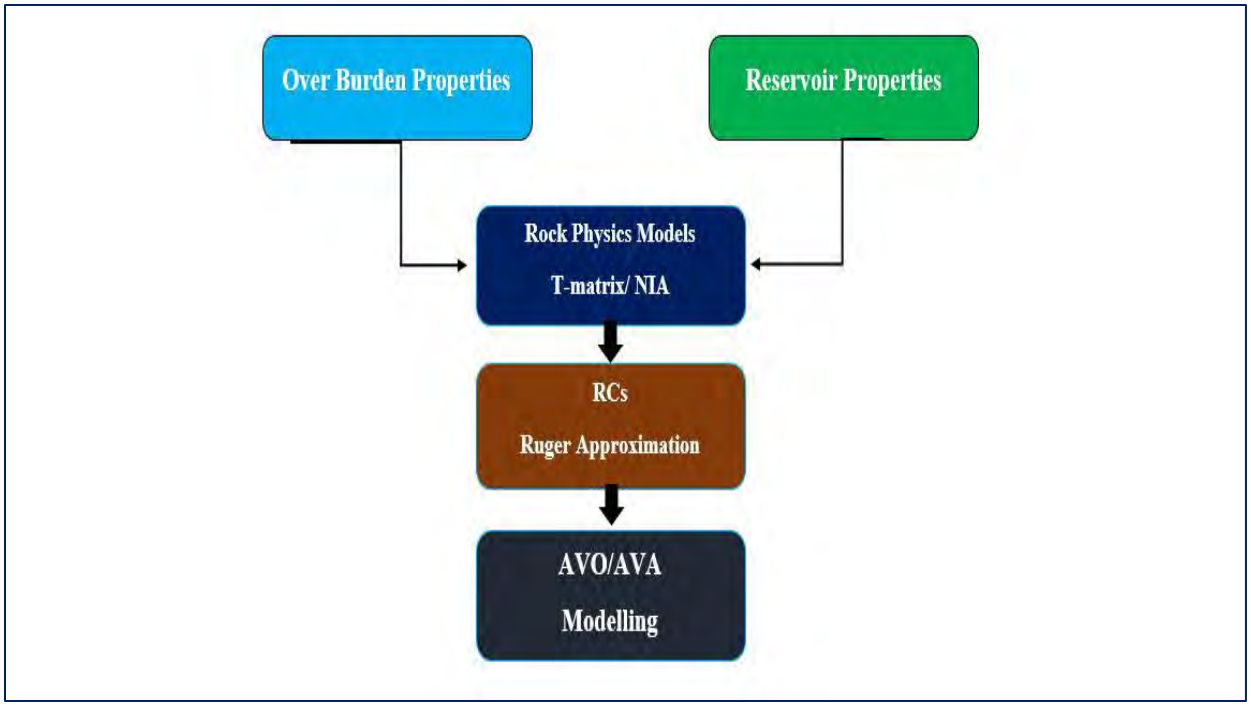

Figure 6.1 Generalized Workflow for AVO/AVA.

6.3 Ruger P-wave Reflection Coefficient

One of the approximation to the full solution of Zeoppritz is given by Rugger (2002) for isotropic medium. Rugger approximation is easy to model as it is linearized equation.

Zoeppritz's equation gives P wave Reflection and Transmission coefficients using elastic parameters as an input. Although the equation gives accurate values as an output, the whole mathematical formulation is a cumbersome procedure. Apart from that the equation is in the form of matrix and therefore inversion of the matrix could be erroneous. The calculation also is time consuming. The equation therefore required an approximation which would be comparatively simpler and less time consuming. For this purpose, many researchers developed mathematical equations that approximates the original Zoeppritz's equation. One such approximation is Ruger approximation. This approximation is linear, comparatively simpler and gives valid results. The Ruger approximation has been used in this dissertation to carry out the AVO analysis.

$$R_p^{ruger}(e) = \frac{1}{2}\frac{\Delta Z}{Z} + \frac{1}{2}\left\{\frac{\Delta V_p}{V_p} - \left(\frac{2v_s}{v_p}\right)^2 \frac{\Delta G}{G}\right\} sin^2 e + \frac{1}{2}\frac{\Delta V_p}{V_p} sin^2 e\, tan^2 e \ , \quad (6.1)$$

Where

$$\Delta Z = Z_2 - Z_1 \ , \quad (6.2)$$

$$Z = \frac{Z1 + Z2}{2} \ , \quad (6.3)$$

$$\Delta V_P = V_{P\_sat} - V_{P\_ovb} \ , \quad (6.4)$$

$$V_p = \frac{Vp_{sat} + Vp\_ovb}{2} \ , \quad (6.5)$$

$$V_S = \frac{Vs\_sat + Vs\_ovb}{2} \ , \quad (6.6)$$

$$G_1 = \rho_{ovb} \text{ x } (V_{S\_ovb})^2 , \quad (6.7)$$

$$G_2 = \rho_{sat} \text{ x } (V_{S\_sat})^2 \ , \quad (6.8)$$

$$\Delta G = G_2 - G_1 \ , \quad (6.9)$$

The approximation gives us RC values with respect to angles on the basis of elastic parameters obtained from different rock physics model.

6.4 Classification Scheme for AVO/AVA

Rutherford and Williams (1989) proposed a classification arrangement of AVO responses for diverse type of gas sands (Figure 6.2) by plotting R (0) versus G to locate top of gas sand. Based on AVO characteristics, gas-sand reflectors can be grouped into three classes defined in terms of reflection coefficient (Ro) at the top of the gas sand. AVO characteristics for each of these class sand are distinct.

6.4.1 Class 1 Sand

It is normally present in a stiff rock, on-shore part and has a greater impedance as compare to the inclosing shale material (Rutherford & Williams, 1989).

6.4.2 Class 2 Sand

This type of sand can have intense AVO effects if sufficient angle/ offset range is existing in the

seismic data. In Figure 6.2, the middle two arcs denote the limits of promising AVO responses in Class 2 sands. As the zero offset reflection coefficients of Class 2 sands are nearby to zero. Great fractional variations in reflectivity from close to distant offset can happen (Figure 6.3), increasing the detectability of these sands (Rutherford & Williams, 1989).

6.4.3 Class 3 Sand

These are produced chiefly in aquatic atmospheres. These sands have lesser impedances than the covering shale (Rutherford & Williams, 1989).

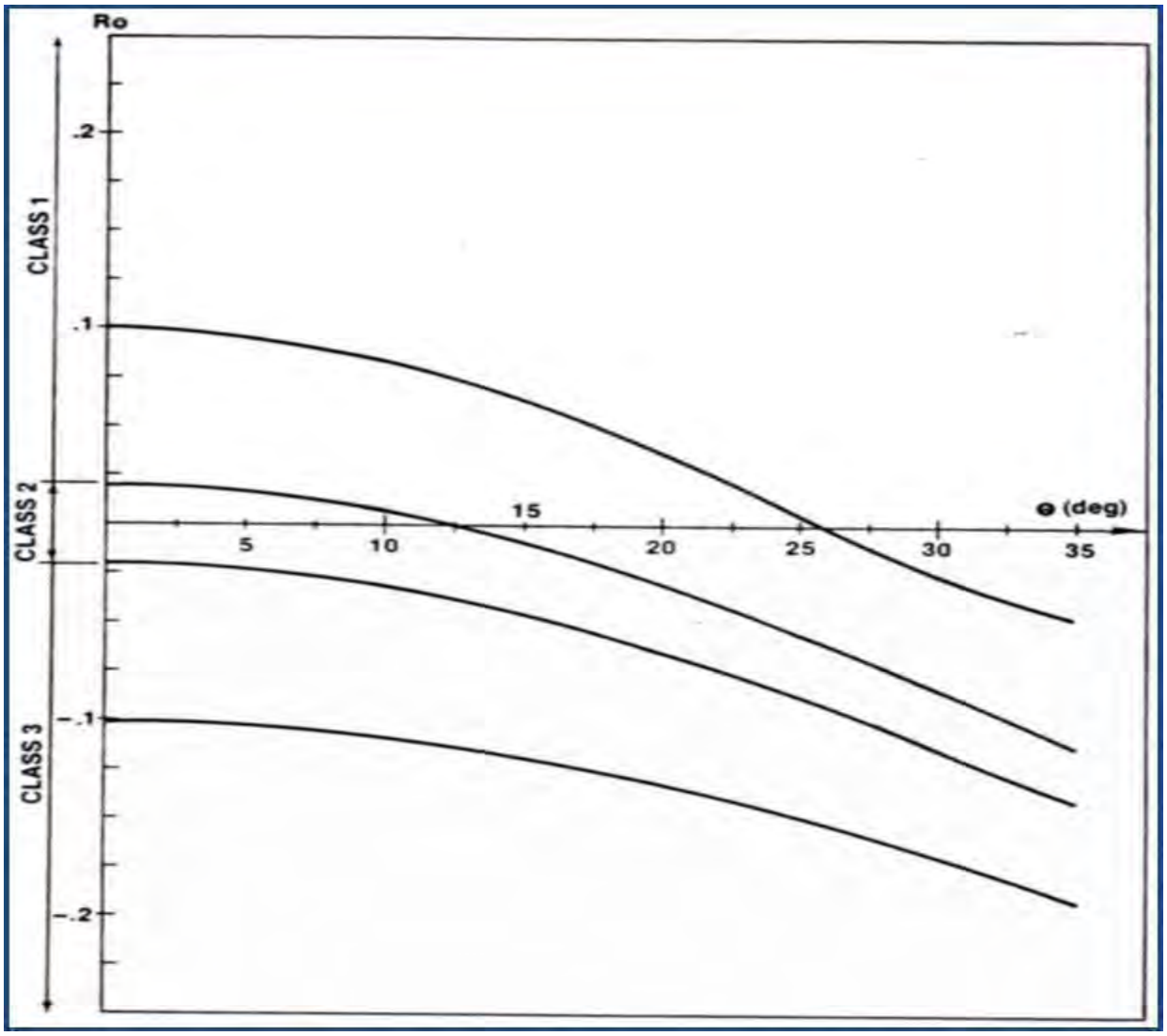

Figure 6.2 P-wave Reflections coefficients with angle on the basis of Zoeppritz equation (Rutherford and Willimas, 1989).

6.5 Castagna Modification

(Castagna, 1997) suggested shale sand layers with potential hydrocarbons should be classified on the basis of their position within the A-B plane where A is the intercept and B is the gradient. Class 1 sands being higher in impedance compared to the above lying rock are placed in the IV quadrant within the A-B plot. This quadrant displays a decreasing normal incident reflection coefficient trend which starts at a positive value while the AVO slope is negative in nature (Castagna et al., 1997). Class II sands have a similar impedance values to the rock unit above it (Castagna et al., 1997). The AVO plot for Class II sands show a high variation and may occur in either of the II, III and IV quadrants within the A-B plot (Castagna and Swan, 1997).

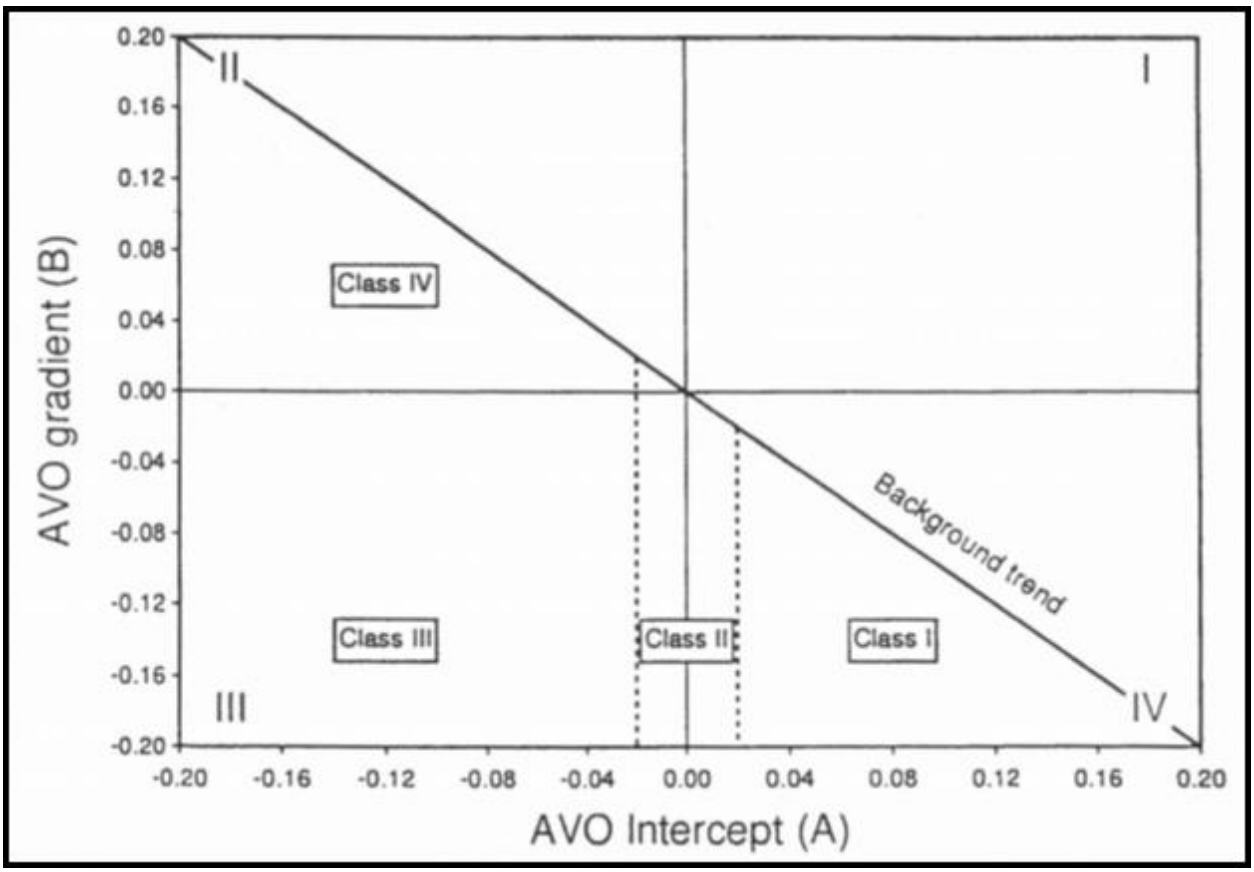

Figure 6.3 Classification of Classes into quadrants on the basis of AVO gradient and intercept (Zhang and Brown, 2001).

6.6 Overburden Properties

In our case study, C-Interval of Lower Goru is our reservoir and shale patch above C-Interval of

Lower Goru is overburden ranged from3268-3334 in well Sawan-07.

Table 6.1: Elastic Properties of Overburden

Properties	Values
P-wave velocity (Vp)	4.2325 Km/sec
S-wave velocity(Vs)	2.4294 Km/sec
Density(ρ)	2.6889 g/cm^3

6.7 Variation of RCs with Angle

Variation of RCs with angle using Rock Physics Models has been seen by changing porosity and saturation respectively.

Varying Porosities using T-matrix

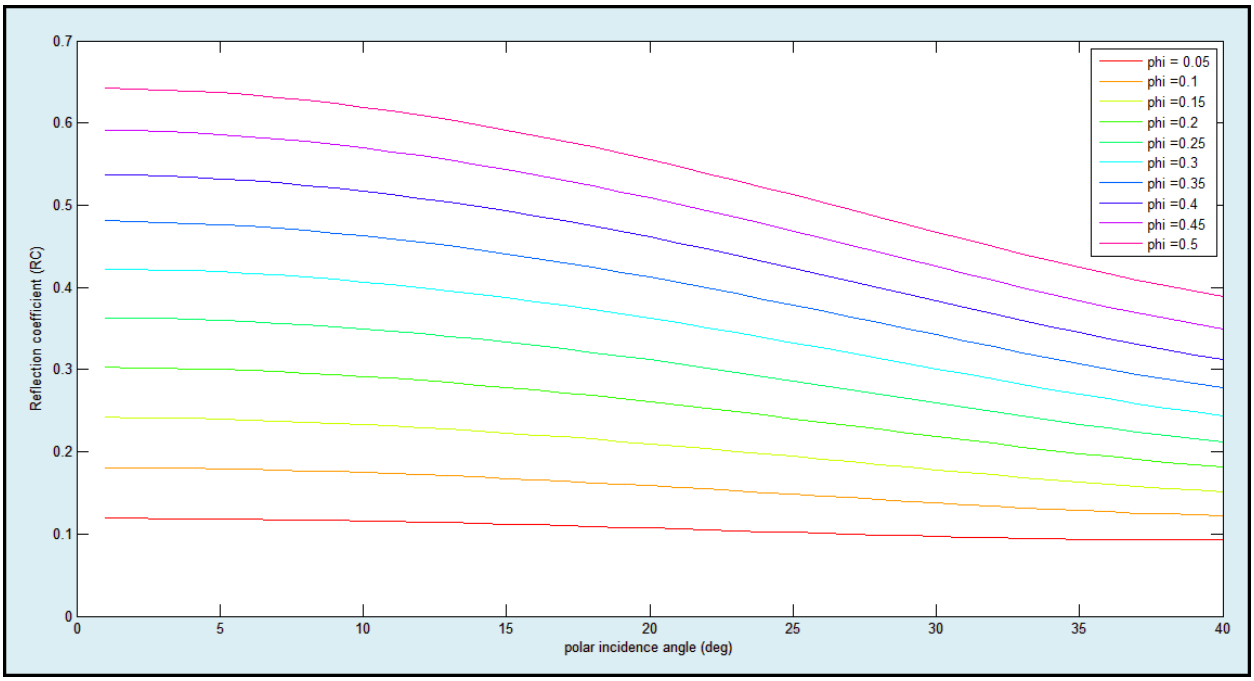

Figure 6.4: Variation of RCs with angle by varying porosities using T-matrix.

Varying Porosities using Non-Interacting Approach (NIA)

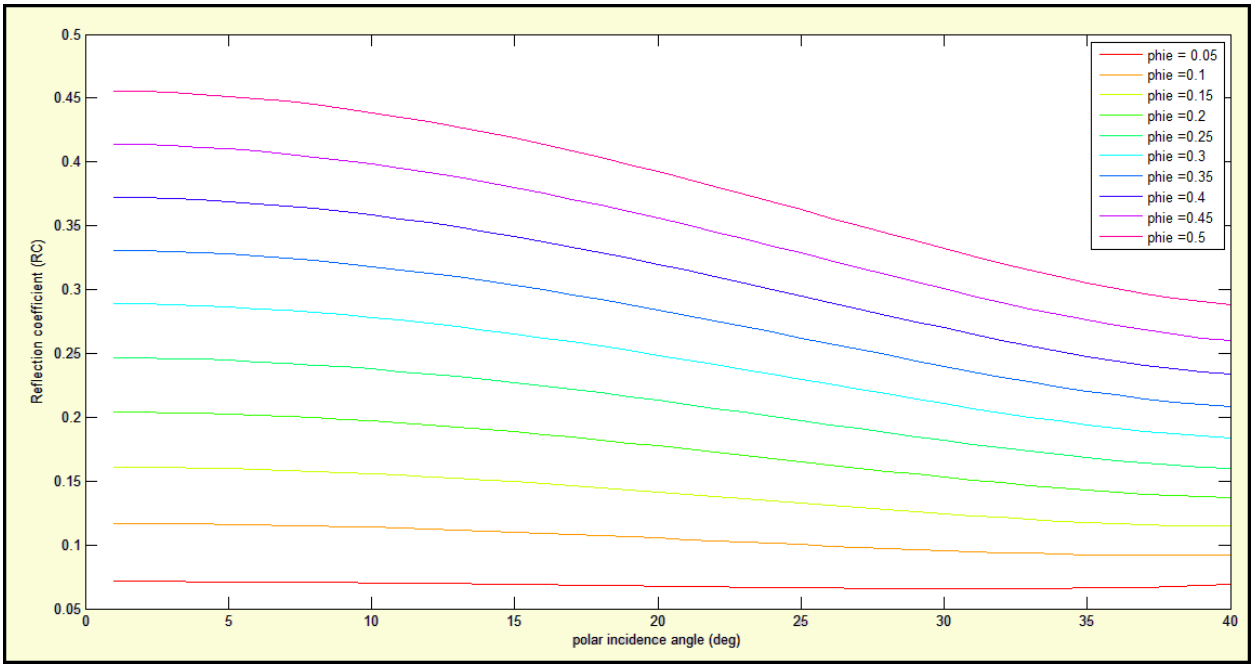

Figure 6.5: Variation of RCs with angle by varying porosities using NIA.

6.7.1 Porosity Variation Results in RCs for RPM

RCs obtained from Rugger equation with elastic properties generated from T-Matrix NIA model clearly be seen to decrease with increase in porosity. The RCs fall in Class I according to the curves given by (Rutherford and Williams, 1989).

T-matrix and NIA models were used to generate elastic parameters which were taken as input for generation of RCs using Rugger equation. The RCs (Figure 6.4 and 6.5) show an evident decrease with increase in porosity. RCs were generated for 0.5%, 1%, 1.5%, 2%, 2.5%, 3%, 3.5%, 4%, 4.5% and 5% porosities. Intercept values for comparatively lower porosity values are lower. RCs for all porosity value show a Class I trend in accordance with (Rutherford and Williams, 1989).

Varying Saturation using T-matrix

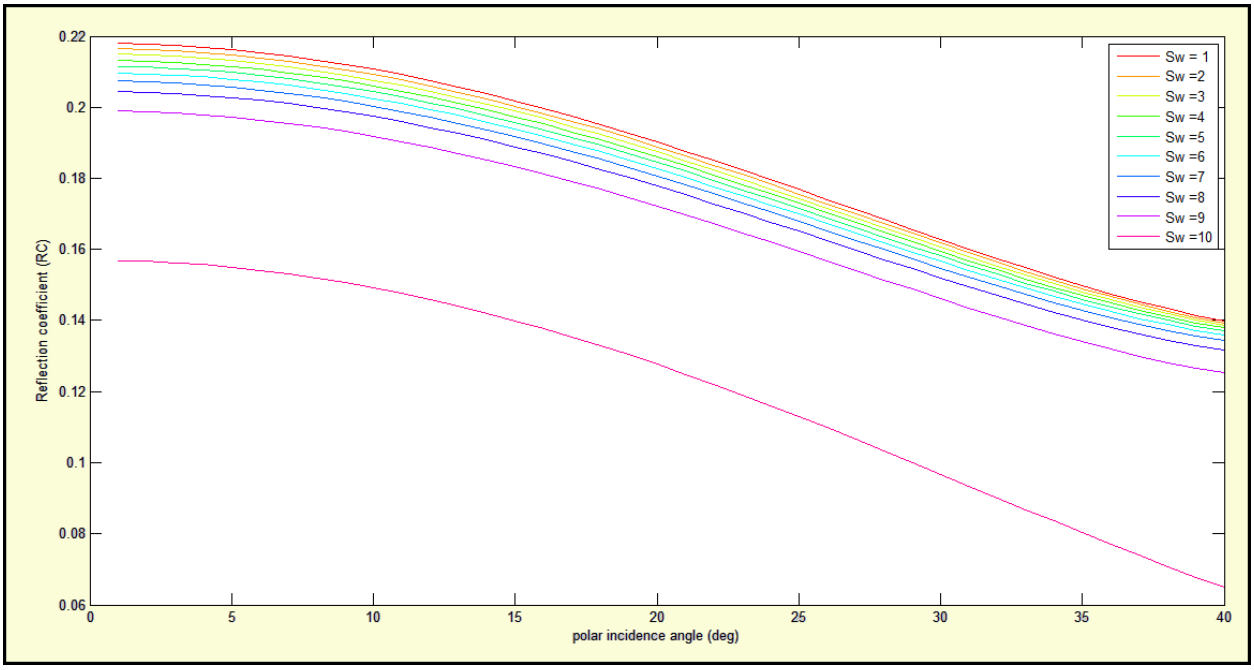

Figure 6.6: Variation of RCs with angle by varying saturation using T-matrix.

Varying Saturation using Non-Interacting Approach (NIA)

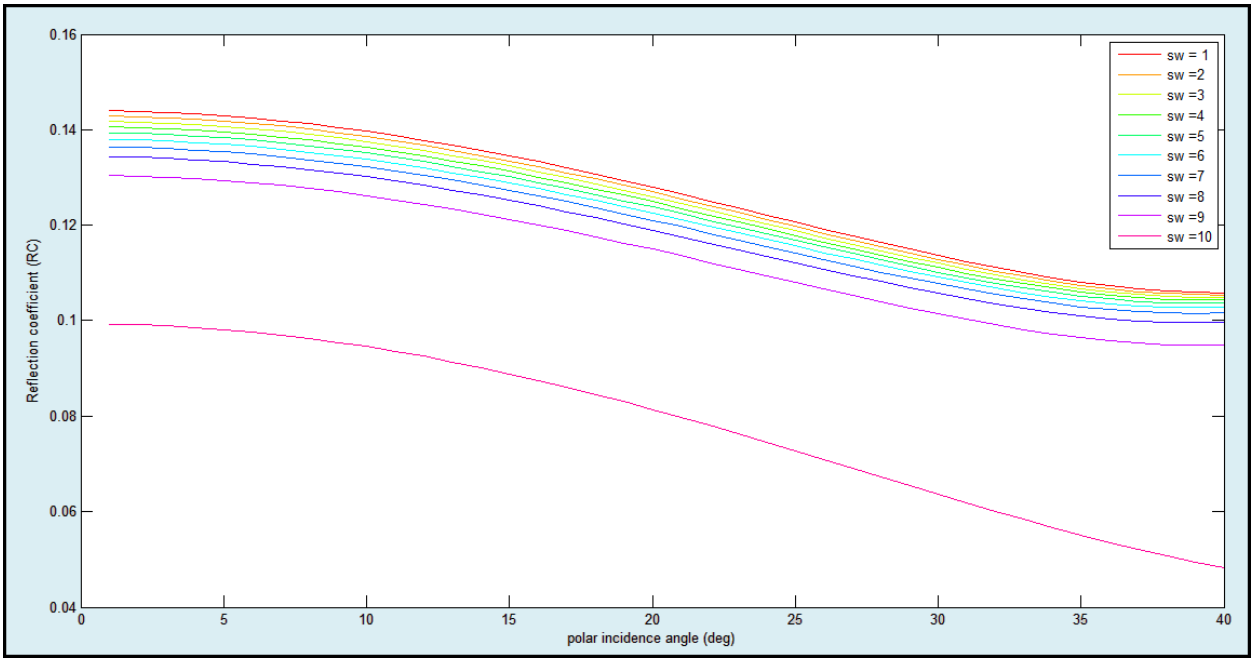

Figure 6.7: Variation of RCs with angle by varying saturation using NIA.

6.7.2 Saturation Variation Results in RCs for RPM

RCs generated using Rugger equation with input values from T-matrix and NIA models (Figure 6.6 and 6.7) show a decreasing trend with angle. RCs were generated for 10%, 20%, 30%, 40%, 50%, 60%, 70%, 80%, 90% and 100%. The intercept decreases with increasing saturation levels. At 100% saturation, RCs show a sharp decrease in intercept. This is due to high percent saturation acting as a layer rather than saturation within another layer.

6.8 Comparison of T-matrix and NIA at Different Porosities Using RCs

Porosity=8%

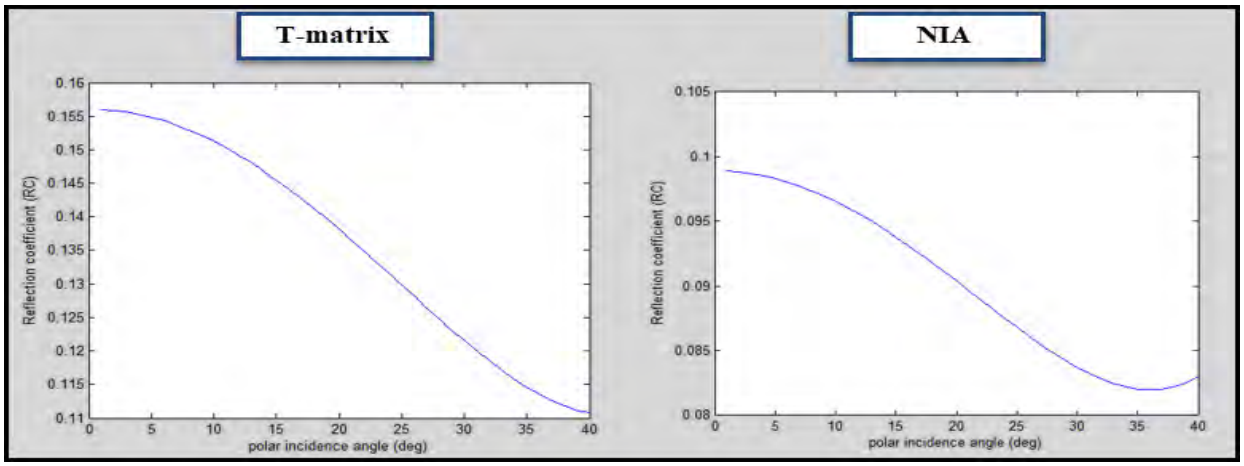

Figure 6.8: Comparison of RPM using RCs at 8% porosity.

Porosity=16%

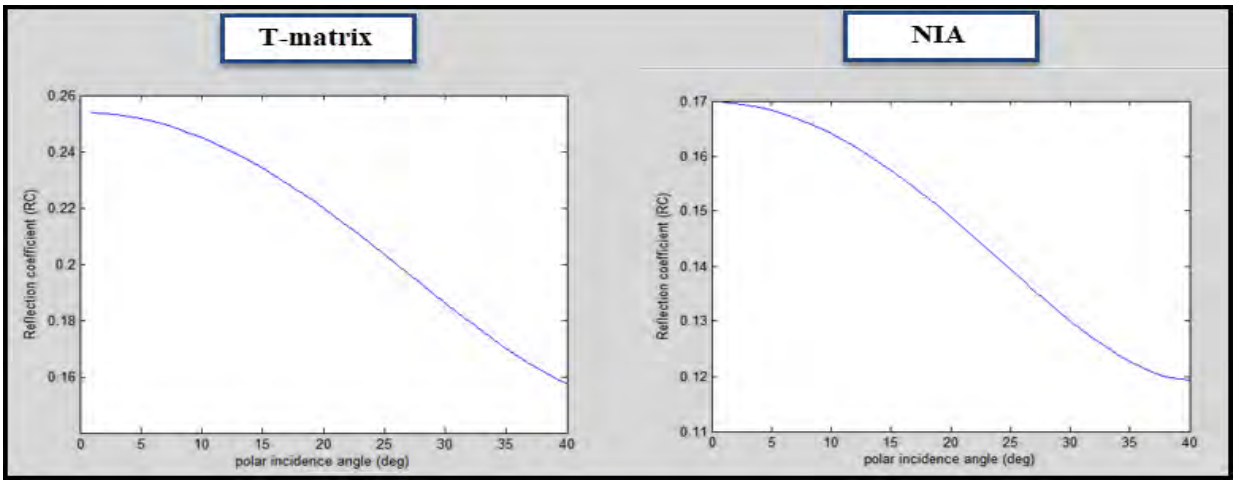

Figure 6.9: Comparison of RPM using RCs at 16% porosity.

Porosity=24%

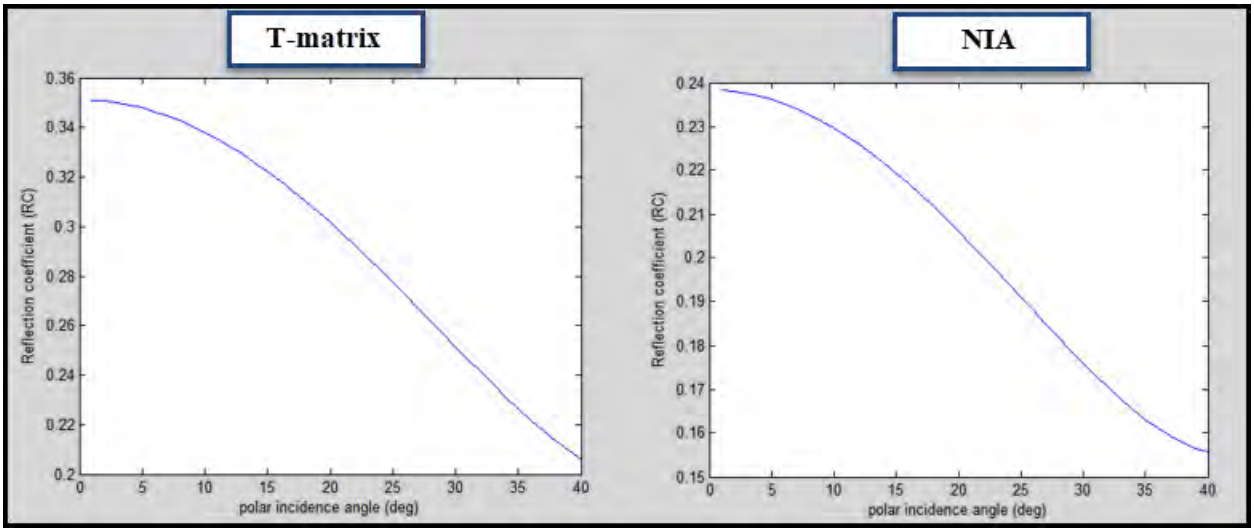

Figure 6.10: Comparison of RPM using RCs at 24% porosity.

Porosity=32%

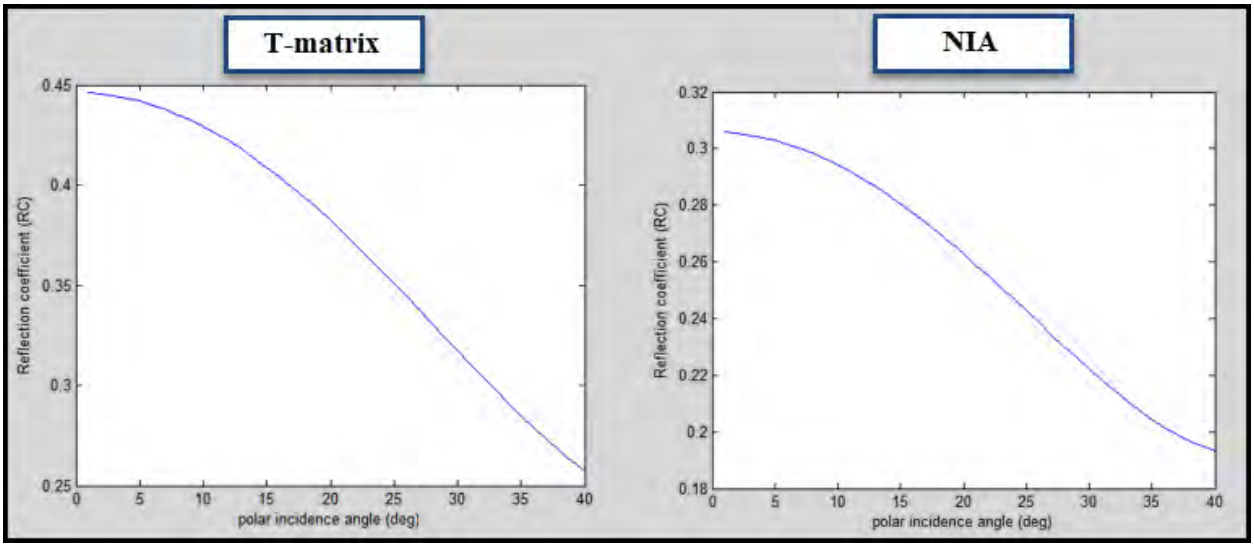

Figure 6.11: Comparison of RPM using RCs at 32% porosity.

6.8.1 Porosity Comparison Results in RCs for RPM

The comparison of the NIA and T-matrix elastic parameters in terms of RCs at 8%, 16%, 24% and 32% porosity (Figure: 6.8, 6.9, 6.10, 6.11) show a slight different in the two curves. Intercept for

T- matrix is less in all figures. RCs decrease with angle with a negative slope. The gradient is more for NIA based curve as compared to T-matrix curve in all plots.

6.9 Comparison of T-matrix and NIA at Different Saturation Using RCs

15% saturation

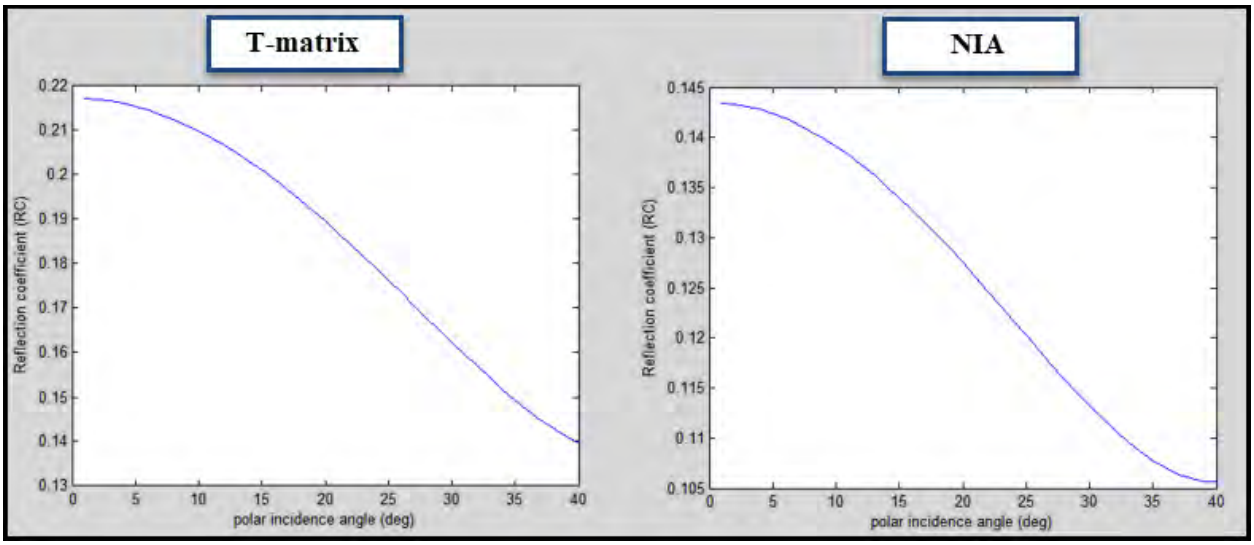

Figure 6.12: Comparison of RPM using RCs at 15% Water Saturation.

Water Saturation=30%

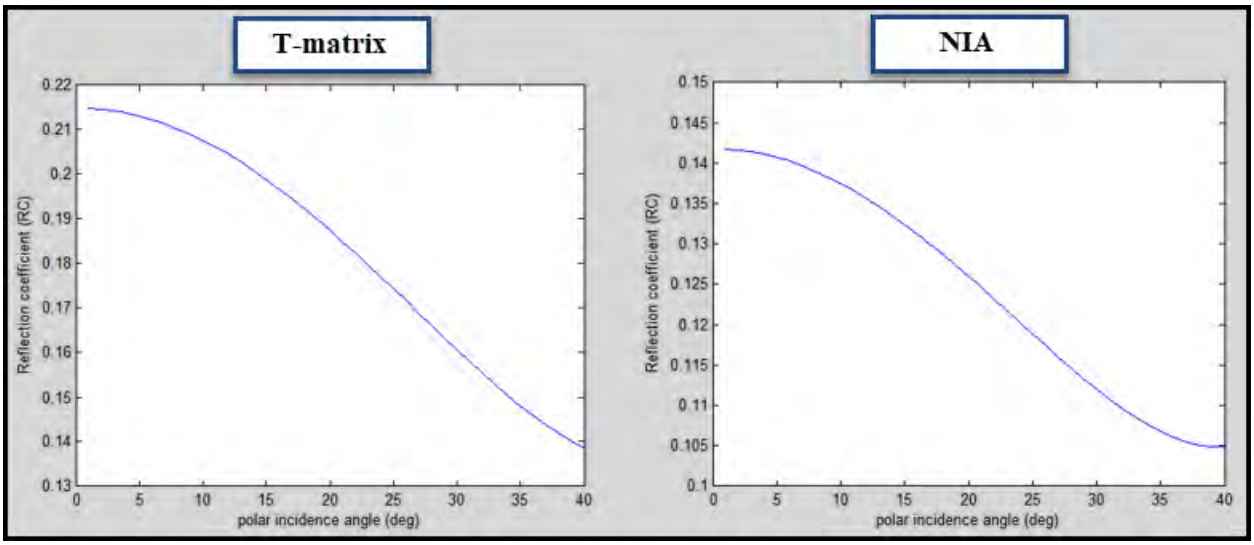

Figure 6.13: Comparison of RPM using RCs at 30% Water Saturation.

Water Saturation=45%

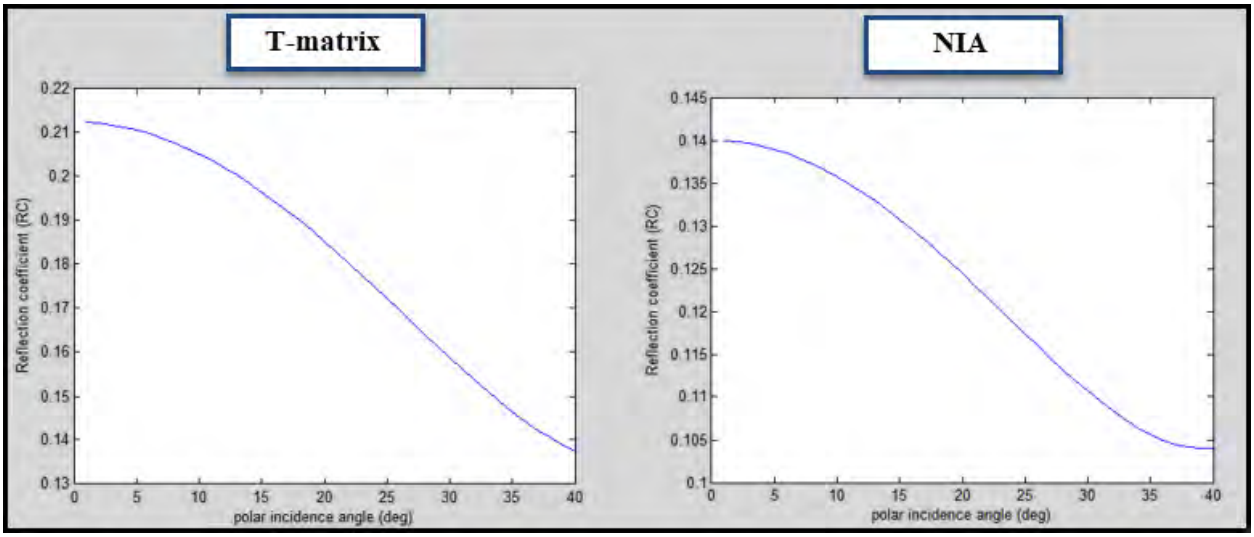

Figure 6.14: Comparison of RPM using RCs at 45% Water Saturation.

Water Saturation=60%

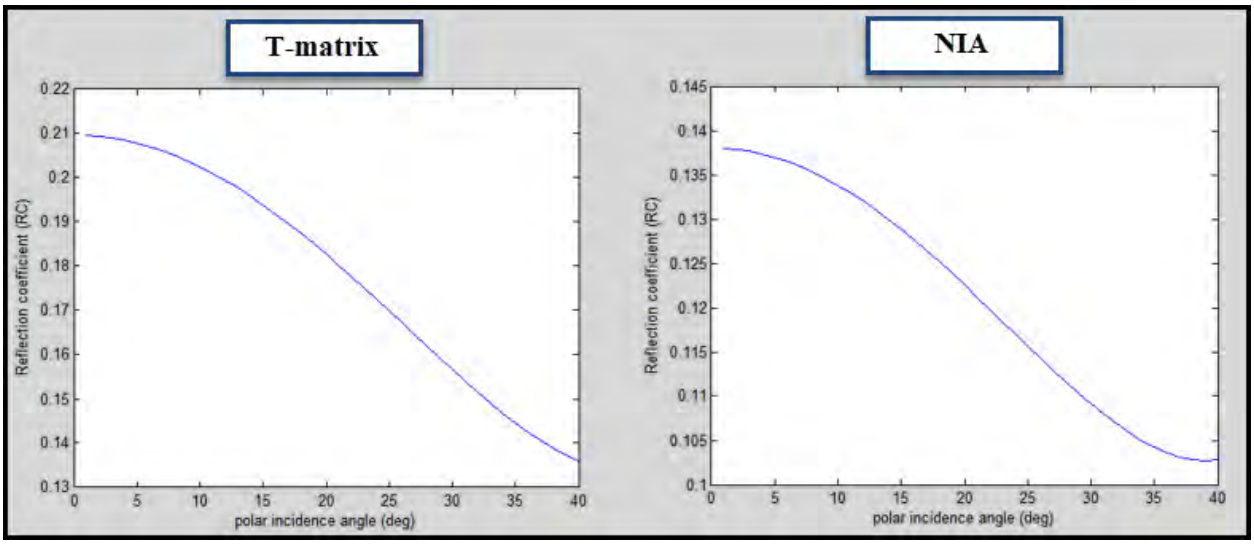

Figure 6.15: Comparison of RPM using RCs at 60% Water Saturation.

6.9.1 Water Saturation Comparison Results in RCs for RPM

For 15%, 30%, 45% and 60% water saturation, RCs obtained from elastic properties extracted from NIA and T-matrix (Figure: 6.12, 6.13, 6.14, 6.15), the intercept value is more for RCs developed from NIA compared to T matrix. In all plots, the slope decreases with angle and is high for T-matrix means a relatively faster decrease in RC values with angle compared to NIA.

6.10 Comparison of T-matrix and NIA at Different Porosities Using AVO

Porosity=8%

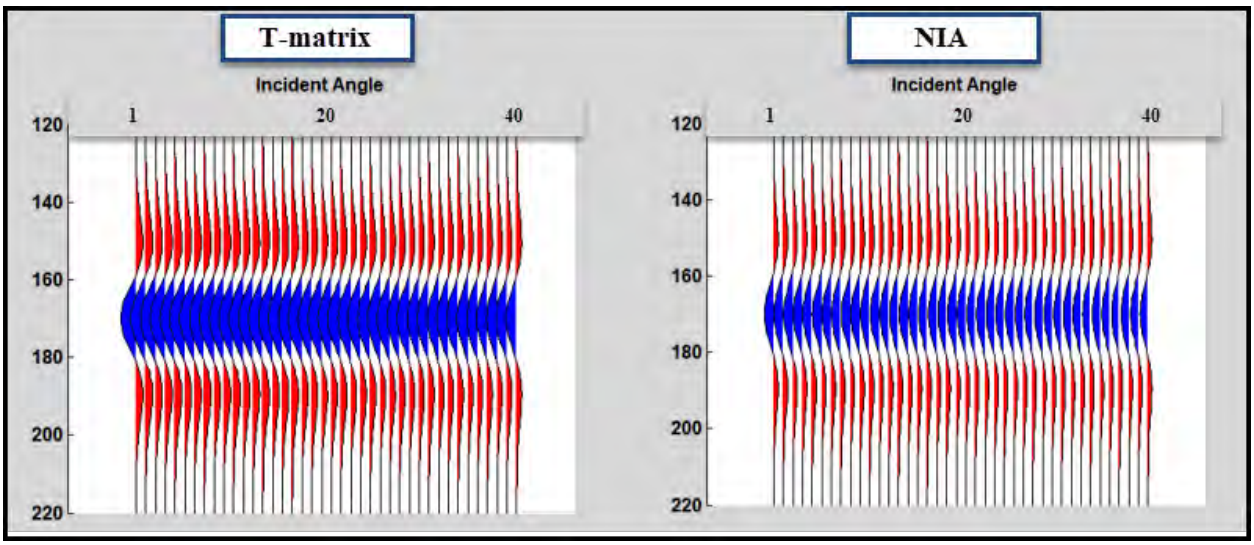

Figure 6.16: Comparison of RPM using RCs at 8% Porosity.

Porosity=16%

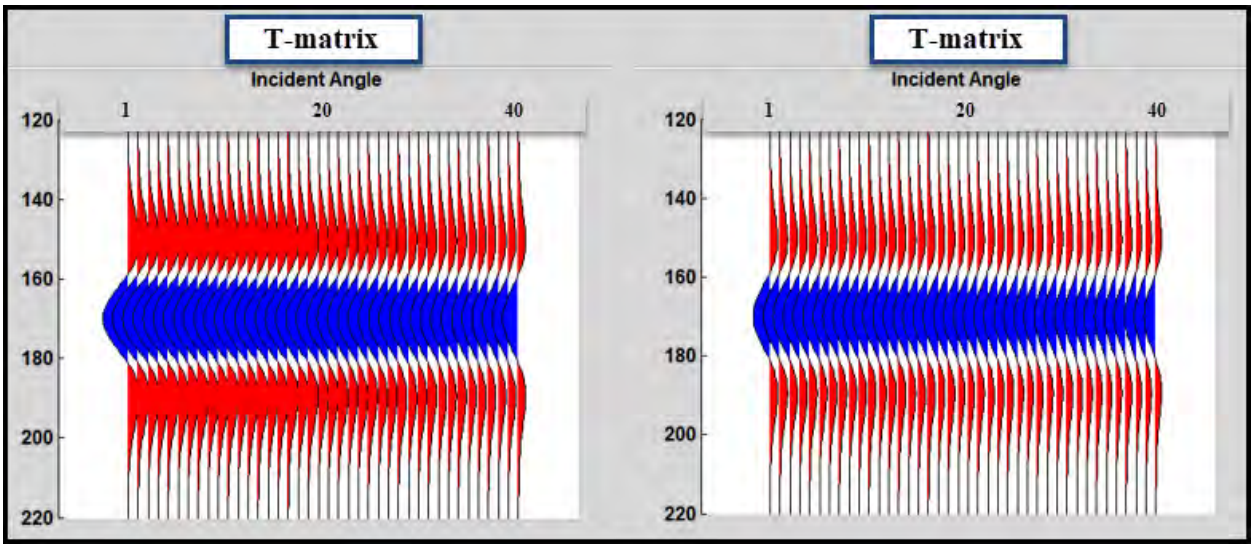

Figure 6.17: Comparison of RPM using RCs at 16% Porosity.

Porosity=24%

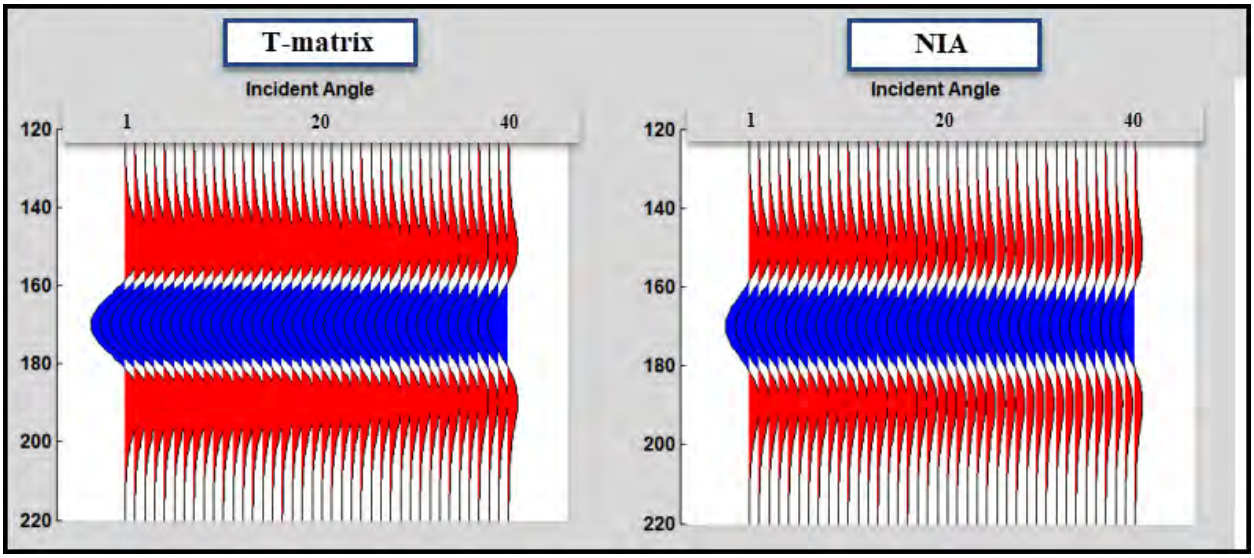

Figure 6.18: Comparison of RPM using RCs at 24% Porosity.

Porosity=32%

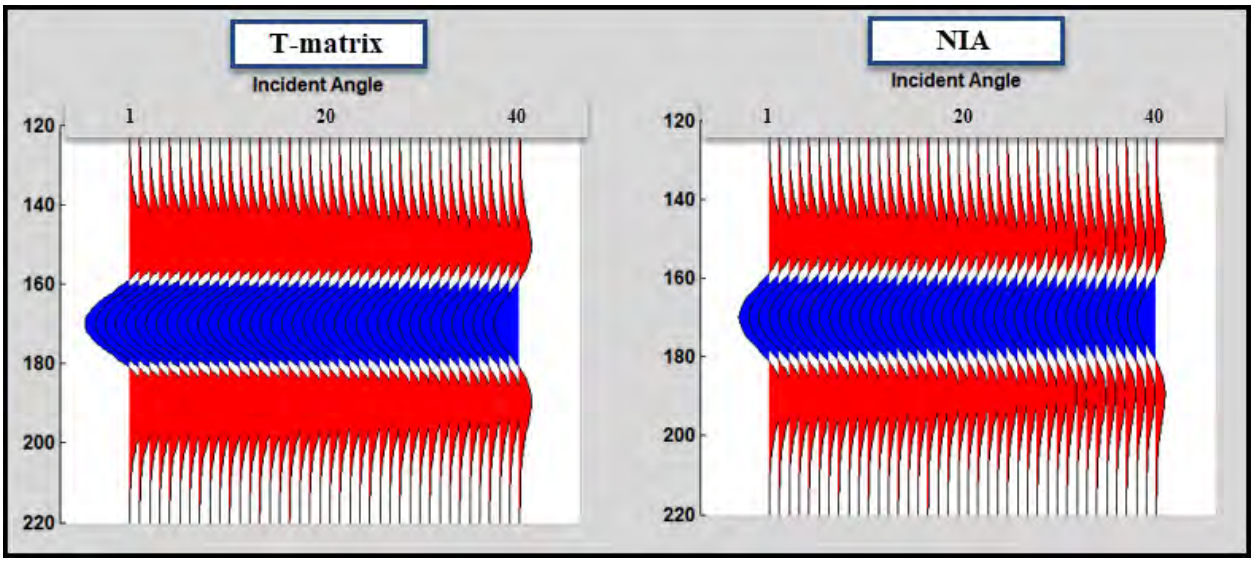

Figure 6.19: Comparison of RPM using RCs at 32% Porosity.

6.10.1 Porosity Comparison Results in AVO for RPM

For 8%, 16%, 24% and 32% porosity, AVO obtained from RCs generated using T-matrix and NIA (Figure: 6.16, 6.17, 6.18, 6.19), amplitude is more for AVO developed from T-matrix

paralleled to NIA. All plots shows that the polarity is high for T-matrix means a relatively due to faster decrease in RC values with angle compared to NIA.

6.11 Comparison of T-matrix and NIA at Different Saturation Using AVO

Water Saturation=15%

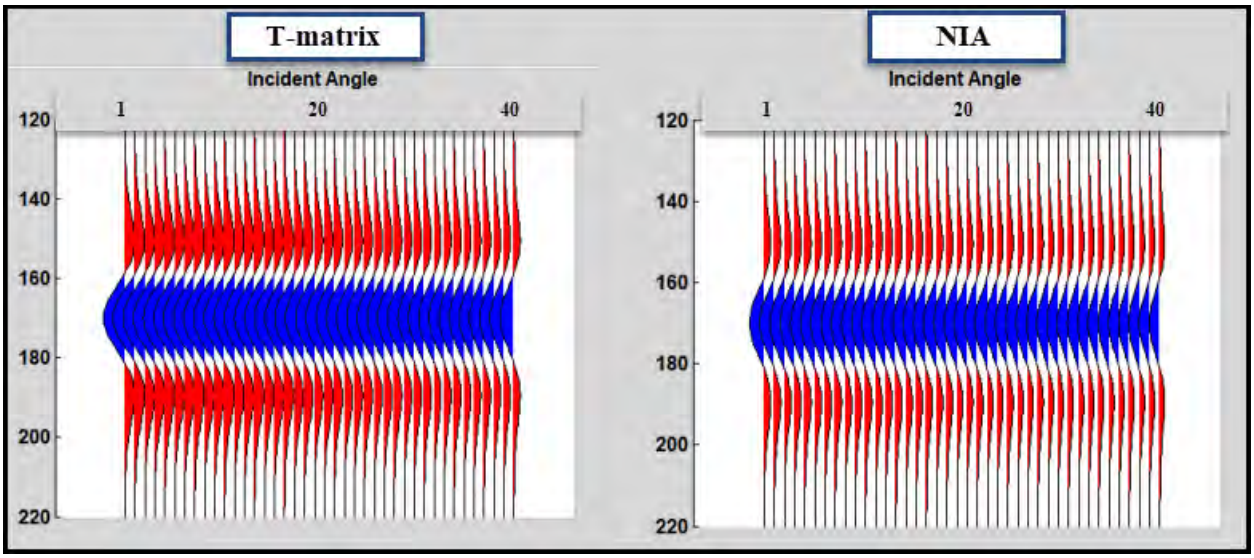

Figure 6.20: Comparison of RPM using AVO at 15% Water Saturation.

Water Saturation=30%

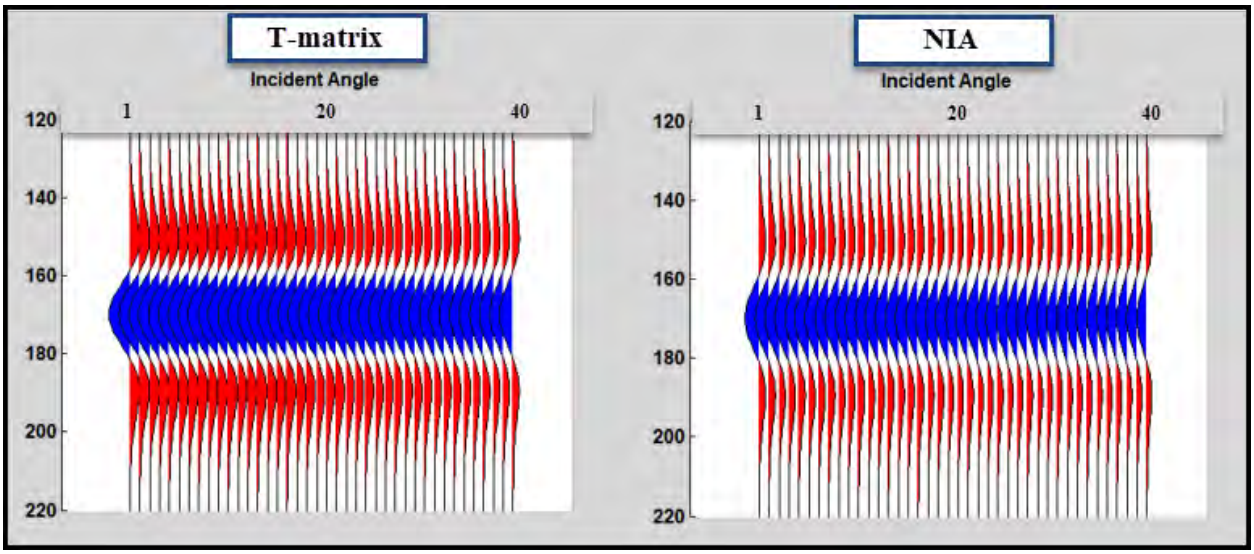

Figure 6.21: Comparison of RPM using AVO at 30% Water Saturation.

Water Saturation=45%

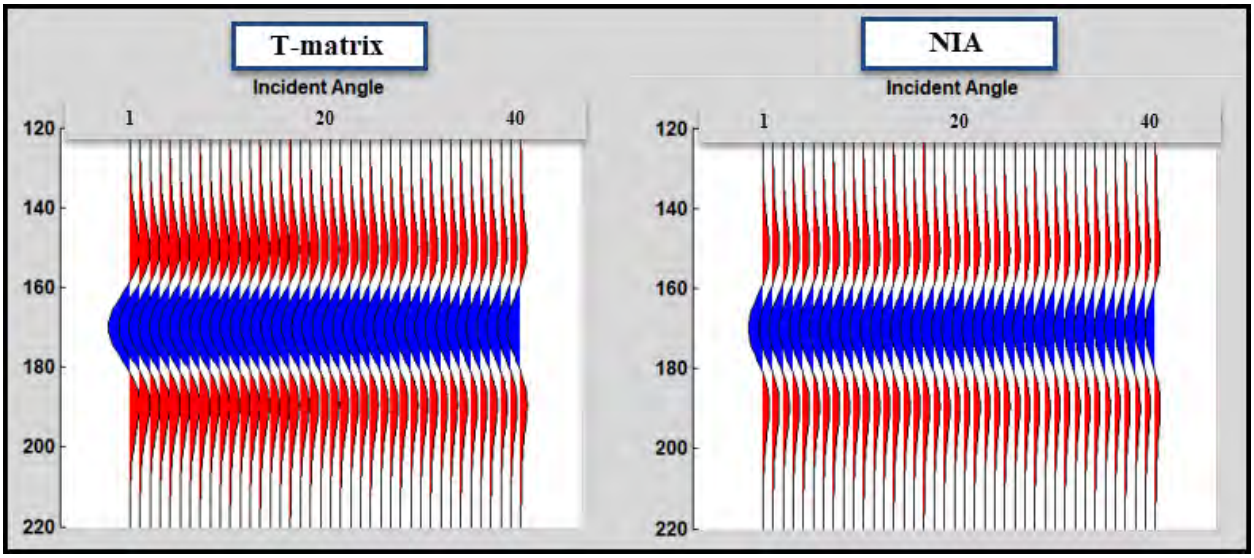

Figure 6.22: Comparison of RPM using AVO at 45% Water Saturation.

Water Saturation=60%

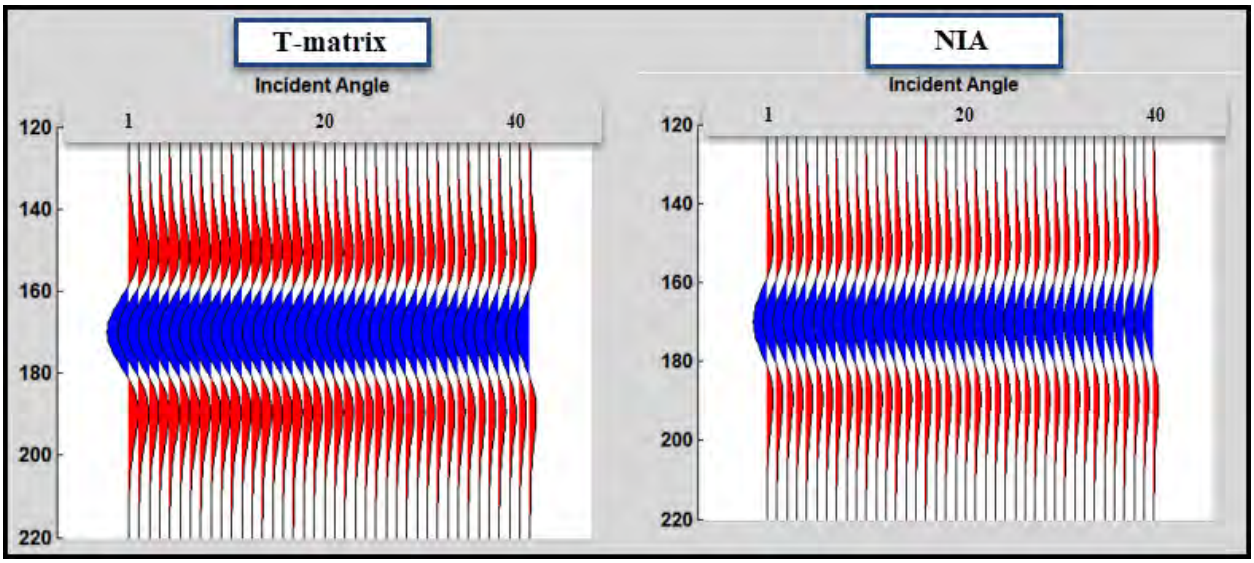

Figure 6.23: Comparison of RPM using AVO at 60% Water Saturation.

Water Saturation=90%

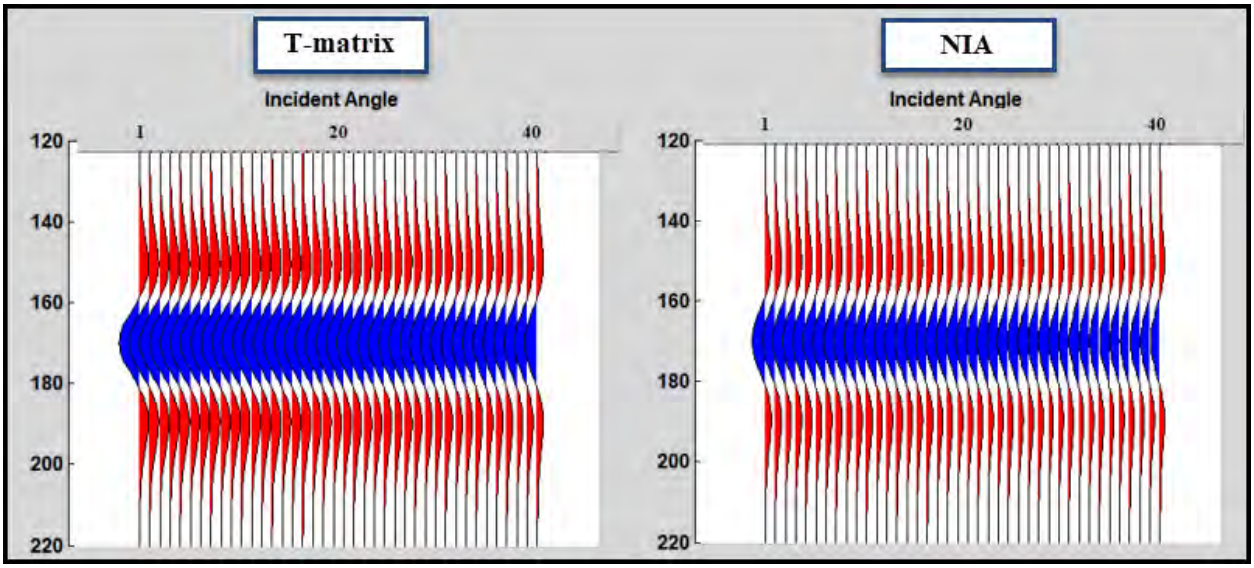

Figure 6.24: Comparison of RPM using AVO at 90% Water Saturation.

Water Saturation=100%

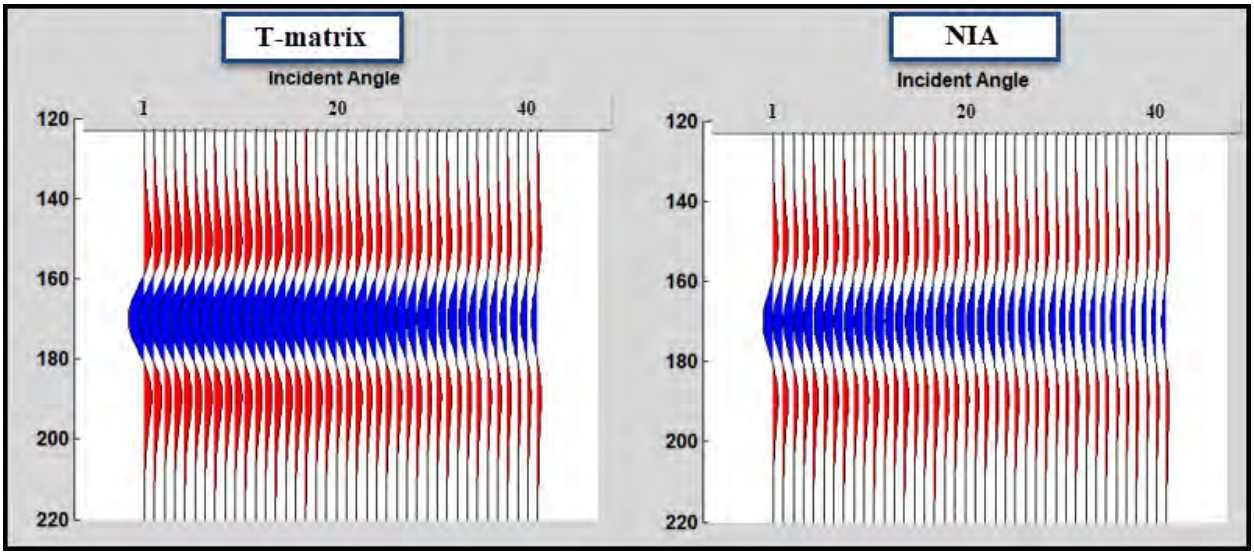

Figure 6.25: Comparison of RPM using AVO at 100% Water Saturation.

6.11.1 Water Saturation Comparison Results in AVO for RPM

The comparison of the NIA and T-matrix Rock Physics Models in terms of AVO at 15%, 30%, 45%, 60%, 90% and 100% water saturation (Figure: 6.20, 6.21, 6.22, 6.23, 6.24, 6.25) shows a minor difference in AVO synthetics generated from both RPMs. On the basis of RCs generated

from the models, we can safely say all (15%, 30%, 45%, 60% and 90%) saturations have almost identical synthetics due to minute contrast upon RC values. In case of 100% saturation, the synthetic shows a reasonable contrast from the rest generated synthetics. This contrast is due to a fluid layer formation which sharply reduces the contrast after replacing the gas within the reservoir. Polarity for T- matrix is greater than NIA due to reflection coefficients and as RCs decrease with angle with a negative slope so the gradient and of course amplitude is less for NIA based synthetic as compared to T-matrix in all plots.

DISCUSSIONS AND CONCLUSIONS

Interpretation of 3D seismic cube of Sawan Area, Lower Indus Basin through generation of depth and time contour maps after demarcation of Lower Goru formation, C sand and fault polygons. With the use of Sawan – 07 well, the interpretation was carried out after synthetic seismogram generation. Presence of horst and graben structures was confirmed within the study area which came to existence under the influence of extensional regime. C-Interval of Lower Goru formation act as reservoir which has been filled by Sembar formation beneath it forming a petroleum play.

Characterization of a potential reservoir within an area is critical. Primarily, this characterization is done through wells drilled within the vicinity of the any area of interest. Reservoir zones investigated in the area using las files from Sawan – 07 well results contained 16.6% total porosity, 12.5% effective porosity and 48% hydrocarbon saturation. The results found for Sawan – 01 well were 11.4% effective porosity, 17.3% total porosity and 34% hydrocarbon saturation while in case of Sawan – 02 well, 12% (Zone A), 6.1% (Zone B) effective porosity, 16.4% (Zone A), 10.7% (Zone B) average total porosity and 32.4% (Zone A), 24% (Zone B) saturation was determined.

Rock Physics Models are important to analyze a reservoir through substitution of fluid and porosity variation which directly impacts upon the elastic parameter values. Using well data of Sawan-07 and with the help of modified T-matrix and Non Interactive Approximation models, dry rock properties under influence of varying porosity obtained for a sand reservoir were inculcated with variation of fluid. The increasing porosity caused decrease in P wave and S wave velocities. Water saturation inculcation produced a similar effect and decrease P and S wave velocities.

Fluid filled sand reservoirs can be further analyzed for presence of gas if variation in reflectivity with respect to intercept angle of wave with a particular interface is observed. AVO analysis provides the means to analyze such behavior. The AVO analysis was carried out with the use of MATLAB coding producing multiple scenarios through substitution of fluid as well as variation in porosity in the zone of interest. Upon observation, the reservoir sands were classified as Class I sands based upon the positive large reflectivity intercept values for each scenario, a decrease in reflectivity with angle and a negative gradient trend. Comparison of T- matrix model and NIA results showed a relatively higher values obtained from T- matrix in comparison with the NIA approach. Synthetics developed for various scenarios upon comparison showed a larger amplitude in case of T – matrix model.

REFERENCES

- Admasu, F., Back, S., & Toennies, K. (2006). Autotracking of faults on 3D seismic data. *Geophysics*, *71*(6), A49-A53.
- Afzal, J., Kuffner, T., Rahman, A., & Ibrahim, M. (2009). Seismic and Well Log based Sequence Stratigraphy of the Early Cretaceous, Lower Goru "C" Sand of the Sawan Gas Field, Middle Indus Platform, Pakistan. PAPG, ATC.
- Ahmed N. Fink P. Sturrock S, Mahmood T. Ibrahim M (2004) Sequence stratigraphy as predictive tool in Lower Goru Fairway, Lower and Middle Indus Platform, Pakistan. PAPG, ATC 2004.
- Aki, K., and P. G. Richards. "Qualitative seismology, University Science (1980).
- Ali, Aamır, and Morten Jakobsen. "Seismic characterization of reservoirs with multiple fracture sets using velocity and attention anisotropy data." Journal of Applied Geophysics 75 3 (2011) 500-602.
- Ali, Aamir, et al. "Resource potential of gas reservoirs in South Pakistan and adjacent Indian subcontinent revealed by post-stack inversion techniques." *Journal of Natural Gas Science and Engineering* 49 (2018): 41-55.
- Ali, Aamir, Muhammad Younas, Matee Ullah, Matloob Hussain, Muhammad Toqeer, Asher Samuel Bhatti, and Azhar Khan. "Characterization of secondary reservoir potential via seismic inversion and attribute analysis: A case study." *Journal of Petroleum Science and Engineering* 178 (2019): 272-293.
- Ali, Aamir, Tiago M. Alves, and Khaista Rehman. "The accuracy of AVA approximations in isotropic media assessed via synthetic numerical experiments: Implications for the determination of porosity." *Journal of Petroleum Science and Engineering* 170 (2018): 563-575.
- Amigun, John Olurotimi, and Oluwaseyi Ayokunle Odole. "Petrophysical properties evaluation for reservoir characterisation of Seyi oil field (Niger-Delta)." *International Journal of innovation and applied studies* 3.3 (2013): 756-773.
- Andersen, Charlotte Faust, and Aart-Jan van Wijngaarden. "Interpretation of 4D AVO inversion results using rock-physics templates and virtual-reality visualization, North Sea

examples." *SEG Technical Program Expanded Abstracts 2007*. Society of Exploration Geophysicists, 2007. 2934-2938.

- Anwer, H.M., Alves, T.M. and Ali, A., 2017. Effects of sand-shale anisotropy on amplitude variation with angle (AVA) modelling: The Sawan gas field (Pakistan) as a key case-study for South Asia's sedimentary basins. *Journal of Asian Earth Sciences*, *147*, pp.516-531.
- Archie, Gustave E "The electrical resistivity log as an aid in determining some reservoir characteristics." Transactions of the AIME 146.01 (1942): 54-62.
- Asquith, George B., Daniel Krygowski, and Charles R. Gibson. *Basic well log analysis*. Vol. 16. Tulsa: American Association of Petroleum Geologists, 2004.
- Aurnhammer, Melanie, and K. D. Tonnies. "A genetic algorithm for automated horizon correlation across faults in seismic images." *IEEE Transactions on evolutionary computation* 9.2 (2005): 201-210.
- Avseth, Per, et al. "Rock physics estimation of cement volume, sorting, and net-to-gross in North Sea sandstones." *The Leading Edge* 28.1 (2009): 98-108.
- Aziz, O., Hussain, T., Ullah, M., Bhatti, A. S., & Ali, A. (2018). Seismic based characterization of total organic content from the marine Sembar shale, Lower Indus Basin, Pakistan. Marine Geophysical Research, 39(4), 491-508.
- Bacon, M., Simm. R., and Redshaw, T. (2007). 3-D seismic interpretation. Cambridge University.
- Badley, M.E., Price, J.D., Dahl, C.R. and Agdestein, T., 1988. The structural evolution of the northern Viking Graben and its bearing upon extensional modes of basin formation. *Journal of the Geological Society*, *145*(3), pp.455-472.
- Badley, Michael E. "Practical seismic interpretation." (1985).
- Barclay, F. Bruun, A., Rasmussen, K. B., Alfaro, J. C., Cooke, A., Cooke, D. A..... .Carcione, Jose M. "Constitutive model and wave equations for linear, viscoelastic, anisotropic med Geophysics 602 (1995): 537-548.
- Berger, A., Gier, S., and Krois, P., 2009, Porosity-preserving chlorite cements in shallow marine volcaniclastic sandstones: evidence from Cretaceous sandstones of the Sawan gas field, Pakistan. American Association of Petroleum Geologists Bulletin, v. 93. pp. 595 615.

- Berryman, James G. "Confirmation of Biot's theory." *Applied Physics Letters* 37.4 (1980): 382-384.
- Bortfeld, Roo. "Approximations to the reflection and transmission coefficients of plane longitudinal and transverse waves." *Geophysical Prospecting* 9.4 (1961): 485-502.
- Bruggeman, From DAG. "Calculation of various physical constants of heterogeneous substances. I. Dielectric constants and conductivities of mixed bodies made of isotropic substances." *Annalen der physik* 416.7 (1935): 636-664.
- Bust, Vivian K., Joshua U. Oletu, and Paul F. Worthington. "The challenges for carbonate petrophysics in petroleum resource estimation." *SPE Reservoir Evaluation & Engineering* 14.01 (2011): 25-34.
- Castagna, John P., and Herbert W. Swan. "Principles of AVO crossplotting." *The leading edge* 16.4 (1997): 337-344.
- Chao, Alexander Wu, and Karl Hubert Mess, eds. *Handbook of accelerator physics and engineering*. World scientific, 2013.
- Coffeen, J.A., 1978. Seismic exploration fundamentals.
- Djebbar, Tiab, and Erle C. Donaldson. *Petrophysics*. Elsevier Engineering Information Incorporated, 2004.
- Dræge A, Jakobsen M, Johansen TA. Rock physics modelling of shale diagenesis. Petroleum Geoscience. 2006 Feb 1;12(1):49-57.
- E.Badley, M. (1987). Practical Seismic Interpretation. Badley, Ashton, and Associates Ltd.
- Eshelby, John Douglas "The determination of the elastic field of an ellipsoidal inclusion, and related problems. Proceedings of the Royal Society of London. Series A. Mathematical and Physical Sciences 241.1226 (1957): 376-396.
- Fatti, Jan L., et al. "Detection of gas in sandstone reservoirs using AVO analysis: A 3-D seismic case history using the Geostack technique." *Geophysics* 59.9 (1994): 1362-1376.
- Fischetti, A. L, and Andrade, A. (2002). Porosity images from well logs. Journal of Petroleum Science and Engineering, 36(3), 149-158.
- Freissinet, C., Glavin, D. P., Mahaffy, P. R., Miller, K. E., Eigenbrode, J. L., Summons, R. E., ... & MSL Science Team. (2015). Organic molecules in the sheepbed mudstone, gale crater, mars. *Journal of Geophysical Research: Planets*, *120*(3), 495-514.

- Gassmann, Fritz. "Elastic waves through a packing of spheres." Geophysics 16.4 (1951): 673-685.
- Grechka, Vladimir, and Mark Kachanov. "Effective elasticity of rocks with closely spaced and intersecting cracksGeophysies 71.3 (2006): D85-D91. Gassmann, Fritz. "Elastic waves through a packing of spheres." Geophysics 16.4 (1951): 673
- Han. De-hua, and Michael L. Batzle. "Gassmann's equation and fluid-saturation effects on seismic velocities." Geophysics69.2 (2004): 398-405
- Hornby, Brian E., Larry M. Schwartz, and John A. Hudson. "Anisotropic effective-medium modeling of the elastic properties of shales." *Geophysics* 59.10 (1994): 1570-1583.
- Hussain, M., Ahmed, N., Chun, W. Y., Khalid, P., Mahmood, A., Ahmad, S. R., & Rasool, U. (2017). Reservoir characterization of basal sand zone of lower Goru Formation by petrophysical studies of geophysical logs. *Journal of the Geological Society of India*, *89*(3), 331-338.
- Ibrahim, M., 2007. Seismic Inversion Data, a Tool for Reservoir Characterization.
- Innanen, Kristopher A. "Inversion of the seismic AVF/AVA signatures of highly attenuative targets." Geophysics 76.1 (2011):R1-R14.
- Jakobsen, M., & Chapman, M. (2009). Unified theory of global flow and squirt flow in cracked porous media. *Geophysics*, *74*(2), WA65-WA76.
- Jakobsen, Morten, and Mark Chapman. "Unified theory of global flow and squirt flow in cracked porous media." Geophysics 74.2 (2009): WA6S-WA76.
- Jakobsen, Morten, and Tor Ame Johansen. "The effects of drained and undrained loading on viscoelastic waves in rock-like composites." International Journal of Solids and Structures 42.5-6 (2005): 1597-1611.
- Katahara, Keith W. "Clay mineral elastic properties." *SEG Technical Program Expanded Abstracts 1996*. Society of Exploration Geophysicists, 1996. 1691-1694.
- Kazmi AH, Jan MQ (1997) Geology and tectonics of Pakistan Graphic Publishers, Karachi, Pakistan.
- Khan, N., Konaté, A.A. and Zhu, P., 2013. Integrated geophysical study of the lower Indus platform basin area of Pakistan. *International Journal of Geosciences*, *4*(9), p.1242.

- Kingston. D. R., Dishroon, C. P., & Williams, P. A. (1983). Global basin classification system. AAPG bulletin.
- Krois, P., Mahmood, T., and Milan, G 1998, Miano field, Pakistan, A case history of model driven exploration. Proceedings of the Pakistan Petroleum Convention, 1998, PAPG Pakistan Petroleum Convention, Abstract No. 90145, p.112.
- Kumar, Dhananjay. "A tutorial on Gassmann fluid substitution: Formulation, algorithm and Matlab code." *matrix* 2.1 (2006).
- Kumar, G. "Effect of fluids on attenuation of elastic waves." 73rd Annual International Meeting, SEG, Expanded Abstracts, 2003. 2003.
- Linde, N., Tryggvason, A., Peterson, J. E., & Hubbard, S. S. (2008). Joint inversion of crosshole radar and seismic traveltimes acquired at the South Oyster Bacterial Transport Site. *Geophysics*, *73*(4), G29-G37.
- Mavko, Gary, Tapan Mukerji, and Jack Dvorkin. The rock physics handbook. Tools for seismic analysis of porous media. Cambridge university press, 2009.
- Modeling Sawan Gas Field - a Case Study, PAPG, ATC.
- Mukerji, T. Avseth, P. Mavko, G., Takahashi, 1. González, E.F., 2001. Statistical rock physics: combining rock physics, information theory, and geostatistics to reduce uncertainty in seismic reservoir characterization. Lead. Edge 20 (3). 313-319.
- Munir, Khyzer, et al "Mapping the productive sands of Lower Goru Formation by using seismic stratigraphy and rock physical studies in Sawan area, southern Pakistan a case study." Journal of Petroleum Exploration and Production Technology 1.1 (2011): 33-42.
- Rüger, Andreas. *Reflection coefficients and azimuthal AVO analysis in anisotropic media*. Society of Exploration Geophysicists, 2002.
- Rutherford, Steven R., and Robert H. Williams. "Amplitude-versus-offset variations in gas sands." *Geophysics* 54.6 (1989): 680-688.
- Shuey. R. T. "A simplification of the Zoeppritz equations." Geophysics 50.4 (1985): 609-614.
- Silversides, K., Melkumyan, A., Wyman, D., & Hatherly, P. (2015). Automated recognition of stratigraphic marker shales from geophysical logs in iron ore deposits. *Computers & Geosciences*, *77*, 118-125.

- Slatt, R. M. (2006). *Stratigraphic reservoir characterization for petroleum geologists, geophysicists, and engineers*. Elsevier.
- Smith, G. C., and P. M. Gidlow. "Weighted stacking for rock property estimation and detection of gas." *Geophysical prospecting* 35.9 (1987): 993-1014.
- Stewart, Andrew L., and Andrew F. Thompson. "Sensitivity of the ocean's deep overturning circulation to easterly Antarctic winds." *Geophysical Research Letters* 39.18 (2012).
- Wandrey, CJ., Law, B.E. and Shah, H.A. 2004. Sembar Goru/Ghazij Composite Total Petroleum System, Indus and Sulaiman-Khirthar Geologic Provinces. Pakistan and India, U.S. Geological Survey Bulletin 2208-C.
- White, J. E. (1986). Biot-Gardner theory of extensional waves in porous rods. *Geophysics*, *51*(3), 742-745.
- Wilcox, Andrew C., et al. "An integrated analysis of the March 2015 Atacama floods." *Geophysical Research Letters* 43.15 (2016): 8035-8043.
- Wyllie, Malcolm Robert Jesse, Alvin Ray Gregory, and Louis Wright Gardner. "Elastic wave velocities in heterogeneous and porous media." *Geophysics* 21.1 (1956): 41-70.
- Xu, Sheng, et al. "Antileakage Fourier transform for seismic data regularization." *Geophysics* 70.4 (2005): V87-V95.
- Yilmaz, Öz, Irfan Tanir, and Cyril Gregory. "A unified 3-D seismic workflow." *Geophysics* 66.6 (2001): 1699-1713.Yin, Xing Yao, Guang-Sen Cheng, and Zhao-Yun Zong. "Non-linear AVO inversion based on a novel exact PP reflection coefficient." Journal of Applied Geophysics 159 (2018): 408-417.
- Zaigham NA, Mallick KA (2000) Prospect of hydrocarbon associated with fossil-rift structures of the southern Indus basin, Pakistan. Am Assoc Pet Geol Bull 84(11):1833-1848.
- Zhang, Y., Ratcliffe, A., Roberts, G., Duan, L, 2014. Amplitude-preserving reverse time migration from reflectivity to velocity reflectivity to velocity and impedance inversion Geophysics 79 (6), S271-S283.
- Zoeppritz, K., 1919. Erdbebenwellen VIIIB. On the reflection and propagation of seismic waves.